UNIVERSITY OF OKLAHOMA

GRADUATE COLLEGE

DIBLOCK CARBON NANOTUBES COMPATIBILIZED IMMISCIBLE POLYMER BLENDS

A DISSERTATION

SUBMITTED TO THE GRADUATE FACULTY

in partial fulfillment of the requirements for the

Degree of

DOCTOR OF PHILOSOPHY

By

FATOUMATA IDE SEYNI

Norman, Oklahoma

2020

DIBLOCK CARBON NANOTUBES COMPATIBILIZED IMMISCIBLE POLYMER BLENDS

A DISSERTATION APPROVED FOR THE
SCHOOL OF CHEMICAL, BIOLOGICAL AND MATERIALS ENGINEERING

BY

Dr. Brian Grady, Chair

Dr. Steven Crossley

Dr. Keisha Walters

Dr. Jeffrey Harwell

Dr. Jivtesh Garg

© Copyright by FATOUMATA IDE SEYNI 2020
All Rights Reserved.

Acknowledgements

First and foremost, I would like to thank my advisors Dr. Harwell and Dr. Grady for giving me the opportunity to pursue my graduate studies. I would like to thank the CBME faculty that I have learned from these past few years. A special thanks to Lisa Morales, for her constant support and encouragements since my first day at OU.

I would like to thank the all the people I have learned from and who have contributed to this work: Dr. Lawrence Barrett for is work synthesizing the nanotubes, Dr. Preston Larson for his help and expertise on SEM and TEM experiments, Dr. Tingting Gu for her help on confocal microscopy, and Dr. Julian Sabisch who I have only know for a couple of weeks but dedicated a significant amount of time to make sure I get good TEM images. I want to thank Dennis McAlister and Andrew D'Amico for fixing and maintaining the lab equipment. My undergraduate researchers, Roukayatou Ouedraogo and Sam Saley for their dedication and help in the completion of the research. I have learned a lot about mentorship working with them.

I would like to thank all the friends that I have met through this journey and who have become family. Those who would regularly check up on me, bring me food, encourage me constantly, and provided mental support through this last year. I want to especially thank Fatima Dembele and the Saho Family for making me part of their families.

Finally, I would like to thank Habsatou Mounkaila and Ide Seyni, my amazing parents, and dedicate this dissertation to them for making sure I got the best education they could afford to give me. I made it this far thanks to their sacrifices.

Table of Contents

List of Tables

List of Figures

Abstract

Plastic pollution is one of the most serious environmental challenges the world is currently facing. From contaminating soil and oceans to harming animals that consume it, the damages caused by mismanaged plastic waste require immediate action. Of the solutions that currently exist to deal with plastic pollution, the best is recycling. However, the wide variety of plastics available, their immiscibility and the necessity to sort them, makes recycling an expensive process. To solve the problem, interfacial agents are used to improve the miscibility between different plastics. The present dissertation summarizes experiments conducted to evaluate the suitability of carbon nanotubes as compatibilizers for immiscible polymer blends. Nanotubes with dual chemistry (i.e diblock CNTs) allowing them to be compatible with two different polymers have previously been synthesized. Asymmetric double cantilever beam (ADCB) studies were conducted to quantitatively measure the ability of the diblock CNTs to compatibilize polystyrene/poly(methyl methacrylate) PS/PMMA blends. TEM analysis shows the diblock CNTs at the interface between the two polymers. The fracture mechanism taking place suggests that the carbon nanotubes have higher affinity to PMMA than PS. The maximum interfacial fracture toughness of 30 J/m^2 obtained was similar to that of block copolymer reinforced interfaces; however, SEM studies of the fractured surfaces also show agglomerates of carbon nanotubes present which may be limiting the efficacy of carbon nanotubes at toughening the interface. Results from varying the annealing time of ADCB samples show that diblock CNTs can also slow down the degradation of polymers at a given temperature

Chapter 1 : Advances in immiscible polymer blends technology

1.1 Plastic production and waste related problems

Polymers commonly known as plastics affect almost every aspect of our daily lives; they are used in the packaging, health care, and automotive industries to cite a few. The mass production of plastics was ignited by the discovery of the first fully synthetic plastic, Bakelite, in 1907. Until 1950, the world produced about 2 million tons of plastic per year. Since then, annual production increased exponentially to reach 381 million tons produced in 2015, roughly the mass of two-thirds of the world population [1]. The cumulative production of plastic was 7.8 billion tons in 2015, and around 8.3 billion tons in 2018 [2]. This massive production of plastics results in massive plastic waste generation. Figure 1.1 shows the primary plastic production and plastic waste generation by industrial sector in 2015. The packaging industry produced 42% of plastics in 2015 and because of the short "in-use" lifetime of packages, was also the dominant generator of plastic waste responsible for almost half of the global total [2].

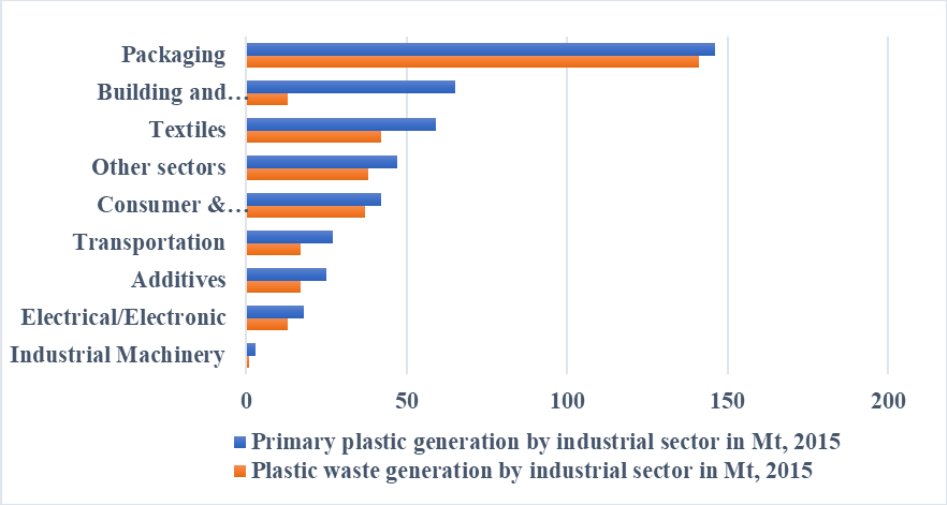

Figure 1.1 Plastic production and plastic waste generation in million tons in 2015. Data obtained from ref 2.

There are four primary ways to dispose of plastic waste: recycling, incineration, disposal in controlled landfills, or discarding it in the natural environment. Prior to 1980, 100% of the plastic produced was discarded as shown in Figure 1.2. By 2015, an estimated 55% of plastics was still discarded while 20% was recycled with remainder incinerated. Cumulatively, about 79% of the total plastic produced between 1950 and 2015 was discarded, 12% incinerated and only 9% was recycled. Discarded waste can cause serious environmental and health problems. To date, around 150 Mt (million-tons) of plastics is believed to have been released in the oceans [3]. The devastating impact of plastics in the environment and on wildlife including animal wounds, death, and reduced population in hundreds of species have been recorded [4]. Over time large macroplastics can fragment into micro or nano-sized plastics. Even though, no clear evidence of micro or nanoplastics effects on human health exists, there are fears that the plastics themselves, the chemicals adsorbed on them, or the chemicals that leach when the plastics fragment can cause serious health problems [5, 6]. Incineration consists of burning waste at high temperatures to produce ash, flue gas, and heat. Several European countries like France, Denmark, and Germany rely on incineration to handle their municipal waste and to produce electric energy. However, there is concern that serious problems on wildlife and human health can result from burning plastic. Besides being expensive to implement, burning plastics releases dioxins into the air, soil, and water which can cause serious respiratory problems like asthma or even cancer [7].

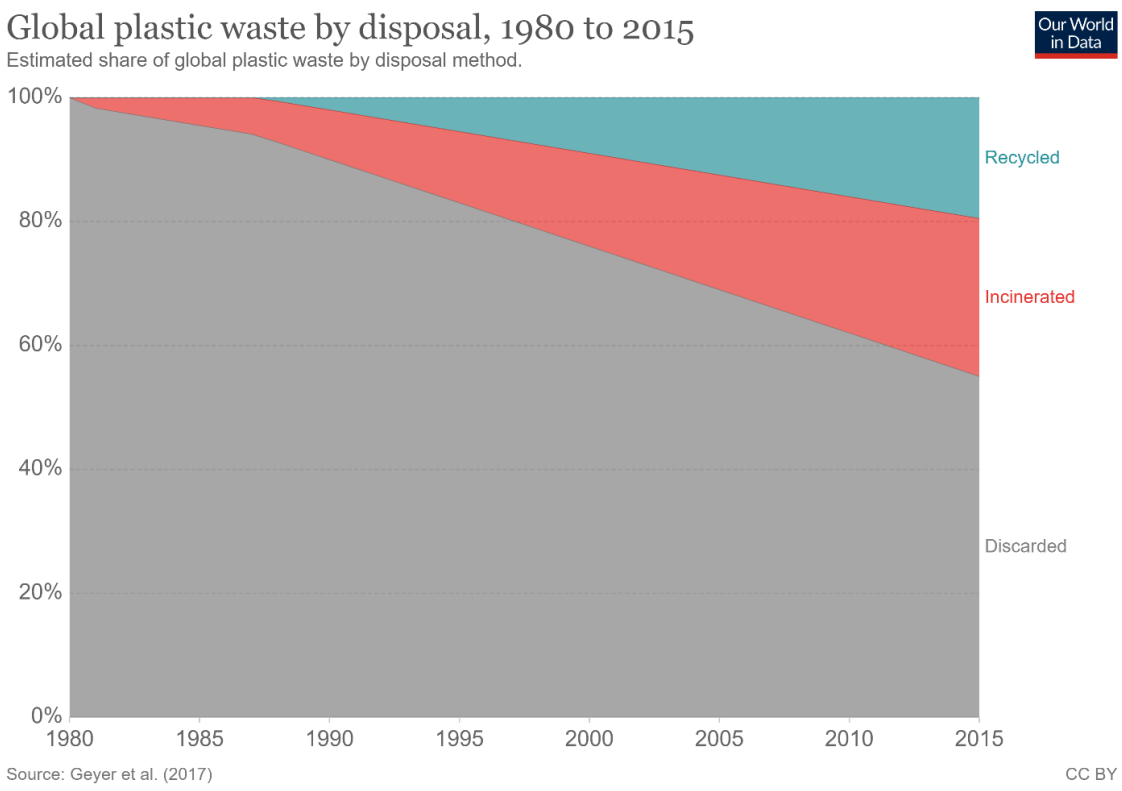

Figure 1.2 Global plastic waste disposal between 1980 and 2015. Chart obtained from ref 1.

The best solution to deal with plastic waste is recycling [8]. Mechanical recycling consists of cleaning plastic from contamination, chopping it down and melting it to form pellets without altering the chemical structure of the plastic. Because recycled plastic loses some of its physical properties, the pellets are usually mixed with virgin plastic to produce materials with acceptable properties or are otherwise incorporated with virgin plastic.

However, mechanical recycling also has several limitations. Since polymers must be melted down and reformed, mechanical recycling is limited to a subset of polymers (i.e. thermoplastics); polymers that cannot be melted down and reformed like thermosets with rigid cross-linked bonds cannot be recycled. The presence of impurities can render a recycled plastic unusable and most polymers are not miscible so considerable energy is expended to sort plastic by type prior to

recycling. Because of the wide variety of polymer types, current technology can only recycle a few kinds of plastics. Even though some recycling facilities collect several different types of plastics, most end up being discarded or incinerated because they do not meet the recycling requirements of the facility [9].

There are three main ongoing research areas to improve on the current plastic recycling limitations: improving chemical recycling efficiency through catalyst development, expanding recycling beyond thermoplastics, and finally minimizing the need for sorting through compatibilizer development [8]. The last area is the focus of this work.

1.2 Mechanical Recycling and immiscible polymer blend compatibilization

The need for sorting plastic prior to recycling renders the process very expensive to implement. Considering the numerous types of polymers produced, being able to blend different types of plastics can significantly decrease costs associated with mechanical recycling. Polymer blends are already used to extend the performance of engineering resins and improve on specific properties of certain polymers like impact and solvent resistance [10]. For example, high impact polystyrene (HIPS) is made by adding rubber to polystyrene to improve the impact resistance of the latter. Another common blend is polyethylene/polyamide (PE/PA) which combines the high stress and good chemical resistance of PA with the high impact resistance and low moisture absorbance of PE [11]. Blending plastic waste is not only more cost-effective and requires less development time, but also gives an opportunity to recycle plastic waste into usable materials. Polymer blends can allow for the synergetic combination of the properties of different polymers and allow for tuning by varying the ratio of the different polymers.

The immiscibility of polymers results from the lack of entanglements at the interface between the polymers in the blend. Consequently, several methods for improving interfacial adhesion and

mechanical properties of polymer blends have been developed. These methods, known as compatibilization techniques, strive to increase interactions between phases and rigidify of the interface [12]. Compatibilizers can be reactive or non-reactive. Reactive compatibilization consists of adding a third component in a blend that can react to form covalent bonds with one of the polymers in the blends or crosslink the two polymers [13, 14]. Non-reactive or physical compatibilization consists of adding a third component that is compatible with both components in the blend [15]. For a compatibilizer to be effective, it needs to 1) relocate at the interface during the mixing process, 2) stabilize the morphology against thermal and shear effects during blending and 3) finally provide adhesion in the solid state.

1.2.1 Copolymers applications and limitations

Copolymers are the most common type of compatibilizer for immiscible polymer blends. They are polymer molecules formed by covalently bonding two or more different types of monomers. Several different architectures of copolymers have been used including block [15-18], random [19, 20], graft [21, 22], and alternating copolymers [23]; a schematic of which can be found in Figure 1.3. Because of their popularity over 45,000 papers can be found on copolymers [24]. Alternating copolymers generally have much poorer performance than polymers with blockiness. For a copolymer with some blockiness to be maximally effective, one block needs to have miscibility with one component in the blend and the other with the other component. Further, each block needs to be above the entanglement molecular weight of its respective miscibility pair and the concentration of the copolymer in the blend need to be slightly the critical micelle concentration (CMC), a concentration above which copolymers will form micelles rather than locate at the interface. These requirements make it challenging to synthesize effective copolymers for compatibilization. Low molecular weight copolymers can easily move to the interface but are not

long enough to entangle with the polymers in the blend and so do not provide good adhesion in the solid state. However, copolymers with chains above the entanglement molecular weight can effectively entangle once at the interface but long chains make it more difficult for those copolymers to reach the interface and are more easily lost in micelles [13].

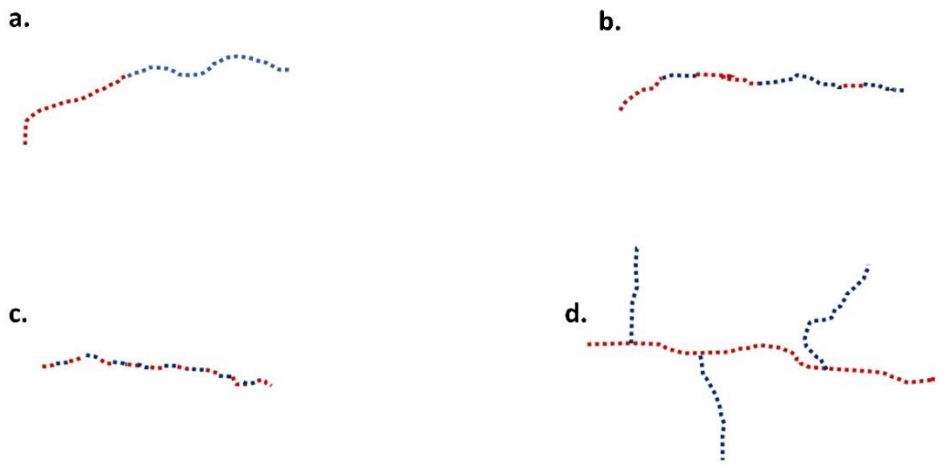

Figure 1.3 Different types of copolymers: (a) diblock, (b) alternating, (c) random, and (d) graft copolymer.

Reactive compatibilization uses a reaction that connects chains across the interface forming block or graft copolymers. In these cases, a third component is added which induces a reaction between the two polymers in the blend. Most commonly, a copolymer is added which is miscible with one polymer in the blend and is also capable of forming covalent bonds with the other polymer in the blend [25, 26]. The reactive unit is typically in low concentration (~1 %). This second type of compatibilization is much more important commercially because it leads to thicker interphases and thus good morphology stability. A drawback of this method is that covalent bonds can be formed in the bulk polymers which can hinder recyclability. Even though reactive

compatibilization is the preferred method, it is limited to a few blends while compatibilization using premade copolymers can be applied to a wide range of blends.

The two main techniques of blending polymers are solution [27] and melt mixing [28]. Either one of these techniques can be used, in principle, regardless of the compatibilization technique used. Limitations to either method comes from the polymers in the blend; for solution mixing to be used, the polymers used in the blend need to have a common solvent whereas for melt mixing, they must melt when heated. Because finding common solvents for different solvents is a challenging task and because separation of the solvent from the dried polymer is expensive, melt mixing is the favored technique commercially. Melt mixing also often promote reactions because of the high temperatures involved. Academically however, solution mixing is often used because less material is needed, molecular weight degradation can be ignored and, if thin films are needed, then they can be formed much easier.

Recently, "particulate compatibilizers" – particles that can adsorb at the interface of immiscible blends and have effects similar to conventional compatibilizers have been developed. These particles form so-called Pickering emulsions by preventing droplet coalescence and stabilizing the morphology thus significantly improving blending. Several types of particles including carbon black, nanoclays and silica have been shown to adsorb at interfaces in immiscible polymer blends. While some of the particles are used without any kind of surface modification, an increasing area of research is concerned with particles with dual surface chemistries – analogous to that of block copolymers.

1.2.2 Janus particle (JP) applications

JPs have been synthesized in a variety of shapes and sizes. We will focus on those shapes that have been used for immiscible polymer blend compatibilization. Three main types of JPs have been used: nanosheets (JNs) which are usually rectangular in shape with one chemistry on one side and another chemistry on the opposite side, "snowman-like" particles made by grafting silica and polymeric particles, and finally spherical JPs made with two different polymers.

The techniques used to synthesize JPs can be classified in three main categories: "masking", phase separation between immiscible particles, and self-assembly of block copolymers, examples of JPs synthesis using these techniques can be seen in Figure 1.4. The masking technique, used to produce JNs, consists of modifying one face without modifying the other. Masking is achieved by selectively masking one face with a material that cannot be polymerized while functionalizing the other side. The second technique consists of incorporating two incompatible substances into a single particle and taking advantage of their immiscibility to induce phase separation. This technique is very versatile and allows for the formation of organic and inorganic JPs or, in the case of snowman-like JPs, particles that are part organic and part inorganic. The last technique used to produce nanoparticles for polymer blend compatibilization is "self-assembly" of copolymers [29, 30]. Usually an ABC triblock copolymer is self-assembled in bulk or solution and produces nanosized symmetric particles that are roughly ellipsoidal in shape. Block B is cross-linked and a JP is formed with chains A and C as the opposite faces. A detailed review of the work done to

synthesize JPs is beyond the scope of this review but several reviews have reported in detail on those techniques [31-38].

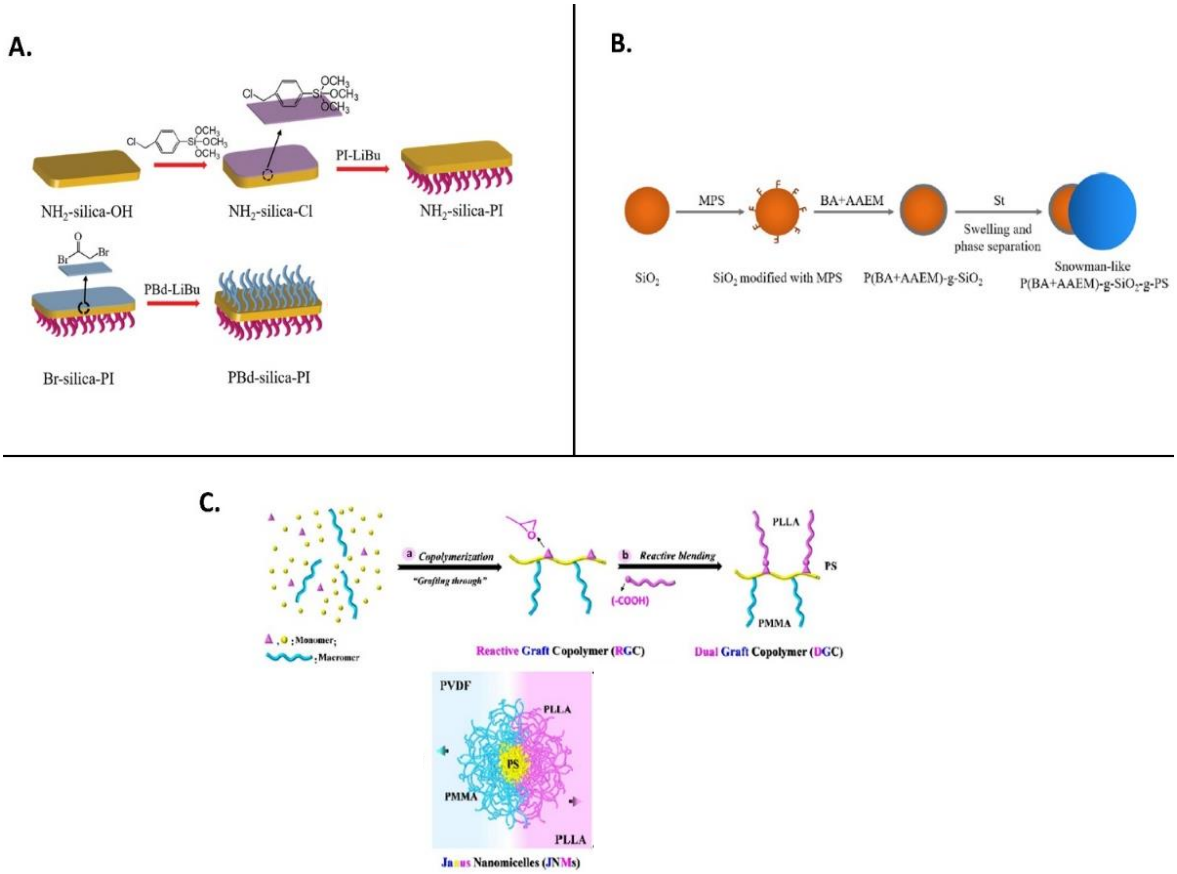

Figure 1.4 Representative Janus particles synthesis techniques. (a) Illustrative fabrication of amphiphilic PBd-silica-PI Janus nanosheets using a masking technique. Reprinted from ref. 40 (b) Schematic representation of the synthesis of snowmanlike JPs using phase separation between immiscible particles technique. Reprinted from ref.45 (c) Schematic view of the formation of Janus nanomicelles using self-assembly of PLLA-PS-PMMA triblock copolymer. Reprinted from ref. 51.

The first type of JPs encountered in immiscible polymer blends compatibilization applications are Janus nanosheets (JNs). Nie and coworkers synthesized silica JNs by selectively grafting PS chains and polyisoprene (PI) chains on opposite sides of the sheets [39]. The PS-silica-PI JNs showed great efficiency at compatibilizing PS-PI blends in contrast to silica nanosheets which had poor dispersion in the blend. These nanosheets have also been shown to improve the mechanical

properties of the compatibilized blends. Han et al., incorporated polybutadiene (PBd)-silica-PI JNs in styrene-butadiene-rubber/natural rubber (SSBR-NR) blends and saw significant improvement in the mechanical properties [40]. Strengthening and toughening of the blends was accomplished with only 3 parts per hundred rubber (3phr); the tensile strength of the composites was 3 times higher than that of the unfilled blends, and twice that of blends filled with unfunctionalized nanosheets. The elongation at break also increased to 470% compared to 320% for unfilled blends. Similarly, Hou et al. added butadiene acrylonitrile rubber (NBR)-silica-epoxide JNs in blends of epoxy resin-nitrile butadiene rubber (EP-LNBR) and obtained composites with improved tensile modulus (2.3 GPA to 33 GPA), tensile strength (73 to 88 MPa), and elongation at break [41]. Lastly, Daitx and co-workers used kaolinite based JNs with an amine group and PMMA chains on either side to compatibilize PS-PMMA blends [42]. They saw a reduction in dispersed phase domain size with addition of the kaolinite JNs and the storage modulus, Young's modulus, and strain at break increased by 50, 35, and 70%, respectively compared to the blends without compatibilizer.

Another common type of JPs encountered are "snowman-like" particles. They are usually synthesized by embedding a silica particle into a polymer nanosphere [43]. These asymmetric particles have shown superior ability to stabilize cocontinuous morphology during annealing at high temperatures [44]. Parpaite and co-workers incorporated SiO_2@PS snowman-like nanoparticles into PS-polyamide-6 (PA6) (80-20, w-w) blends and observed a decrease in size of the PA6 dispersed phase [45]. The complex viscosity increased as a function of JPs over the entire frequency range used which was attributed to the formation of a rigid network at the interface. A similar study was conducted by Caro and co-workers, who also observed a decrease in the PA6 phase diameter from 13.3 μm for unfilled blends to 7.2 μm for composites. They analyzed the

rheological response of the composite using the Palierne model and found a decrease in the interfacial tension (IFT) from 7.4 mN-m to 1.95 mN-m at 3 phr of JHNPs in the blends. However, other researchers found that it was necessary to graft a polymer either on the silica side or both sides of these snowman-like JPs to make them more compatible with the polymers in a blend. Nie et al. produced JPs by successive grafting of brushes on polydivinylbenzene (PDVB)@SiO_2 JPs [46]. They grafted polybutadiene (PB) onto the PDVB side and polyisoprene (PI) chains onto the SiO_2 side. Their results showed that the brush-modified PB-PDVB@SiO_2-PI nanoparticles decreased domain sizes and stabilized bicontinuous morphologies of PS-PBd rubber blends during thermal annealing for 9 hours whereas the original snowman-like JPs did not decrease domain size and selectively located in the PBd phase. Xu et al. used snowman-like JPs with dodecyl mercaptan (DM) grafted on the PDVB side and 3(trimethoxylsilyl) propyl methacrylate (MPS) chains on the SiO_2 side to compatibilize liquid isoprene rubber (LIR)-epoxy resin(ER) blends [47]. The JPs decreased the LIR domain sizes and also decreased the glass transition temperature (T_g) difference of the two polymers in the blend which are both signs of improved compatibility. The impact strength of the composite also improved when up to 3% JPs were added compared to that of the unfilled LIR-ER blend. More recently, Cheng et al. [48] used similar PDVB@ SiO_2 nanoparticles to make JPs but only grafted polymer on the SiO_2 side. They used triethylene-tetramine (TETA)-SiO_2@PDVB NPs to compatibilize acrylic resin-ER blends. The strong interfacial adhesion and high desorption energy of the TETA-SiO_2@PDVB NPs resulted in toughening the blends. The impact strength and tensile strength of the composites were 60% and 280%, respectively, higher than that of the blends without added particles.

Wang et al. used a “self-assembly” technique to produce in-situ Janus nanomicelles by incorporating small amounts of reactive poly (styrene-co-glycidylmethacrylate)-graft-poly

(methyl methacrylate) (PMMA) in polyvinylidene fluoride (PVDF)-poly(lactic acid) (PLLA) blends [49, 50]. In-situ formed nanomicelles stabilized the morphology and the elongation at break after melt mixing for 10 minutes was 320% compared with 5% for the blend without the JPs. A common triblock copolymer used for the production of Janus particles is PS-PB-PMMA (SBM) triblock terpolymer [51, 52]. Here particles are formed by crosslinking PB which forms the core of the JP with PS and PMMA hemispheres. Barwinkel et al. [53] and Bryson et al. [54] used SBM terpolymer to produce JPs to compatibilize polyphenyl ether (PPE)-styrene-acrylonitrile (SAN) atnd PS-PMMA blends, respectively. In both cases, the JPs stabilized the morphology of the blends and reduced the dispersed phase sizes resulting in "raspberry-like" structures. Similarly, Bahrami and coworkers [55, 56] synthesized JPs using SBM to compatibilized 60-40 (w-w) Poly(2,6-dimethyl-1,4-phenylene ether)-SAN blend. They also observed that "raspberry-like" structures of JPs-covered PPE-phases in a SAN matrix were formed, as shown in Figure 1.5, when the optimum fraction of JPs was added to the blend.

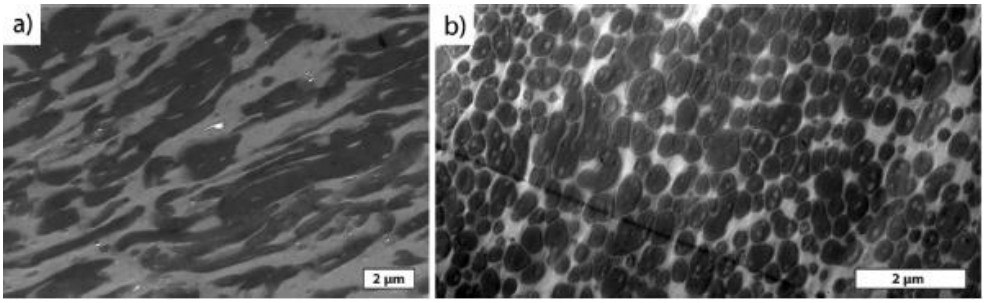

Figure 1.5 Morphology of PPE (dark)-SAN (bright) blend (60-40 w-w), as neat blend and compatibilized with 10 wt.% of SBM JPs. TEM overview of the PPE-SAN blend without (a) and with compatibilization (b). "Raspberry-like" structures can be observed for the compatibilized blend in (b). Reproduced from ref. 56**.**

Another structure is used to compatibilize immiscible blends which cannot be classified as JPs but are inspired by the JP structure. These materials are made by grafting two different polymers onto a particle (i.e silica) but contrary to a typical JP that has two distinct chemistries on opposite sides,

the polymers chains are randomly distributed. Wang and coworkers used an "attaching onto" technique by successively grafting epoxide chains via the reaction of epoxide monomers and long poly(methyl methacrylate) (PMMA) molecules on the surface to form reactive epoxy-PMMA-graft-SiO_2 (Epoxy-M-SiO_2) nanoparticles [57]. Incorporating these Epoxy-M-SiO_2 nanoparticles into a PVDF-PLLA (50-50, w-w) blend by melt mixing resulted in in-situ formation of PLLA on the surface of SiO_2 by the reaction of the carboxylic acid groups with epoxide groups on the surface of SiO_2. The nanoparticles were exclusively located at the interface by the formation JPs with pregrafted PMMA tails entangled with the PVDF phase and the in-situ grafted PLLA chains embedded in the PLLA phase. They functioned as compatibilizers by suppressing the coalescence of PVDF domains and improving the adhesion between the two phases; a domain size reduction from ~10 μm to ~1.9 μm was obtained after adding the Epoxy-PMMA-SiO_2 NPs to the blend. The mechanical properties of the blends also improved significantly with the elongation at break and tensile strength increasing by 50% and 29%, respectively. Guo and coworkers used a similar technique to modify the surface of silica nanoparticles but instead of using two different polymers, they attached mono hydroxyl group terminated PS-PMMA random copolymers via the condensation reaction between the hydroxyl groups of the silica particles and the copolymer [58]. They used the nanoparticles to stabilize dispersed and cocontinuous PS-PMMA blends prepared by solvent evaporation; here too the silica JPs were found to densely pack at the PS and PMMA interface.

The effectiveness of JPs shows the potential for particles with the right surface chemistries to serve as effective compatibilizers for immiscible polymer blends while mitigating the micellization problem of diblock copolymers.

1.3 Carbon nanotubes: applications in immiscible polymer blends

Carbon nanotubes (CNTs) are tubular nanostructured carbon materials that are long and slender with walls made of hexagonal carbon rings and end caps containing pentagonal rings; their structure resembles that of rolled up graphene sheets. They can be single-walled (SWCNTs) or multi-walled (MWCNTs); and their properties depends not only on their type, but also their degree of graphitization and their diameter. Three methods are used to produce CNTs; arc discharge, visible light vaporization and chemical vapor deposition (CVD). The first two methods use graphite as the carbon source while CVD can use carbon monoxide (CO), methane, acetylene, benzene, and alcohols. The production methods used determines the quality of tubes, distribution of diameters and lengths, degree of entanglement, and amount of impurities. CVD is the preferred and most scalable method [59].

CNTs have incredible properties; they are both thermally and electrically conductive and are one of the stiffest and strongest man-made materials with elastic modulus of 10^3 GPa and 500 GPa, respectively [60]. CNTs have been used in both homopolymers and polymer blends to produce electrically conductive polymer nanocomposites with enhanced thermal and mechanical properties [61, 62].

CNTs are used in immiscible polymer blends to produce conductive composites at low filler compositions. When conductive fillers like CNTs are added to polymers, they form a conductive network above a critical concentration, called the percolation threshold. Because of their high aspect ratios combined with their superior electrical properties, carbon nanotubes have been shown to produce conductive composites at much lower filler loadings than other fillers like carbon black [63]. The low filler content allows for the preservation of the flexibility of the polymer matrix since high content of a stiff filler negatively affects flexibility. Polymer blends have been used to

further decrease the electrical percolation threshold through the concept of double percolation first introduced by Sumita et al. [64] for carbon black [65, 66]. Double percolation refers to the percolation of a filler in one phase of a polymer blend (first percolation), which itself percolates in the blend (second percolation). Contrarily to spherical particles like carbon black or silica that can be made to locate at the interface in certain polymer blends, carbon nanotubes strongly prefer to locate in one of the phases in blends regardless of mixing sequence because of their high aspect ratio [67]. Double percolation is achieved by adding CNTs to the continuous phase in a droplet morphology or one of the continuous phases in a co-continuous blend. Despite not locating at the interface, CNTs have been shown to toughen immiscible blends through two mechanisms. (1) The same percolated network that allows CNTs to conduct electricity in an insulating polymer matrix can also improve the stress transfer ability of the composite by transferring stress along the axis of the CNTs network. In PC/PBT [68], PC/PLA [69, 70], and PP/EVA [71] blends, the presence of a CNTs improved the impact strength. (2) Some compatibility has been observed when CNTs selectively locate in their preferred phase in an immiscible polymer blend because the presence of CNTs changes the viscosity ratio of the blend (which can, in some cases, improve mechanical properties and also prevents coalescence of minor phase domains during blending). [72, 73]. This observation has been made for PCL/PLA [74], HDPE/PA6 [75, 76], and PVDF/PA6 [77] blends.

However, optimum compatibilization can only be obtained when compatibilizers can readily locate at and strengthen interfaces of immiscible blends. The selective localization of CNTs in blends is controlled by both thermodynamic and kinetic factors. The first one comes from the tendency of minimizing the free energy of the system, and the driving force is the difference in interfacial energies between the fillers and the respective polymers in the blend. Even for highly compatible blends of polycarbonate (PC) and styrene acrylonitrile (SAN) where the interfacial

energy of MWCNTs/PC was just slightly lower than that of MWNCTs/SAN, the tubes still completely relocate to the PC phase after just 5 minutes of mixing [78]. Even tough wettability of CNTs by respective polymers in a blend is the driving force for CNTs to move from an unfavorable to a favorable phase, kinetic factors also play an important role in the final localization of CNTs in a blend. The speed of CNT migration from the unfavorable blend component to the favorable component depends on several factors like the viscosity of the homopolymers in the blend, the aspect ratio of the CNTs and the mixing parameters (mixing time, temperature, shear force, etc.). For the same PC/SAN blend mentioned above, increasing the viscosity of the PC hindered the migration of CNTs from SAN to the high viscosity PC [74]. Similar behavior was found for LDPE/PVDF/CNTs [79], PLA/PCL/CNTs [80, 81], PA12/PE/CNTs [82], and PC/PTT/CNs [68] nanocomposites. Goldel et al. [78] have reported that transfer of high aspect ratio nanoparticles like CNTs through a blend interface is faster than that of spherical shapes particles (i.e. carbon black) due to a so-called "Slim-Fast Mechanism" (SFM). Since CNTs, in general, move quickly through interfaces to locate in their thermodynamically favored phases; the most important aspect of producing CNTs for immiscible polymer blend compatibilization is their affinity to the respective polymers in the blend.

"Patchy" carbon nanotubes have been synthesized by physically wrapping a PS-b-PE-b-PMMA triblock copolymer [83]. The PE middle block selectively adsorbs on the nanotubes while the PS and PMMA blocks separate into a patchy PS/PMMA corona. These nanotubes were shown to have strong interfacial activity in a PS/PMMA blend and decreased the domain size of dispersed PMMA domains in PS. TEM images showed that the nanotubes laid parallel to the blend interface. Carbon nanotubes are strong along the axial direction [84, 85] but weaker radially [86, 87]. So, even though

these patchy nanotubes can stabilize the morphology of immiscible polymer blends, they do not use the full potential of the nanotubes.

1.4 Objectives of this work

The objective of this work is to show that a highly anisotropic NP, i.e. a carbon nanotube, with different chemistry along its length as shown in Figure 1.6, can compatibilize polymer blends. Functionalization, which consists of covalently or non-covalently attaching functional groups to nanotube walls, has been used to change the location of multiwalled carbon nanotubes (MWCNTs) in a blend [88]. Since affinity to respective polymers in a blend is the most important factor governing the location of nanotubes in blends, we have synthesized a diblock nanotube that has similarities in structure to diblock copolymers and JPs; one side has a higher affinity to polymer 1 and the other side has a higher affinity to polymer 2 and thus can reside at the interface in a blend.

Using Janus particles means that composites can be made with scrap immiscible plastics with good mechanical properties at low filler concentrations while eliminating the micellization problem present in copolymer compatibilized blends. Because of their high aspect ratio and strength, CNTs can absorb more energy than block copolymers and strengthen immiscible polymer blend interfaces at lower concentrations. They also have superior mechanical, electrical, and thermal properties compared to other carbon nanofillers and particles. So being able to produce polymer blends compatibilized with block nanotubes offers the possibility of making composite materials with improved mechanical, electrical, and thermal properties for a wide range of applications. Nanotubes at the interface in polymer blends offers the possibility of triple percolation [23], where an immiscible polymer blend forms a co-continuous structure and nanotubes percolate at the interface. These types of composites would further decrease the amount of filler needed to produce conductive materials; much less than in double percolated composites.

The main chapter of this thesis is concerned with the third criteria of compatibilization: adhesion between immiscible polymers in the solid state. Asymmetric double cantilever beam (ADCB) tests are fracture tests used to quantify the adhesion of immiscible polymer interfaces. These tests are used to measure the interfacial fracture toughness of copolymer reinforced immiscible polymer blend interfaces. In this work, we have developed a procedure to perform ADCB experiments with CNTs and the findings are compared against those of copolymers.

In the first appendix, preliminary work conducted on rheological measurements in the melt state will be presented. While ADCB experiments focus on the mechanical properties of reinforced interfaces in the solid state, rheological experiments evaluate the effectiveness of block CNTs at stabilizing the morphology of the blend during processing. Results from these experiments will complement the findings of this work and prove whether all criteria of compatibilization can be met using diblock CNTs.

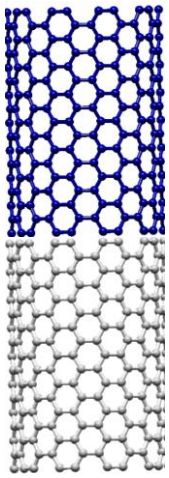

Figure 1.6 Schematic representation of a block carbon nanotube with two different chemistries along its length represented by the blue and grey atom colors.

Chapter 2 : Adhesion Fracture Tests

2.1 Introduction

Adhesion is related to the strength of coupling that can occur between any pair of materials. In glassy polymers, adhesion is created by heating the two materials above their glass transition temperature (T_g) to allow for interdiffusion; it is also referred to as welding or crack-healing [89]. Adhesion between two different materials is controlled by the entanglement between the materials. Materials that are immiscible have very narrow interfaces resulting in low adhesion. However, their adhesion can be greatly improved if a third material that is miscible with both polymers is present at the interface and entangles with both polymers.[90]

Tests of adhesion are fracture tests where a crack is propagated along an interface. In these tests, the results are given as G_c, the critical energy release rate which is the energy dissipated per unit crack area formed, with units of energy over surface. G_c is analogous to the interfacial fracture toughness; a propriety that describes the ability of a material to resist failure. [91]

The value of G_c depends on the type of fracture test employed. The toughness of the PS/PMMA interface was found to be around 200 J/m^2 when measured using symmetric compact tension or double torsion experiments [92]. However, that value fell to around 3 J/m^2 when an asymmetric double cantilever beam (ADCB) sample is used [93]. The large value obtained for symmetric tests were due to the tendency of crazes to grow in the PS during crack propagation. The crazes dissipate much energy and cause a high measured toughness. The excess crazing can be avoided by using an asymmetric fracture test to drive the crack towards the PMMA. Since the PMMA requires a higher stress to craze than PS, the crack will be forced to remain at the interface. This same effect of sample asymmetry has been observed in several other glassy polymer pairs,

PMMA/polyphenylene oxide (PPO) [94], and PS/poly 2-vinyl pyridine (PVP) [95]. In each system, the lower crazing material is stiffened so that the craze can be deflected from that surface.

ADCB fracture toughness tests on immiscible polymer interfaces have been conducted for surfaces reinforced with diblock, random, and multiblock copolymers [96-98]. The studies were conducted to measure the strength of a compatibilized interface and combined with surface analysis techniques also understand the mechanisms involved in the failure of those interfaces. The purpose of this work is to investigate the fracture toughness of an immiscible polymer pair interface reinforced with diblock CNTs.

The experimental system is the immiscible pair of PS and PMMA homopolymers. Both polymers have approximatively the same glass transition temperature (~5°C difference), similar elastic moduli but different crazing stresses. “Bare” interfaces between these two polymers are very weak so improved mechanical strength can be correlated with the presence of diblock CNTs. Since the system has been extensively studied, the performance of the diblock CNTs can be evaluated against that of copolymers.

2.2 Experimental Methods

2.2.1 Materials

Homopolymers

PS (M_w = 192,000) in pellet form and PMMA (M_w=120,000) in granular form were purchased from Sigma Aldrich. The homopolymers were dried at 80°C under vacuum for at least 24 hours to remove any residual solvent or other impurities. These molecular weights are far above the entanglement molecular weights of both polymers.

Carbon nanotubes

The nanotubes used in this work were synthesized by Lawrence Barrett, PhD as part of his doctoral work. All chemicals used were purchased from Sigma Aldrich ACS regent grade > 98% or higher. Three types of CNTs were synthesized: unfunctionalized (pristine surface), PS-functionalized and a diblock functionalized (half pristine, half PS-functionalized) CNTs. Vermiculite was used as support for nanotube growth and different tube chemistries resulted from switching the gas during the polymerization from ethylene to acetonitrile; the latter gives a tube that has ~1 nitrogen atom for every 60 carbon atoms. These diblock nanotubes were between 1-10 μm long and the transition length between blocks was ~300 nm. To functionalize the CNTs, 1 gram of nanotubes suspended in 100 ml of benzene was reacted with 0.1 benzoyl peroxide for an hour to form radicals on the nanotube surface, then reacted with a 1:1.3 molar ratio of BPO in TEMPO for 1 hour, and finally was filtered and washed with benzene. Styrene was added to the suspended CNTs in benzene and polymerized at 80°C for 24 hours. Polymerized nanotubes were washed three times in benzene to remove unattached PS. Diblock tubes after polymerization were found to be 9.6 wt% polymer.

2.2.2 Fracture toughness tests

Tensile tests

The elastic moduli of the homopolymers are important in the calculation of the fracture toughness. Tensile tests were performed using a United STM-2K tensile tester. Samples were compression molded using a Carver Laboratory Press at 160°C for 10 minutes and were then cut using an ASTM D-1708 die from Dewes-Gumbs on a manual expulsion press. Cutting PS and PMMA samples at room temperature is impossible because they are both brittle and glassy. For cutting of the samples to be possible, the compression molded samples were reheated above the T_g of the polymers and immediately cut before they cooled down. The dog-bone shaped samples were then tested at room temperature.

Dispersion of nanotubes in solvent

The dispersion of nanotubes in solvent is an important step in getting well dispersed nanotubes at the interface. Two solvents were used: toluene and cyclohexane. Bath sonication was used to disperse the desired amount of nanotubes in the solvent.

Sample preparation

PS and PMMA sheets (5 cm x 6 cm) were compression molded at 160°C. The thickness of the sheets were 2.0 mm and 2.4 mm, respectively. The dispersed carbon nanotubes are deposited on the PMMA sheet. The solvent was evaporated under the hood overnight then in a vacuum at 60°C for 24 hours to completely remove the solvent. Dried PMMA and PS sheets were joined together in a compression molder at 160°C under slight pressure. The adhered sheets were then cut in strips 6-8 mm wide and 60 mm long. A schematic of a sample is represented in Figure 2.2.

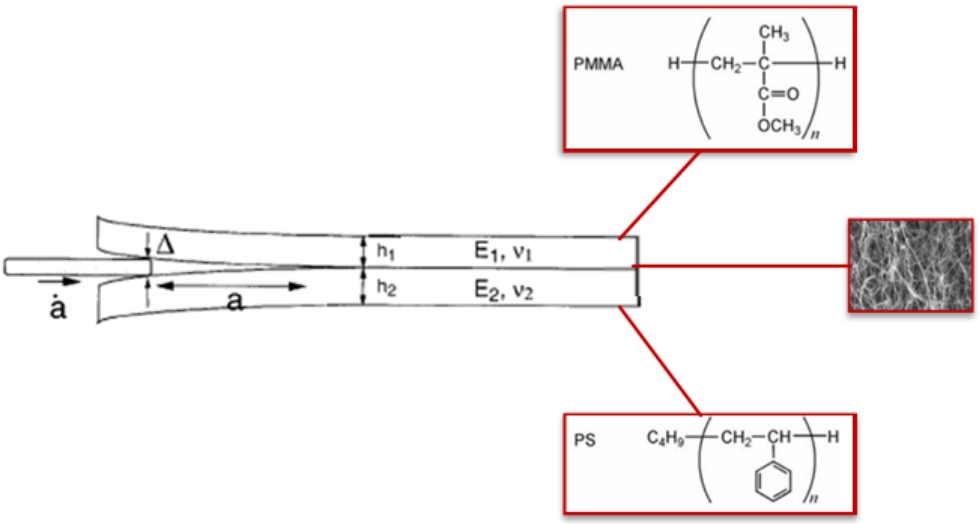

Figure 2.1 Schematic representation of an ADCB sample.

The thickness ratio of the two beams is very important to make sure that the G_c value measured reflects the toughness of the interface. Since PS/PMMA has been extensively studied, the optimum ratio for their ADCB samples has already been determined. Systematic studies by Sikka et al.[97] and Bernard et al.[93] have showed that the optimum ratio is between 1.1-1.2, with PS being the thicker beam. As can be seen in Figure 2.3, when the PS beam is too thin or too thick, crazes grow away from the interface increasing the value of the measured G_c. The optimum ratio of beam thicknesses is the one where the crack stays at the interface and gives a minimum value of G_c for a bare interface.

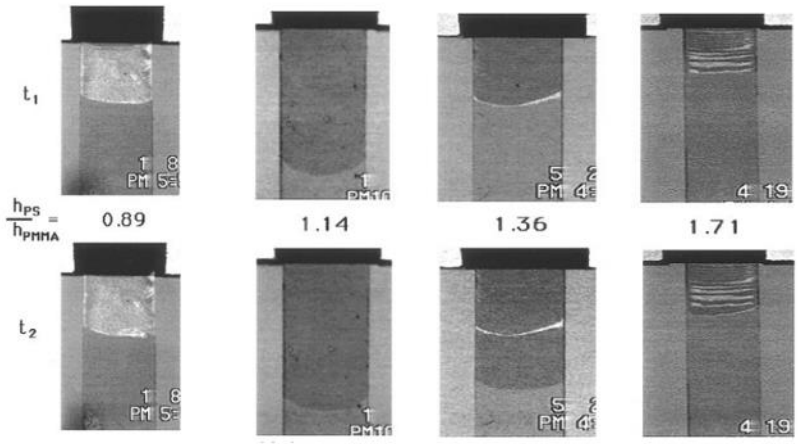

Figure 2.2 Video frames representative of the fracture experiments at indicated h_{PS}/h_{PMMA} values. Fracture specimens are ~8 mm wide. Taken from ref.[97]

Fracture toughness measurements

The ADCB experiments are not very common and no standard apparatus for the test exists. Based on the information in the literature, a testing apparatus was built using a servo motor, Figure 2.4.

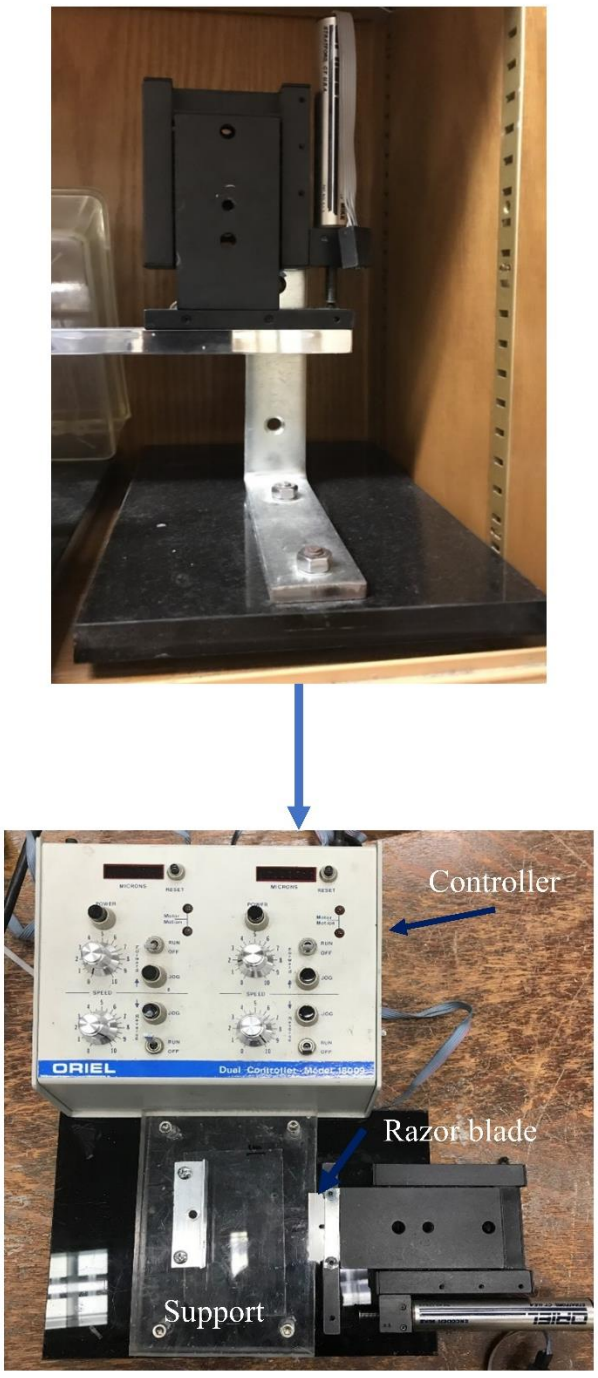

Figure 2.3 ADCB samples testing apparatus

To ensure the set up was appropriate, tests were conducted on bare PS/PMMA interfaces first to make sure the razor blade was introduced exactly at the interface because small deviations can initiate the crack in one of the polymers and cause errors in the measured toughness. In Figure 2.5,

SEM images of the surfaces of the polymers after testing can be seen. Some imperfections are present on the PMMA surface, but no crazes or plastic deformation were present after the test; confirming that the testing apparatus was adequate for the tests.

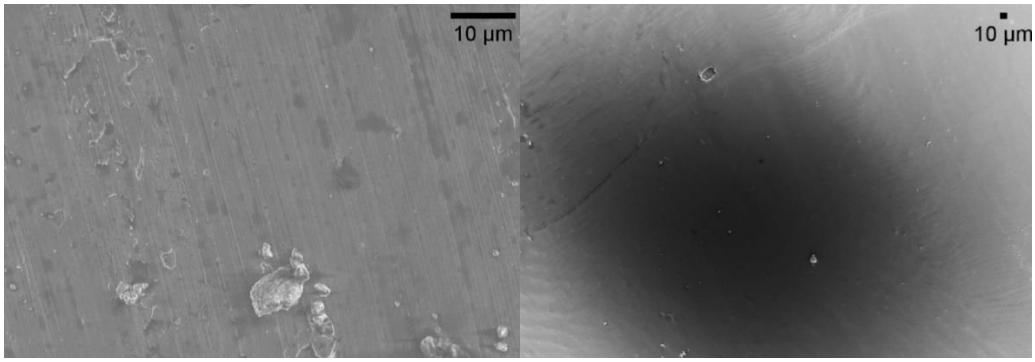

Figure 2.4 SEM micrographs of PMMA (left) and PS (right) surface after testing their bare interface fracture toughness.

Fracture tests were performed using the servo motor set up seen in Figure 2.4. A razor blade is introduced at the interface at a speed of 3 x 10^{-6} m/s using the servo motor. A video of the crack advance at the interface was captured and several frames were taken. The image analysis software ImageJ was used to measure the crack length a from the razor blade to the crack tip; Figure 2.6 shows examples of how a was measured. G_c of the interface was obtained using Equation 2.1, given by Creton et al. [99] and derived from a model of a cantilever beam on an elastic foundation proposed by Kannimen [100].

$$G_c = \frac{3\Delta^2 E_1 h_1^3 h_2^3}{8a^4}\left[\frac{(E_1 h_1^3 C_2^2 + E_2 h_2^3 C_1^2)}{\left(E_1 h_1^3 C_2^3 + E_2 h_2^3 C_1^3\right)^2}\right] \qquad (2.1)$$

With $C_1 = 1 + 0.64h_1/a$ and $C_2 = 1 + 0.64h_2/a$. E_1 and E_2 are the elastic moduli of polymers 1 and 2 respectively, measured here with a United STM-2K tensile tester; h_1, and h_2 are the thicknesses of the two beams, and Δ is the thickness of the razor blade.

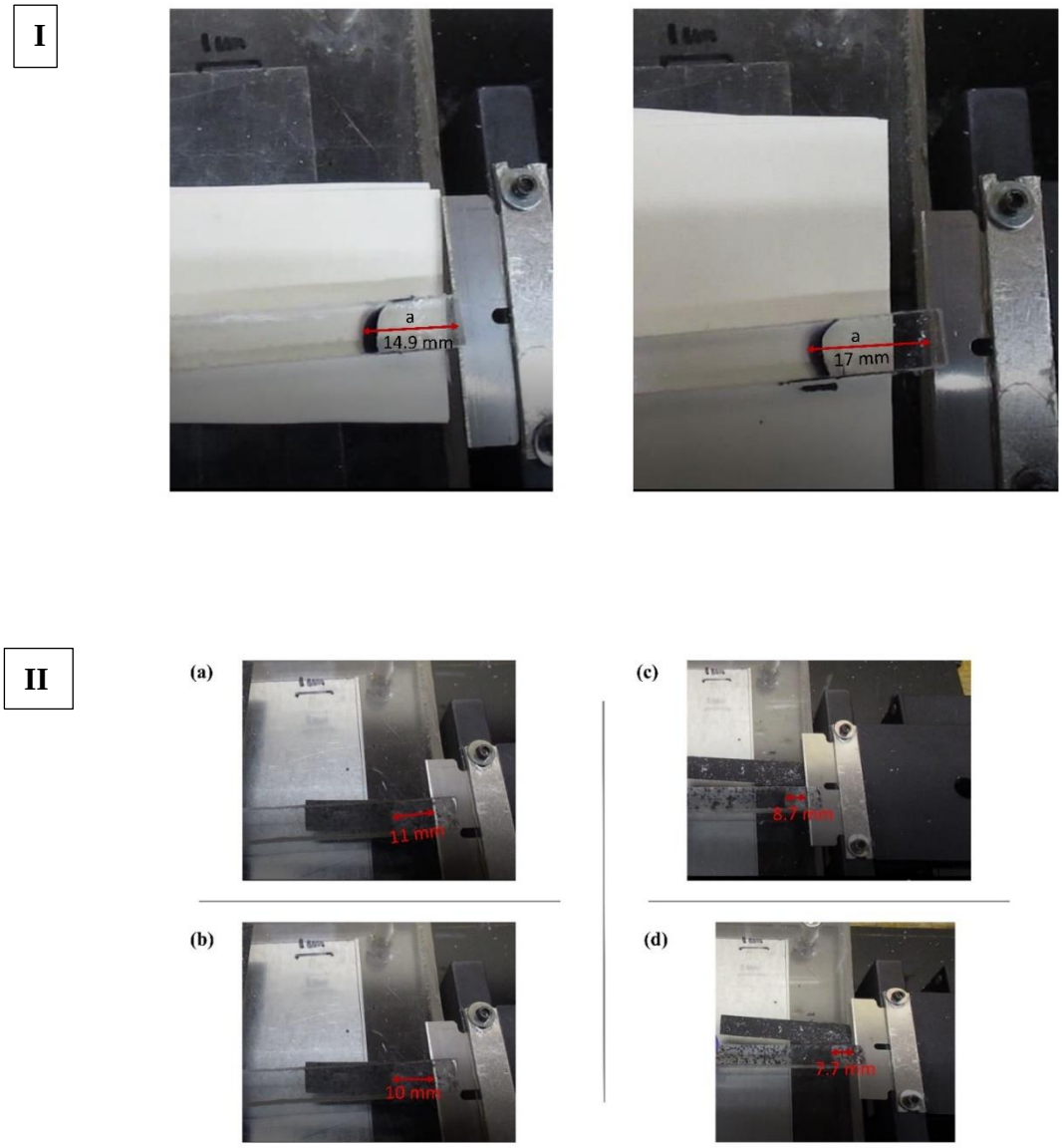

Figure 2.5 Examples of crack length measurements on (I) bare interfaces and (II) diblock CNT reinforced interfaces.

Transmission electron microscopy (TEM)

TEM was used to observe the location of the nanotubes at the interface of an ADCB sample. A table saw was used to cut a cross-section (~1mm wide) of an ADCB sample containing the

interface. The sample was then microtomed into 690 nm thin slices using a glass knife and imaged using JEOL 2010F field emission transmission electron microscope.

Scanning electron microscopy (SEM)

Plastic deformation on the surfaces of the polymers were examined using a scanning electron microscope (SEM). The two beams were split apart, after the test, and sputter coated with 5-6 nm of AuPd before imaging. Images of the PS and PMMA surfaces were captured to analyze the dispersion pattern of the nanotubes and the extent of plastic deformation on both surfaces.

A summary of the steps involved in ADCB fracture tests is provided in Figure 2.7.

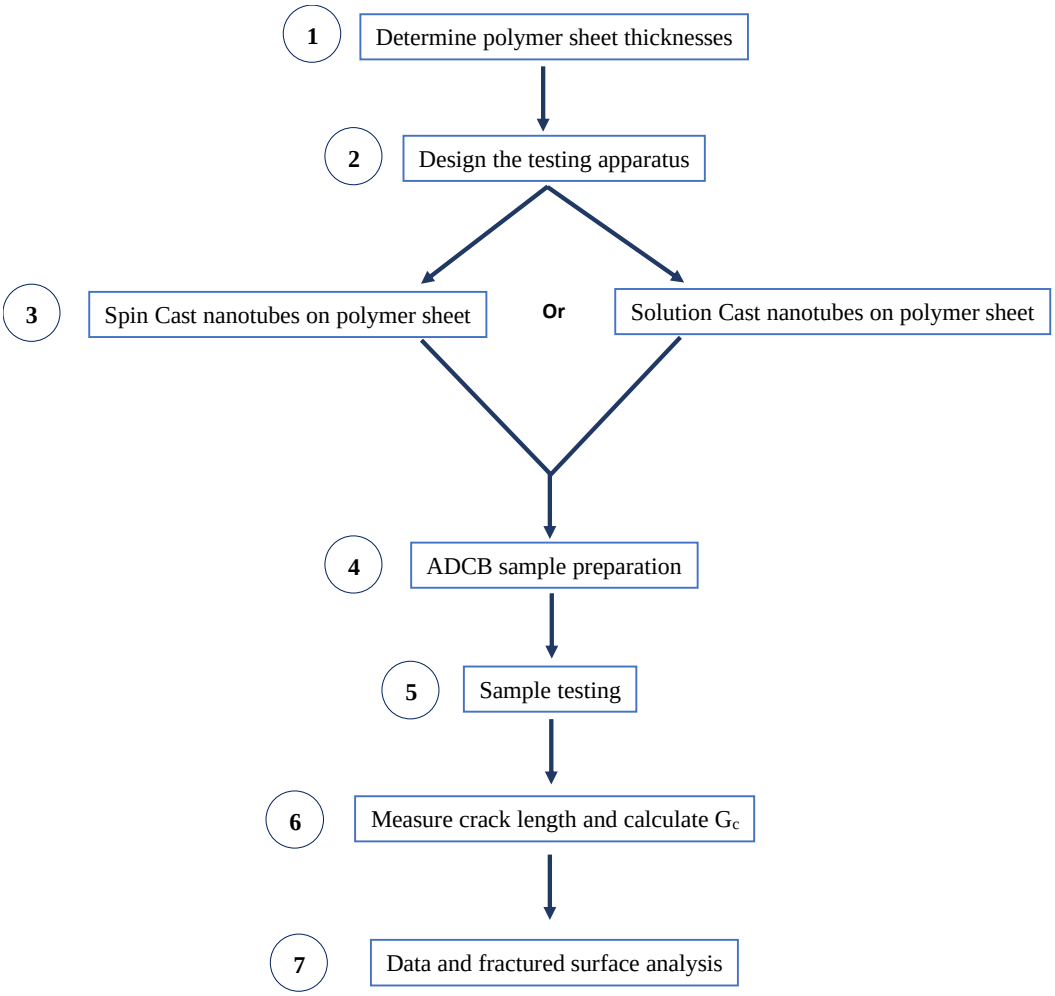

Figure 2.6 Details of steps involved in ADCB experiments

2.3 Results and Discussion

2.3.1 Dispersion of nanotubes

Dispersing nanotubes in solvent is an important step to full advantage of their mechanical properties. CNTs have great physical properties as individual tubes but their bundles are very weak and can serve as crack initiators in composites. Different strategies were tested to obtain the best possible dispersion. In all previous ADCB sample studies with PS/PMMA, toluene was used to dissolve the copolymers and spin coat them on PS. Toluene was the solvent selected here and bath sonication was used to disperse the nanotubes. The choice of bath over horn sonication is because the latter has been shown to break nanotubes to a greater extent. A "good" dispersion is one that has as few aggregates as possible while minimizing individual tube breakage. For diblock CNTs especially, minimizing breakage is important because the diblock structure must be preserved (if the nanotubes were to break in half for example, they won't be more efficient than mixing two different types of nanotubes).

Since the amount of diblock nanotubes available was limited, the dispersion time studies were conducted on single chemistry tubes. Figure 2.8 shows optical microscope images of nanotubes coated on a PS sheet after different dispersion times in toluene. The dispersion improves slightly after sonicating from 5 to 15 minutes but after 20 minutes much less aggregates were present. The dispersion time was limited to 20 minutes to ensure good dispersion.

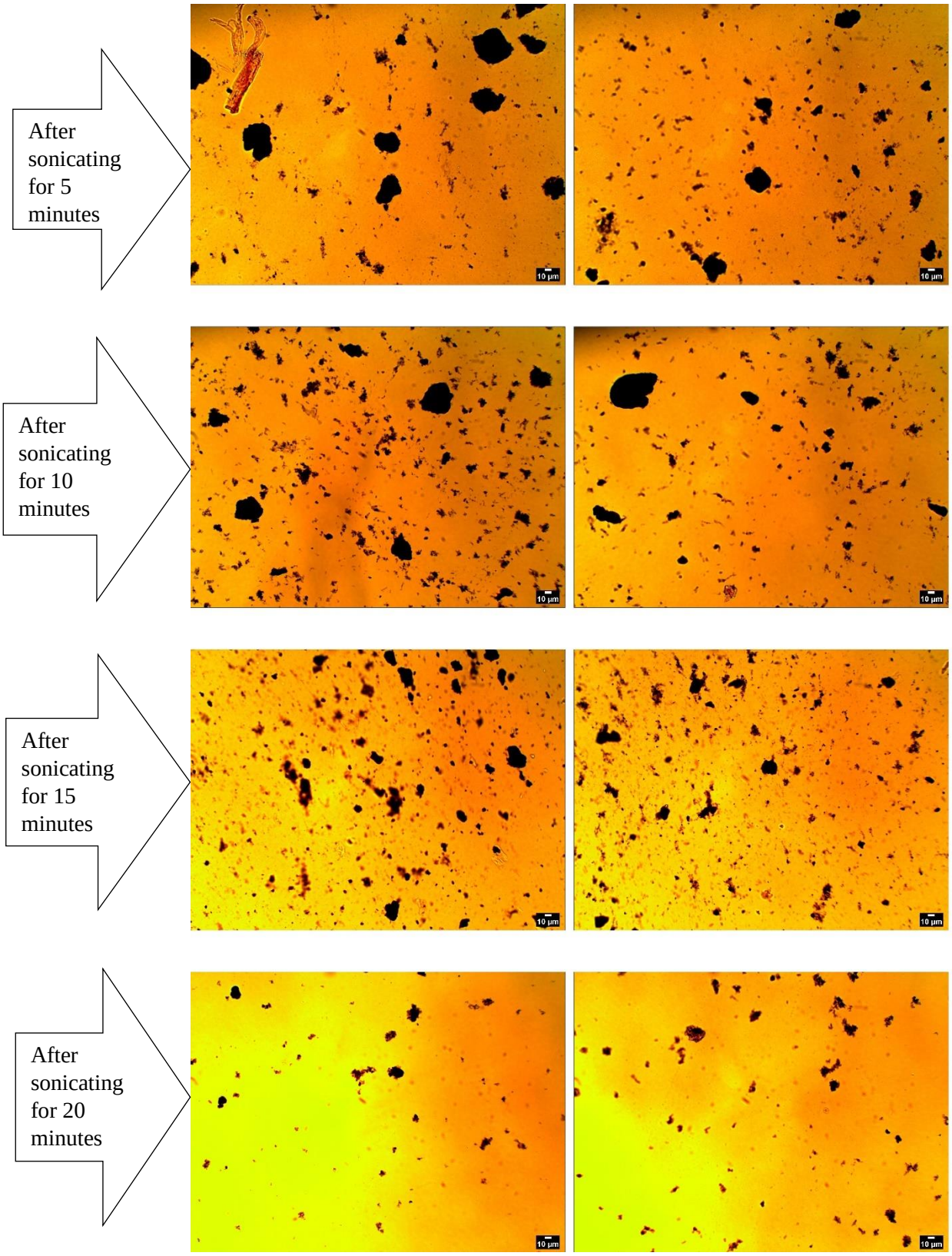

Figure 2.7 CNTs dispersed on PS after different sonication times in toluene

The main difference between copolymers and CNTs is that the former could be dissolved in toluene while the latter can only be dispersed. Hence, for copolymers, small quantities of solvent can be used and the polymer concentration is changed to obtain the desired copolymer thickness at the interface. For CNTs a significant amount of solvent is required for a good dispersion (i.e to disentangle tubes from aggregates). So, several consecutive spin coating steps had to be done to get all the nanotube sample at the interface. Figure 2.9 shows optical microscopy images of different diblock CNT samples dispersed on a PS wafer. A total of 2 ml of toluene was used to disperse the nanotubes. The higher the CNT content the bigger the aggregate sizes because the concentration of nanotubes increases with nanotube content which decreases the dispersion quality. Keeping a constant concentration would mean increasing the volume of solvent as the amount of nanotubes increased. Since toluene is a solvent for both polymers, having a high solvent volume is not desirable because the polymer would dissolve. significantly

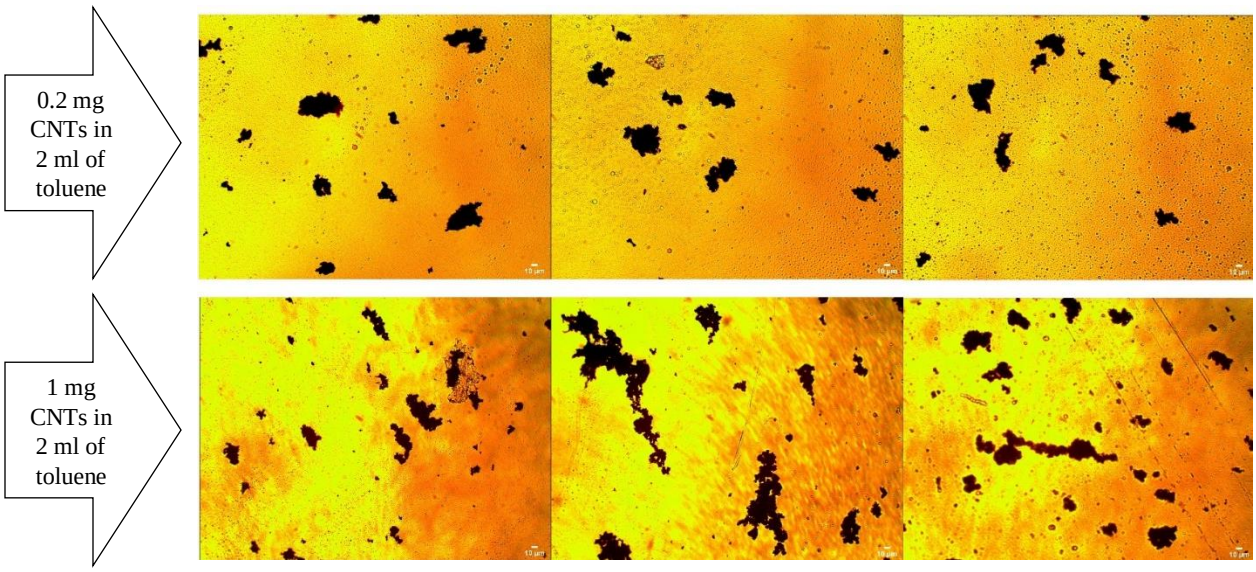

Figure 2.8 Diblock CNTs dispersed on PS

Other solvents to disperse the nanotubes were investigated. Solvents tested were tetrahydrofuran (THF), dimethylformamide (DMF), and chloroform. Out of the three, THF was the one that provided the best dispersion; the nanotubes stayed suspended the longest. THF couldn't be used because it is a much better solvent for both PS and PMMA. Attempts to spin coat nanotubes on either polymer with THF as a solvent resulted in significant polymer dissolution. So, dispersing the nanotubes in toluene for 20 minutes was the best option for the spin coated samples.

For reasons that will be explained in the next section, contrarily to copolymers, the spin coating method was not adequate for nanotubes. The alternative to spin coating was solution casting and for that a solvent that wouldn't dissolve at least one of the polymers had to be used. The only solvent that could be found was cyclohexane; it dissolves PS but not PMMA. For those samples, more solvent could be used since there was no risk of dissolving PMMA. The nanotubes were dispersed in 5 ml of cyclohexane and again several consecutive solution casting steps were used to put all the desired amount of nanotubes on the polymer sheet.

2.3.2 Spin Coated samples

For block copolymers, the value of G_c was shown to depend on the areal chain density, $\sum$, defined as the number of copolymer chains per nm^2. For nanotubes, no technique is available to measure the $\sum$ value so instead the mass of nanotubes used was changed. The values of G_c for the block nanotubes as a function of the amount of nanotubes dispersed in toluene are shown in Figure 2.10. An increase in G_c occurs up to a certain surface coverage then the values starts to decrease. For diblock copolymers, in certain cases, G_c was shown to increase with increasing $\sum$ up to a maximum value above which further addition of copolymer results in a decrease of G_c. This behavior was attributed to excess copolymers forming additional lamellar micelles close to the interface which results in subsidiary weak interfaces [101]. In this case, nanotubes cannot form micelles, but

aggregates can weaken the interface. A possible explanation here is that at the surface coverage where the decrease in G_c was observed too many nanotube bundles were present which weakened the interface.

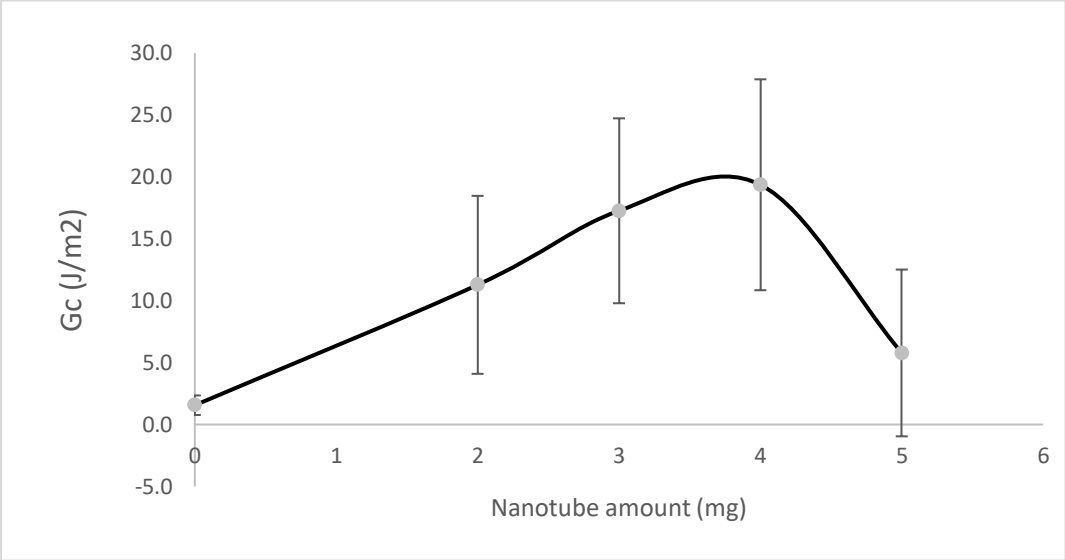

Figure 2.9 Interfacial fracture toughness as a function of diblock CNTs mass dispersed in toluene

When the maximum G_c values obtained are compared with different types of nanotubes, Figure 2.11, the diblock CNTs have the highest reinforcing effect as expected.

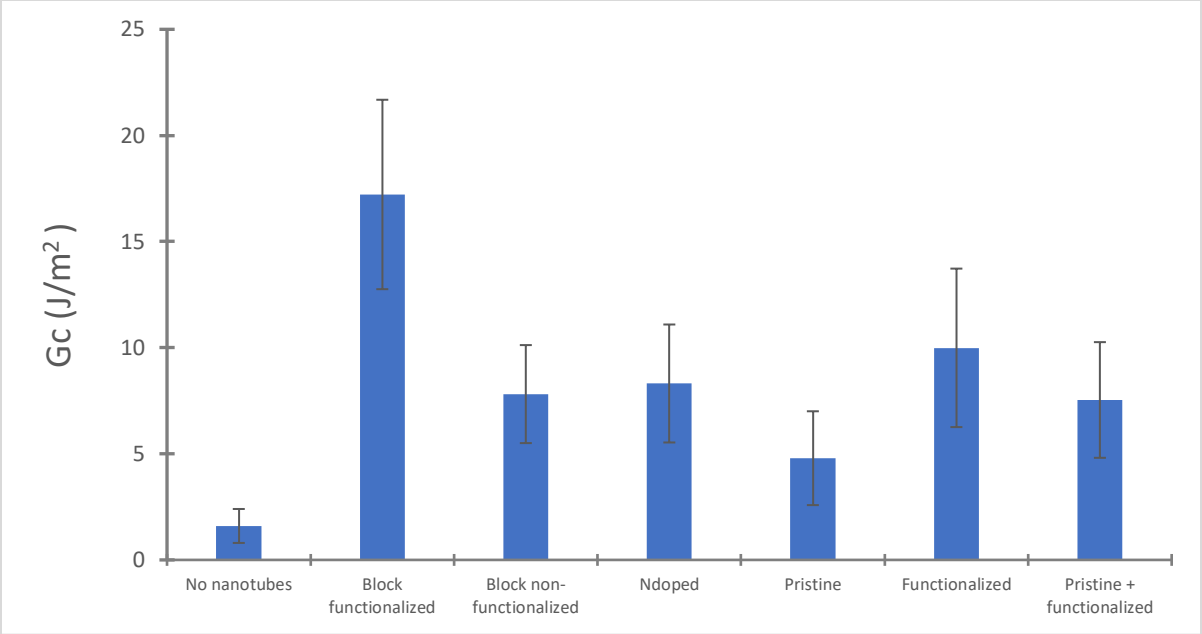

Figure 2.10 Maximum interfacial fracture toughness values for different types of nanotubes

There were two main limitations to this experimental procedure. First, the amount of nanotubes at the interface cannot be determined. For copolymers, ellipsometry experiments can be conducted to measure the thickness of the spun copolymer layer which is used to calculate $\sum$. Ellipsometry is an optical technique that measures the polarization upon reflection or transmission of light and compares it to a model thus it cannot be used for nanotubes (i.e they absorb light) and no other technique could be found to measure the amount of nanotubes at the surface. The second issue was that multiple spin coating steps had to be conducted in order to put all the nanotubes contained in toluene; because toluene is a solvent for PMMA, the polymer slightly melted changing the thickness of the polymer sheet. Since maintaining the thickness is paramount to the experiments, spin coating was deemed inadequate for nanotubes and a different procedure had to be developed.

2.3.3 Solution coated samples

Results from the ADCB tests are given as plots of fracture toughness, G_c, versus mass of carbon nanotubes and are displayed on Figure 2.12. G_c for the bare interface fracture toughness was

measured here to be 3.5 J/m^2. This value was obtained previously for PS/PMMA interfaces [93, 98] confirming that the crack remained at the interface. This value is over 100 times and 140 times less than the bulk fracture toughness of PS and PMMA. In immiscible polymer blends without compatibilizer, the adhesion at the interface is controlled by the thickness of the interface, a_I, and the entanglement density at the interface, Σ. For PS/PMMA interfaces, Fernandez et al. [102] used neutron reflection to measure a_I and found a value less than 20 Å which explains the weakness of the interface. When compatibilizers are added, the entanglement density at the interface increases increasing the thickness of the interface which results in enhanced G_c compared to the bare interface [89].

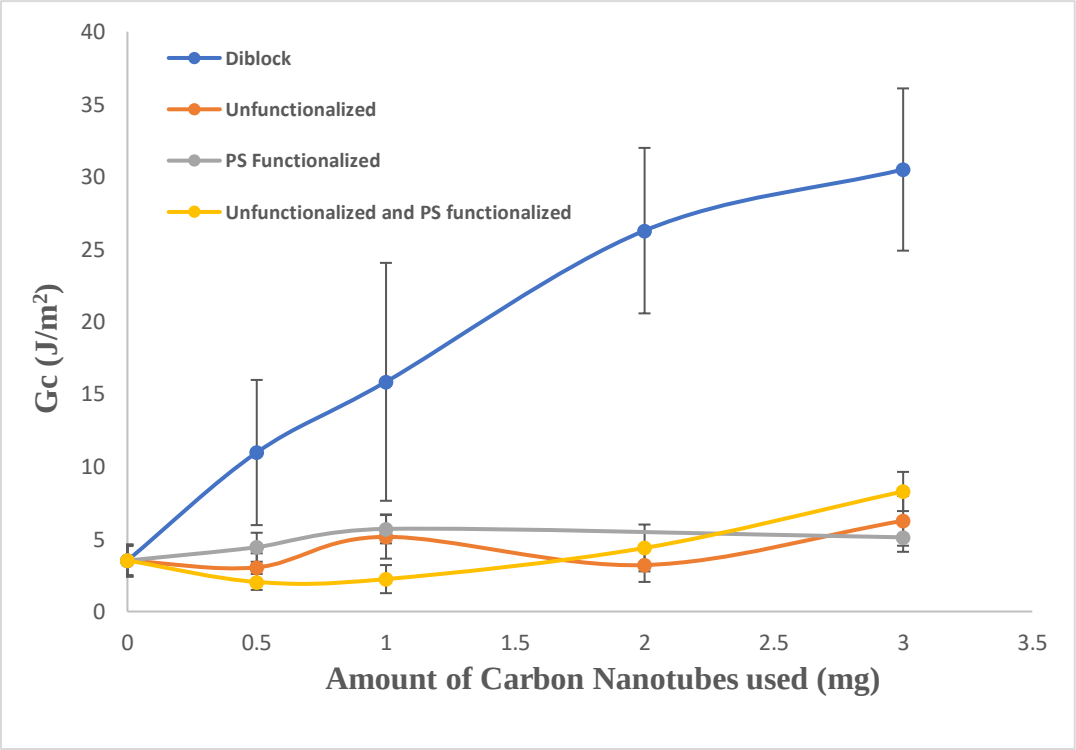

Figure 2.11 Interfacial fracture toughness, Gc, of PS/PMMA interfaces reinforced with diblock, unfunctionalized, PS-functionalized, and a mixture of pristine and functionalized CNTs plotted as a function of CNTs mass.

The results for single chemistry tubes shown in Figure 12 are in accordance with previous work that showed that single chemistry tubes always prefer to relocate in one phase in an immiscible polymer blend [74, 78] and thus have no reinforcing effect on an interface. For our system, unfunctionalized CNTs prefer the PMMA phase while PS-functionalized CNTs prefer the PS phase [103]. After welding, the CNTs relocate in their preferred phase. In a blend, single chemistry tubes can toughen the overall blend by forming percolated networks in one of the phases but they do so without changing the properties of the interface between the two phases. For the diblock functionalized CNTs, however, an almost 10 times increase in G_c was obtained with CNTs addition. The results demonstrate that these block nanotubes are improving adhesion between PS and PMMA.

Further analysis of the sandwiched PS/CNTs/PMMA samples were attempted. A TEM micrograph of the diblock CNTs at the interface between PS and PMMA is shown in Figure 2.13. This sample was obtained by cutting a small area of a sample that contained the interface, microtoming a slice of that interface using a glass knife, and imaging with a TEM. Attempts at repeating the same procedure for bare interfaces and interfaces reinforced with unfunctionalized, PS-functionalized, and a physical mixture of the previous two CNTs were unsuccessful. For the bare interfaces, the force applied when slicing with the glass knife was enough to split the two polymer beams apart. The samples with the nanotubes (except diblock CNTs), all either teared apart after being sliced or had holes that made the samples impossible to image. Qualitatively, these results confirm that adhesion was indeed obtained with the diblock CNTs but not for the single chemistry nanotubes. Their presence barely improved the toughness of the interface, as shown in Figure 2.12, which made them impossible to microtome and observe under electron microscopy.

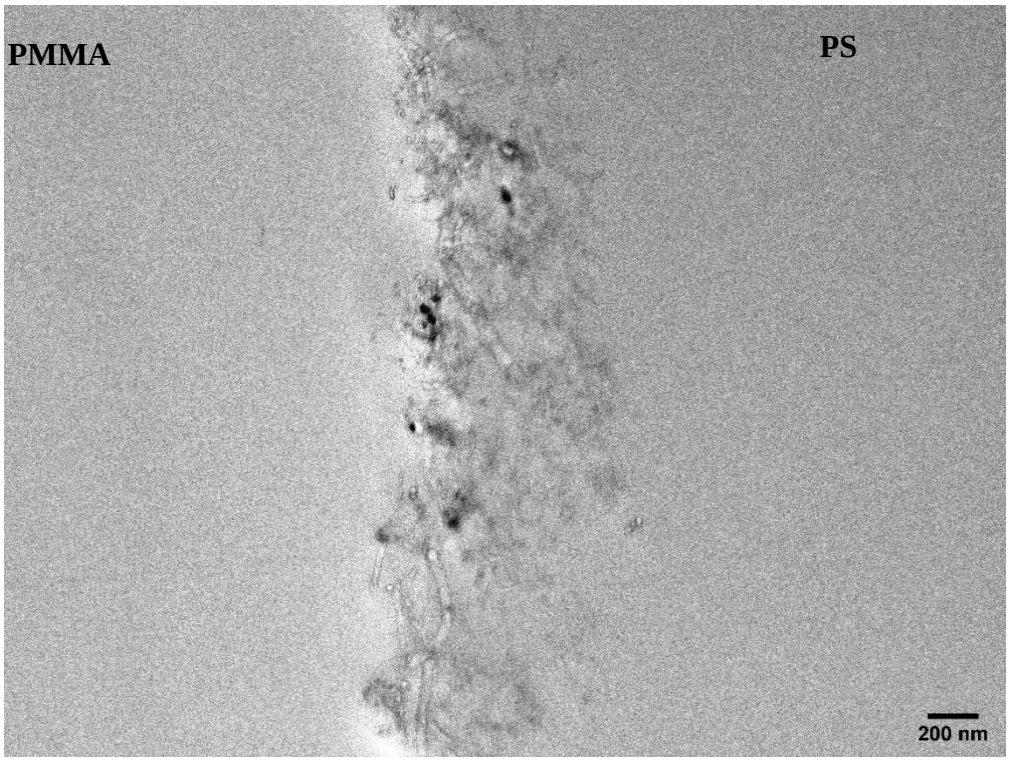

Figure 2.12 TEM image of a cross-section of an ADCB specimen with block CNTs at the interface between PS and PMMA.

The data showed some differences and discrepancies with the results obtained for the spin coated samples. Fracture toughnesses for the diblock CNTs are much higher with solution casting and a drop at the highest surface coverage tested was not observed. Also, for the single chemistry tubes no reinforcement is seen whereas slight improvements in $G_c$were obtained with spin coating. During spin coating, 95% - 98% of the material can be flung off leaving only 2% - 5% of the on the substrate [104]. So, the solution cast samples had a much higher CNTs surface coverage than the spin coated ones. What these results suggest is that significant human errors were introduced during the initial experiments. The testing apparatus was not optimized at the time. The remaining CNTs on the PS substrate after spin coating were so low (i.e < 0.25 mg) that the apparent improvements in fracture toughness obtained were most likely due to cracks deviating in one or both of the polymer surfaces. These results show that using the right asymmetry for the samples

was not enough, inappropriate testing conditions could still cause the crack to deflect from the interface and introduce errors. So, having the right testing apparatus was also essential to conducting the tests.

Table 2.1 shows a comparison between the maximum values of G_c obtained for diblock CNTs from solution casting and those obtained with copolymers in previous experiments. The maximum G_c of 30 J/m^2 obtained for diblock CNTs is the same as what was reported by Bernard et al.[93] but slightly lower than what was obtained by Eastwood et al.[98]. However, this value might not be the highest possible because the quantity of nanotubes available was limited a wider range of surface coverages couldn't be tested. But these results show that at the least diblock CNTs can be as effective as copolymers at providing adhesion between immiscible blends.

Table 2.1 Comparison of fracture toughness between diblock CNTs and diblock copolymers

Reference	Compatibilizer	Gc, max J/m^2
This work	Diblock CNTs	~30
Bernard et al. [93]	Diblock copolymer	~30
Eastwood et al. [98]	Diblock copolymer	~40
Bernard et al. [93]	Random copolymer	~20

To better contrast these results, it is important to consider the different limitations that exist for copolymers and CNTs. In copolymer compatibilized blends, the main limitations are the molecular weight of the blocks and the micellization that happens at high concentrations. ADCB experiments conducted with copolymers have shown that for a given copolymer (diblock, random…), as long as the MW for each block was above the entanglement MW, the maximum fracture toughness remained the same; only the surface coverage at which that maximum occurs depends on the MW

[93, 97, 98]. That's because polymer chains fail either by chain pullout (lower energy needed) or chain scission (requires more energy); as long as copolymer blocks are long enough to entangle with both homopolymers, the energy require for chain scission does not change with increasing copolymer molecular weight. For CNTs, the limitations are nanotube breakage and aggregates. The ability of nanotubes to absorb energy depends on their lengh; the longer the tube the more energy can be dissipated. Unfortunately, there is no dispersion technique that currently exists which prevents either from happening. Even though good adhesion is attained for the diblock CNTs; the value is still much lower than possible for CNT reinforced interfaces. Tube breakage during bath sonication and the presence of large aggregates are limiting the performance of CNTs. Individually dispersed, nanotubes are 30-100 times stronger than steel [61]. Near perfect adhesion can be obtained for perfectly dispersed and adhered nanotubes at the interface because the energy it would take to break them exceeds that of breaking either one of the polymers.

According to Brown [91], 2 hours of welding may not be enough to reach thermodynamic equilibrium at the interface. We wanted to investigate whether longer welding times would increase the interfacial fracture toughness. Test for interfaces reinforced with 2 mg diblock CNTs were conducted for times as long as 24 hours. Increasing the welding time up to 12 hours increased G_c but the value decreased for longer times, as can be seen in Figure 2.13. The same experiment was conducted for bare interfaces and the PS and PMMA were not adhered for welding times greater than 2 hours because the polymers were degrading. So, adhesion was improving with the diblock CNTs even though the polymers started degrading. Pristine MWNTs have been shown to increase the degradation temperature in PMMA [105] as well as in PS [106] in thermogravimetric analysis experiments. Thermo-oxidative degradation of polymers can occur either because polymers are processed above their degradation temperature or exposed to high temperatures for

long periods of times. These results suggest that CNTs can not only decrease the degradation temperature but also decrease the rate of degradation at a given temperature. These results may also explain why ADCB samples have been prepared by welding for just 2 hours.

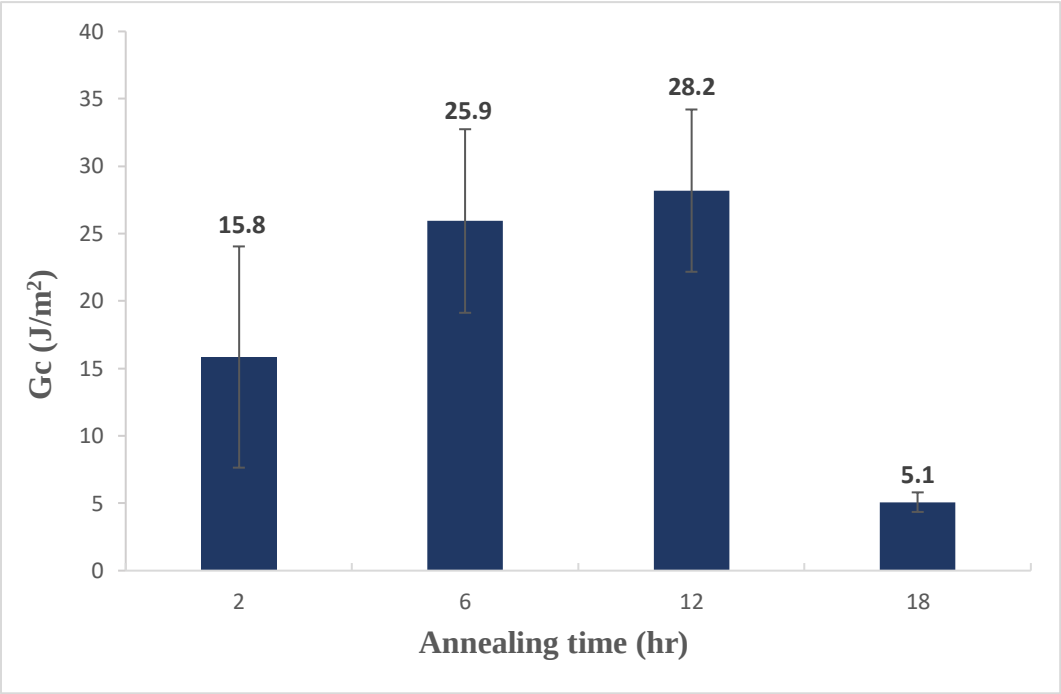

Figure 2.13 Fracture toughness of interfaces reinforced with 2 mg diblock CNTs annealed for different lengths of time.

Fracture tests are also conducted to better understand how interfaces between immiscible polymers fail. Fracture regime mechanisms for immiscible polymer interfaces have been developed based on work done with block copolymers. Previous studies have identified three different fracture regimes correlated to the lengths of the blocks and the number of chains of copolymer at the interface [96, 99, 107, 108]. Regime I correspond to copolymers with blocks longer than the critical molecular weight for entanglement, M_e. Failure at low interfacial coverage for these types of copolymers has been shown to occur by chain scission [99]; copolymers are present on both polymer surfaces after the fracture tests. As Σ increases, the maximum stress that can be sustained at the interface starts to increase and eventually exceeds the plastic deformation, crazing, stress of

the weaker polymer. Crazing is characterized by an abrupt increase of the fracture toughness because of the amount of polymer chains that undergo plastic deformation in the craze. Final failure occurs via copolymer chains disentangling and then pulling out or breaking. Regime II occurs for intermediate length copolymer chains, just at or slightly above the entanglement molecular weight [107, 108]. For these copolymers, failure initially occurs by chain pullout at low surface coverage. Similar to the previous regime, there is a critical surface coverage at which the stress required to pullout a chain will exceed that necessary to plastically deform one of the polymers and the failure mechanism transitions from copolymer chain pullout to plastic deformation of one of the homopolymers followed by copolymer chains disentangling/pulling out or breaking. The third regime corresponds to copolymer chains that are below the entanglement molecular weight [99]. For these copolymers, the stress required to pullout the chains will never exceed the plastic deformation stress and chain pullout remains the only fracture mechanism throughout the whole regime. No significant improvement is obtained for this regime, no more than 5 – 10 J/m^2 [99]. For Regime I and II, surface analysis shows that all the copolymer used for the fracture tests is present on the opposite side of where pullout occurred.

Understanding the mechanism of failure for the diblock CNTs can help synthesize more effective nanotubes. The fractured surfaces were analyzed using SEM. SEM micrographs in Figure 3.3a show that CNTs are present mostly on the PMMA side of the interface after fracture when 0.5 mg of diblock functionalized nanotubes are used which would suggest that pullout from the PS occurred. As the amount of CNTs is increased, plastic deformation on the PS surface can be observed which means that G_c increases as the amount of nanotubes increase. Nanotube-reinforced interfaces fail either by delamination of the tubes from the polymers, crack deflection into one or both polymer surfaces, or by nanotube breakage. CNTs ability to absorb energy depends on their

length. Short nanotubes will mostly fail by delamination. Long nanotubes on the other hand, will fail by a combination of delamination and crack deflection into one or both polymer surfaces. For these long tubes, depending on their adhesion with the polymers, can also break. Micrographs 3.3b-d do not show clearly that nanotubes are only on the PMMA side of the interface, but visually the presence of nanotubes could be seen on both polymers after the test. For nanotubes, their presence on both surfaces after fracture tests does not necessarily mean that the tubes are breaking; it might just mean that nanotube bundles are coming apart during the test since they are easier to break than individual nanotubes or that the nanotubes are short enough to delaminate from both surfaces. CNTs are not ideal for understanding fracture mechanisms of immiscible polymer blends. Because aggregates are present, nanotubes may be observed on either polymer surface after fracture tests even if individual tubes are pulling out of one of interfaces. CNTs lengths are also usually normally distributed, so of all three failure modes can occur simultaneously. Because of the difficulty in dispersing nanotubes and the distribution of lengths, systematic failure mechanisms like the ones provided for copolymers are difficult to develop with CNT reinforced interfaces.

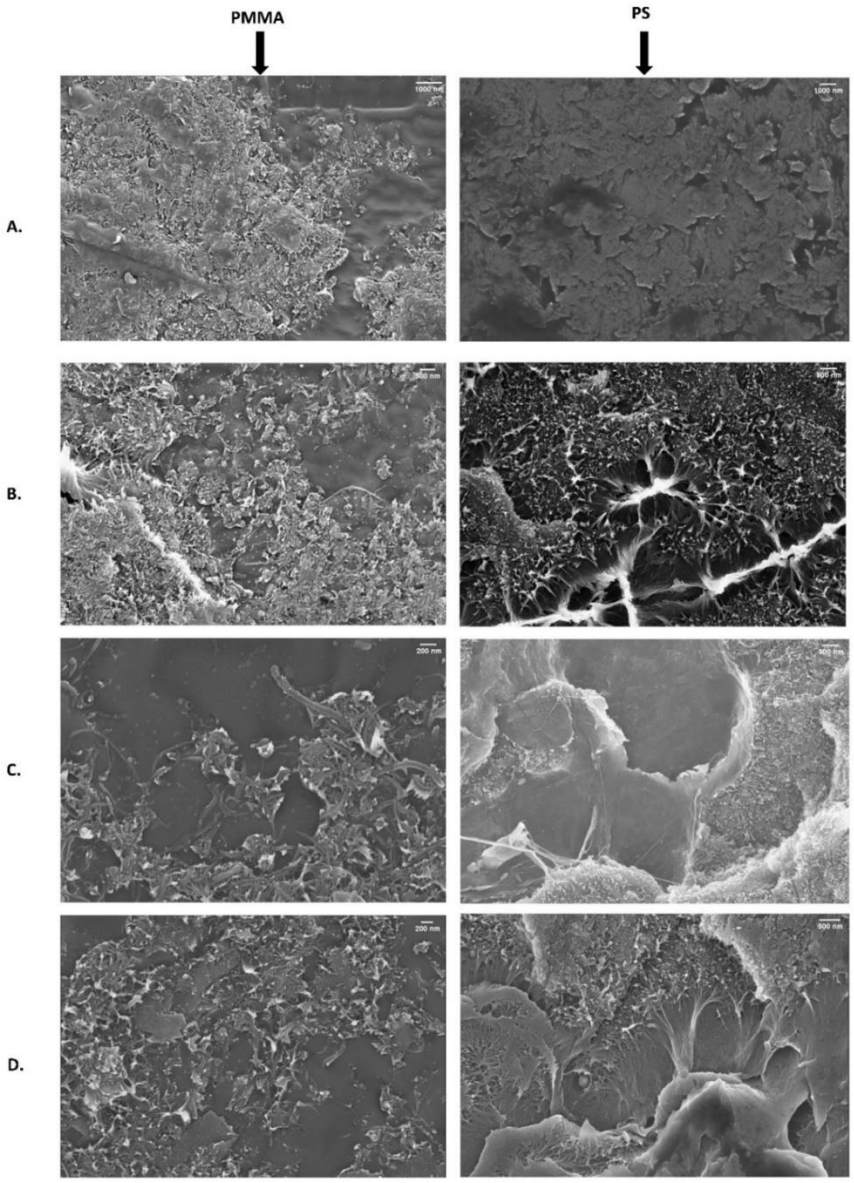

Figure 2.14 SEM micrographs of PS and PMMA surfaces after ADCB tests for interfaces reinforced with (A) 0.5 mg diblock CNTs, (B) 1 mg diblock CNTs, (C) 2 mg diblock CNTS, (D) 3 mg diblock CNTs.

Analyzing the polymer surfaces after fracture tests can still provide insight on the adhesion of nanotubes with either polymer. Since plastic deformation is occurring on the PS side of the interface, the adhesion between the PS-functionalized nanotubes and PS is weaker than between PMMA and unfunctionalized nanotubes. To increase the interfacial adhesion on the PS side of the

interface, the grafting density of PS could be increased, although increasing the number of N defects may also negatively influence the mechanical strength of the nanotubes. If PS grafted to CNTs are too short to entangle with the PS homopolymer then increasing the molecular weight of the grafted polymer would also be appropriate. The entanglement molecular weight for PS is ~13,000 – 18,000 g/mol; the molecular weight of the PS grafted on the nanotubes should be in at the entanglement molecular weight or higher to provide good adhesion. Also, improving the dispersion of the nanotubes at the interface can also improve G_c.

2.3.4 Conclusions and Recommendations

We have shown that diblock CNTs synthesized to be compatible with two different polymers can improve the adhesion of an immiscible PS/PMMA blend. A testing procedure was developed, and a testing apparatus was designed to quantitatively measure the interfacial adhesion provided by the diblock CNTs. The fracture toughness of the interface increased from 3 J/m^2 to 30 J/m^2 when diblock CNTs were added. The maximum fracture toughness of 30 J/m^2 obtained in this work is comparable to maximum values obtained for diblock copolymers under similar testing conditions. Nanotubes have so far been shown to preferentially locate in one phase of an immiscible blend; however, the results demonstrate that CNTs with carefully designed chemistries can also improve the strength of immiscible interfaces.

Further experimentation on bulk mechanical (i.e tensile tests) and electrical properties of diblock CNTs/immiscible polymer blends should be conducted to compliment the results of the fracture tests. For single chemistry tubes, even though they do not enhance interfacial adhesion, they have been shown to toughen immiscible blends through the formation of a percolated network. So, additional experiments with diblock CNTs can give more insight on the factors that govern toughness of immiscible polymer blends; for instance, how much of a difference does improving

the interfacial adhesion (on top of CNT network formation) make on the mechanical properties of the composites. Researchers have also speculated that having carbon fillers that both compatibilize a blend and form a percolated network in the blends will results in a so-called triple percolation which will further decrease the percolation threshold. Electrical conductivity experiments will give insight on whether that hypothesis is true for diblock CNTs. Increasing welding time for ADCB samples showed that diblock CNTs could slow the rate of degradation of the polymers. Thermogravimetric analysis (TGA) on polymer/CNTs has also shown that nanotubes can increase the degradation temperature [103]. Similar TGA studies should be conducted with diblock CNTs to examine the thermal stability of diblock CNTs/homopolymer and diblock CNTs/blend composites.

JPs of different size and shapes have been shown to improve the mechanical properties of immiscible polymer blends. Fracture tests on interfaces reinforced with different types of JPs will provide an understand of how the shapes, sizes, and structure of nano and micro-size particles affect the adhesion of immiscible polymer blends. For example, spherical JPs disperse better than nanotubes so they may provide better adhesion even though nanotubes have better mechanical properties. Comprehensive tests will also provide a deeper analysis of the fundamental differences between nanoparticle and copolymer reinforced interfaces.

Finally, experiments conducted on PS/PMMA interfaces reinforced with pentablock and triblock copolymers have shown that their optimum G_c was almost twice that of diblock copolymers because they can cross the interface multiple times [98]. So, synthesizing and testing multiblock CNTs can further improve the interfacial adhesion. Those experiments also showed the importance of the molecular weight (M_w) of the copolymer blocks; molecular weight above the M_e are more effective. We were not able to determine the M_w of the PS on the diblock CNTs; short lengths may

have limited the adhesion on the PS side of the interface. It is important to develop techniques to quantitatively measure the M_w of the grafted polymer to ensure it is above M_e.

In these experiments, we have showed that diblock CNTs meet at least two of the criteria of compatibilization; they locate at the interface in a blend and provide adhesion in the solid state. The last criterion, coalescence suppression and morphology stabilization, can be verified by conducting rheology experiments. The details of which are explained in the first appendix.

References

[1] H. Richie, "Plastic Pollution," ed, 2018.

[2] R. Geyer, J. R. Jambeck, and K. L. Law, "Production, use, and fate of all plastics ever made," *Science advances,* vol. 3, no. 7, p. e1700782, 2017.

[3] C. J. Rhodes, "Plastic pollution and potential solutions," *Science progress,* vol. 101, no. 3, pp. 207-260, 2018.

[4] C. M. Rochman, M. A. Browne, A. J. Underwood, J. A. Van Franeker, R. C. Thompson, and L. A. Amaral-Zettler, "The ecological impacts of marine debris: unraveling the demonstrated evidence from what is perceived," *Ecology,* vol. 97, no. 2, pp. 302-312, 2016.

[5] M. Revel, A. Châtel, and C. Mouneyrac, "Micro (nano) plastics: A threat to human health?," *Current Opinion in Environmental Science & Health,* vol. 1, pp. 17-23, 2018.

[6] M. E. Iñiguez, J. A. Conesa, and A. Fullana, "Microplastics in Spanish table salt," *Scientific reports,* vol. 7, no. 1, pp. 1-7, 2017.

[7] W. R. Lea, "Plastic incineration versus recycling: a comparison of energy and landfill cost savings," *Journal of Hazardous Materials,* vol. 47, no. 1-3, pp. 295-302, 1996.

[8] J. M. Garcia and M. L. Robertson, "The future of plastics recycling," *Science,* vol. 358, no. 6365, pp. 870-872, 2017.

[9] E. Recycling, "Recycling Plastic: Complications & Limitations," ed, 2009.

[10] L. Utracki, "Introduction to polymer blends," in *Polymer blends handbook*: Springer, Dordrecht, 2003, pp. 1-122.

[11] J. Araujo, M. Vallim, M. Spinacé, and M. A. De Paoli, "Use of postconsumer polyethylene in blends with polyamide 6: effects of the extrusion method and the compatibilizer," *Journal of applied polymer science,* vol. 110, no. 3, pp. 1310-1317, 2008.

[12] L. A. Utracki and C. A. Wilkie, *Polymer blends handbook*. Springer, 2002.

[13] H. K. Jeon, J. Zhang, and C. W. Macosko, "Premade vs. reactively formed compatibilizers for PMMA/PS melt blends," *Polymer,* vol. 46, no. 26, pp. 12422-12429, 2005.

[14] M. Xanthos and S. Dagli, "Compatibilization of polymer blends by reactive processing," *Polymer Engineering & Science,* vol. 31, no. 13, pp. 929-935, 1991.

[15] C. Macosko, P. Guegan, A. K. Khandpur, A. Nakayama, P. Marechal, and T. Inoue, "Compatibilizers for melt blending: Premade block copolymers," *Macromolecules,* vol. 29, no. 17, pp. 5590-5598, 1996.

[16] J. A. Galloway, H. K. Jeon, J. R. Bell, and C. W. Macosko, "Block copolymer compatibilization of cocontinuous polymer blends," *Polymer,* vol. 46, no. 1, pp. 183-191, 2005.

[17] Y. Ding *et al.*, "Compatibilization of immiscible PLA-based biodegradable polymer blends using amphiphilic di-block copolymers," *European Polymer Journal,* vol. 118, pp. 45-52, 2019.

[18] I. Fortelný and J. Jůza, "Analysis of the effect of block copolymers on interfacial tension in immiscible polymer blends," *Polymer,* vol. 150, pp. 380-390, 2018.

[19] M. Lee, T. Lodge, and C. Macosko, "Can random copolymers serve as effective polymeric compatibilizers?," *Journal of Polymer Science Part B: Polymer Physics,* vol. 35, no. 17, pp. 2835-2842, 1997.

[20] J. Benkoski, G. Fredrickson, and E. Kramer, "Effects of composition drift on the effectiveness of random copolymer reinforcement at polymer–polymer interfaces," *Journal of Polymer Science Part B: Polymer Physics,* vol. 39, no. 20, pp. 2363-2377, 2001.

[21] T. Tamiya, X. Cui, Y.-I. Hsu, T. Kanno, T.-A. Asoh, and H. Uyama, "Enhancement of interfacial adhesion in immiscible polymer blend by using a graft copolymer synthesized from propargyl-terminated poly (3-hydroxybutyrate-co-3-hydroxyhexanoate)," *European Polymer Journal,* p. 109662, 2020.

[22] C.-L. Zhang, L.-F. Feng, X.-P. Gu, S. Hoppe, and G.-H. Hu, "Efficiency of graft copolymers as compatibilizers for immiscible polymer blends," *Polymer,* vol. 48, no. 20, pp. 5940-5949, 2007.

[23] M. Arlen and M. Dadmun, "The reinforcement of polystyrene and poly (methyl methacrylate) interfaces using alternating copolymers," *Polymer,* vol. 44, no. 22, pp. 6883-6889, 2003.

[24] M. Lazzari and M. Torneiro, "A Global View on Block Copolymers," *Polymers,* vol. 12, no. 4, p. 869, 2020.

[25] P. Agrawal, A. W. Rodrigues, E. M. Araújo, and T. J. Mélo, "Influence of reactive compatibilizers on the rheometrical and mechanical properties of PA6/LDPE and PA6/HDPE blends," *Journal of materials science*, vol. 45, no. 2, pp. 496-502, 2010.

[26] D. Chen, H. Wang, and Y. Li, "Reactive compatibilization: formation of double-grafted copolymers by in situ binary grafting and their compatibilization effect," *ACS applied materials & interfaces,* vol. 9, no. 38, pp. 33091-33099, 2017.

[27] M. A. Mansilla, A. J. Marzocca, C. Macchi, and A. Somoza, "Natural rubber/styrene-butadiene rubber blends prepared by solution mixing: Influence of vulcanization temperature using a Semi-EV sulfur curing system on the microstructural properties," *Polymer Testing,* vol. 63, pp. 150-157, 2017.

[28] G. Sui, D. Liu, Y. Liu, W. Ji, Q. Zhang, and Q. Fu, "The dispersion of CNT in TPU matrix with different preparation methods: solution mixing vs melt mixing," *Polymer,* vol. 182, p. 121838, 2019.

[29] Y. Liu, V. Abetz, and A. H. Müller, "Janus cylinders," *Macromolecules,* vol. 36, no. 21, pp. 7894-7898, 2003.

[30] A. Walther, X. André, M. Drechsler, V. Abetz, and A. H. Müller, "Janus discs," *Journal of the American Chemical Society,* vol. 129, no. 19, pp. 6187-6198, 2007.

[31] A. Walther and A. H. Muller, "Janus particles: synthesis, self-assembly, physical properties, and applications," *Chemical reviews,* vol. 113, no. 7, pp. 5194-5261, 2013.

[32] Q. Yang and K. Loos, "Janus nanoparticles inside polymeric materials: interfacial arrangement toward functional hybrid materials," *Polymer Chemistry,* vol. 8, no. 4, pp. 641-654, 2017.

[33] E. Poggi and J.-F. Gohy, "Janus particles: from synthesis to application," *Colloid and Polymer Science,* vol. 295, no. 11, pp. 2083-2108, 2017.

[34] F. Liang, B. Liu, Z. Cao, and Z. Yang, "Janus colloids toward interfacial engineering," *Langmuir,* vol. 34, no. 14, pp. 4123-4131, 2017.

[35] H. Su, C.-A. H. Price, L. Jing, Q. Tian, J. Liu, and K. Qian, "Janus particles: Design, Preparation, and Biomedical Applications," *Materials Today Bio,* p. 100033, 2019.

[36] H. Yabu, "Fabrication of Nanostructured Composite Microspheres Based on the Self-Assembly of Polymers and Functional Nanomaterials," *Particle & Particle Systems Characterization,* vol. 36, no. 9, p. 1900178, 2019.

[37] A. Kirillova, C. Marschelke, and A. Synytska, "Hybrid Janus particles: challenges and opportunities for the design of active functional interfaces and surfaces," *ACS applied materials & interfaces,* vol. 11, no. 10, pp. 9643-9671, 2019.

[38] N. Safaie and R. C. Ferrier Jr, "Janus nanoparticle synthesis: Overview, recent developments, and applications," *Journal of Applied Physics,* vol. 127, no. 17, p. 170902, 2020.

[39] H. Nie, X. Liang, and A. He, "Enthalpy-enhanced Janus nanosheets for trapping nonequilibrium morphology of immiscible polymer blends," *Macromolecules,* vol. 51, no. 7, pp. 2615-2620, 2018.

[40] X. Han, X. Liang, L. Cai, A. He, and H. Nie, "Amphiphilic Janus nanosheets by grafting reactive rubber brushes for reinforced rubber materials," *Polymer Chemistry,* vol. 10, no. 38, pp. 5184-5190, 2019.

[41] Y. Hou *et al.,* "Janus Nanosheets Synchronously Strengthen and Toughen Polymer Blends," *Macromolecules,* vol. 52, no. 10, pp. 3863-3868, 2019.

[42] T. S. Daitx, C. G. Jacoby, C. I. Ferreira, P. H. Schneider, and R. S. Mauler, "Kaolinite-based Janus nanoparticles as a compatibilizing agent in polymer blends," *Applied Clay Science,* vol. 182, p. 105291, 2019.

[43] Q. Yang, X. Miao, and K. Loos, "Fabrication of Nano-Sized Hybrid Janus Particles from Strawberry-Like Hierarchical Composites," *Macromolecular Chemistry and Physics,* vol. 219, no. 19, p. 1800267, 2018.

[44] W. You and W. Yu, "Onset reduction and stabilization of cocontinuous morphology in immiscible polymer blends by snowmanlike Janus nanoparticles," *Langmuir,* vol. 34, no. 37, pp. 11092-11100, 2018.

[45] T. Parpaite, B. Otazaghine, A. Caro, A. Taguet, R. Sonnier, and J. Lopez-Cuesta, "Janus hybrid silica/polymer nanoparticles as effective compatibilizing agents for polystyrene/polyamide-6 melted blends," *Polymer,* vol. 90, pp. 34-44, 2016.

[46] H. Nie, C. Zhang, Y. Liu, and A. He, "Synthesis of Janus rubber hybrid particles and interfacial behavior," *Macromolecules,* vol. 49, no. 6, pp. 2238-2244, 2016.

[47] W. Xu, J. Chen, S. Chen, Q. Chen, J. Lin, and H. Liu, "Study on the compatibilizing effect of Janus particles on liquid isoprene rubber/epoxy resin composite materials," *Industrial & Engineering Chemistry Research,* vol. 56, no. 47, pp. 14060-14068, 2017.

[48] W. Cheng *et al.,* "Compatibilization Behavior of Double Spherical TETA–SiO2@ PDVB Janus Particles Anchored at the Phase Interface of Acrylic Resin/Epoxy Resin (AR/EP) Polymer Blends," *ACS omega,* vol. 4, no. 18, pp. 17607-17614, 2019.

[49] H. Wang, W. Dong, and Y. Li, "Compatibilization of immiscible polymer blends using in situ formed janus nanomicelles by reactive blending," *ACS Macro Letters,* vol. 4, no. 12, pp. 1398-1403, 2015.

[50] H. Wang, Z. Fu, W. Dong, Y. Li, and J. Li, "Formation of interfacial janus nanomicelles by reactive blending and their compatibilization effects on immiscible polymer blends," *The Journal of Physical Chemistry B,* vol. 120, no. 34, pp. 9240-9252, 2016.

[51] R. Erhardt *et al.,* "Amphiphilic Janus micelles with polystyrene and poly (methacrylic acid) hemispheres," *Journal of the American Chemical Society,* vol. 125, no. 11, pp. 3260-3267, 2003.

[52] R. Erhardt *et al.,* "Janus micelles," *Macromolecules,* vol. 34, no. 4, pp. 1069-1075, 2001.

[53] S. Bärwinkel, R. Bahrami, T. I. Löbling, H. Schmalz, A. H. Müller, and V. Altstädt, "Polymer foams made of immiscible polymer blends compatibilized by Janus particles—effect of compatibilization on foam morphology," *Advanced Engineering Materials,* vol. 18, no. 5, pp. 814-825, 2016.

[54] K. C. Bryson, T. I. Löbling, A. H. Müller, T. P. Russell, and R. C. Hayward, "Using Janus nanoparticles to trap polymer blend morphologies during solvent-evaporation-induced demixing," *Macromolecules,* vol. 48, no. 12, pp. 4220-4227, 2015.

[55] R. Bahrami, T. I. Löbling, A. H. Gröschel, H. Schmalz, A. H. Müller, and V. Altstädt, "The impact of Janus nanoparticles on the compatibilization of immiscible polymer blends under technologically relevant conditions," *ACS nano,* vol. 8, no. 10, pp. 10048-10056, 2014.

[56] R. Bahrami, T. I. Löbling, H. Schmalz, A. H. Müller, and V. Altstädt, "Synergistic effects of Janus particles and triblock terpolymers on toughness of immiscible polymer blends," *Polymer,* vol. 109, pp. 229-237, 2017.

[57] H. Wang, Z. Fu, X. Zhao, Y. Li, and J. Li, "Reactive nanoparticles compatibilized immiscible polymer blends: synthesis of reactive SiO2 with long poly (methyl

methacrylate) chains and the in situ formation of janus SiO2 nanoparticles anchored exclusively at the interface," *ACS applied materials & interfaces,* vol. 9, no. 16, pp. 14358-14370, 2017.

[58] Y. Guo, Q. Liu, C. Peng, E. Wang, A. Joy, and M. Cakmak, "Colloid silica nanoparticles trapped morphology of polymer blends during solvent evaporation," *European Polymer Journal,* vol. 107, pp. 164-172, 2018.

[59] B. P. Grady, *Carbon nanotube-polymer composites: manufacture, properties, and applications.* John Wiley & Sons, 2011.

[60] L. Vaisman, H. D. Wagner, and G. Marom, "The role of surfactants in dispersion of carbon nanotubes," *Advances in colloid and interface science,* vol. 128, pp. 37-46, 2006.

[61] J. Hilding, E. A. Grulke, Z. George Zhang, and F. Lockwood, "Dispersion of carbon nanotubes in liquids," *Journal of dispersion science and technology,* vol. 24, no. 1, pp. 1-41, 2003.

[62] J. Yang, X. Qi, N. Zhang, T. Huang, and Y. Wang, "Carbon nanotubes toughened immiscible polymer blends," *Composites Communications,* vol. 7, pp. 51-64, 2018.

[63] S. Hom, A. R. Bhattacharyya, R. A. Khare, A. R. Kulkarni, M. Saroop, and A. Biswas, "Blends of polypropylene and ethylene octene comonomer with conducting fillers: influence of state of dispersion of conducting fillers on electrical conductivity," *Polymer Engineering & Science,* vol. 49, no. 8, pp. 1502-1510, 2009.

[64] M. Sumita, K. Sakata, S. Asai, K. Miyasaka, and H. Nakagawa, "Dispersion of fillers and the electrical conductivity of polymer blends filled with carbon black," *Polymer bulletin,* vol. 25, no. 2, pp. 265-271, 1991.

[65] P. Pötschke, A. R. Bhattacharyya, and A. Janke, "Morphology and electrical resistivity of melt mixed blends of polyethylene and carbon nanotube filled polycarbonate," *Polymer,* vol. 44, no. 26, pp. 8061-8069, 2003.

[66] P. Pötschke, S. Pegel, M. Claes, and D. Bonduel, "A novel strategy to incorporate carbon nanotubes into thermoplastic matrices," *Macromolecular Rapid Communications,* vol. 29, no. 3, pp. 244-251, 2008.

[67] Z.-Y. Xiong, L. Wang, Y. Sun, Z.-X. Guo, and J. Yu, "Migration of MWCNTs during melt preparation of ABS/PC/MWCNT conductive composites via PC/MWCNT masterbatch approach," *Polymer,* vol. 54, no. 1, pp. 447-455, 2013.

[68] T. Huang, J.-L. Li, J.-H. Yang, N. Zhang, Y. Wang, and Z.-W. Zhou, "Carbon nanotubes induced microstructure and property changes of polycarbonate/poly (butylene terephthalate) blend," *Composites Part B: Engineering,* vol. 133, pp. 177-184, 2018.

[69] Y. h. Wang *et al.*, "Morphology and property changes of immiscible polycarbonate/poly (L-lactide) blends induced by carbon nanotubes," *Polymer international,* vol. 62, no. 6, pp. 957-965, 2013.

[70] Y.-h. Wang *et al.*, "Super toughened immiscible polycarbonate/poly (L-lactide) blend achieved by simultaneous addition of compatibilizer and carbon nanotubes," *RSC advances,* vol. 4, no. 103, pp. 59194-59203, 2014.

[71] L. Liu, Y. Wang, Y. Li, J. Wu, Z. Zhou, and C. Jiang, "Improved fracture toughness of immiscible polypropylene/ethylene-co-vinyl acetate blends with multiwalled carbon nanotubes," *Polymer,* vol. 50, no. 14, pp. 3072-3078, 2009.

[72] S. S. Ray, S. Pouliot, M. Bousmina, and L. A. Utracki, "Role of organically modified layered silicate as an active interfacial modifier in immiscible polystyrene/polypropylene blends," *Polymer,* vol. 45, no. 25, pp. 8403-8413, 2004.

[73] D. Wu, L. Wu, M. Zhang, W. Zhou, and Y. Zhang, "Morphology evolution of nanocomposites based on poly (phenylene sulfide)/poly (butylene terephthalate) blend," *Journal of Polymer Science Part B: Polymer Physics,* vol. 46, no. 12, pp. 1265-1279, 2008.

[74] A. Göldel, G. Kasaliwal, and P. Pötschke, "Selective localization and migration of multiwalled carbon nanotubes in blends of polycarbonate and poly (styrene-acrylonitrile)," *Macromolecular rapid communications,* vol. 30, no. 6, pp. 423-429, 2009.

[75] Y. Li and H. Shimizu, "Conductive PVDF/PA6/CNTs nanocomposites fabricated by dual formation of cocontinuous and nanodispersion structures," *Macromolecules,* vol. 41, no. 14, pp. 5339-5344, 2008.

[76] F. Xiang *et al.*, "Largely enhanced ductility of immiscible high density polyethylene/polyamide 6 blends via nano-bridge effect of functionalized multiwalled carbon nanotubes," *Polymers for Advanced Technologies,* vol. 22, no. 12, pp. 2533-2542, 2011.

[77] J. Yang, C. Feng, J. Dai, N. Zhang, T. Huang, and Y. Wang, "Compatibilization of immiscible nylon 6/poly (vinylidene fluoride) blends using graphene oxides," *Polymer international,* vol. 62, no. 7, pp. 1085-1093, 2013.

[78] A. Göldel, A. Marmur, G. R. Kasaliwal, P. Pötschke, and G. Heinrich, "Shape-dependent localization of carbon nanotubes and carbon black in an immiscible polymer blend during melt mixing," *Macromolecules,* vol. 44, no. 15, pp. 6094-6102, 2011.

[79] J.-K. Yuan, S.-H. Yao, A. Sylvestre, and J. Bai, "Biphasic polymer blends containing carbon nanotubes: heterogeneous nanotube distribution and its influence on the dielectric properties," *The Journal of Physical Chemistry C,* vol. 116, no. 2, pp. 2051-2058, 2012.

[80] D. Wu, Y. Zhang, M. Zhang, and W. Yu, "Selective localization of multiwalled carbon nanotubes in poly (ε-caprolactone)/polylactide blend," *Biomacromolecules,* vol. 10, no. 2, pp. 417-424, 2009.

[81] D. Wu *et al.*, "Selective localization of nanofillers: effect on morphology and crystallization of PLA/PCL blends," *Macromolecular Chemistry and Physics,* vol. 212, no. 6, pp. 613-626, 2011.

[82] L. Zonder, S. Mccarthy, F. Rios, A. Ophir, and S. Kenig, "Viscosity Ratio and Interfacial Tension as Carbon Nanotubes Distributing Factors in Melt-Mixed Blends of Polyamide 12 and High-Density Polyethylene," *Advances in polymer technology,* vol. 33, no. 4, 2014.

[83] T. Gegenhuber, M. Krekhova, J. Schöbel, A. H. Gröschel, and H. Schmalz, "“Patchy” carbon nanotubes as efficient compatibilizers for polymer blends," *ACS Macro Letters,* vol. 5, no. 3, pp. 306-310, 2016.

[84] C. Wei, K. Cho, and D. Srivastava, "Tensile strength of carbon nanotubes under realistic temperature and strain rate," *Physical Review B,* vol. 67, no. 11, p. 115407, 2003.

[85] M.-F. Yu, O. Lourie, M. J. Dyer, K. Moloni, T. F. Kelly, and R. S. Ruoff, "Strength and breaking mechanism of multiwalled carbon nanotubes under tensile load," *Science,* vol. 287, no. 5453, pp. 637-640, 2000.

[86] R. S. Ruoff, J. Tersoff, D. C. Lorents, S. Subramoney, and B. Chan, "Radial deformation of carbon nanotubes by van der Waals forces," *Nature,* vol. 364, no. 6437, pp. 514-516, 1993.

[87] I. Palaci, S. Fedrigo, H. Brune, C. Klinke, M. Chen, and E. Riedo, "Radial elasticity of multiwalled carbon nanotubes," *Physical review letters,* vol. 94, no. 17, p. 175502, 2005.

[88] P. Liu, "Modifications of carbon nanotubes with polymers," *European Polymer Journal,* vol. 41, no. 11, pp. 2693-2703, 2005.

[89] H. Brown, "The adhesion between polymers," *Annual Review of Materials Science,* vol. 21, no. 1, pp. 463-489, 1991.

[90] H. R. Brown, "Relation between the width of an interface between two polymers and its toughness," *Macromolecules,* vol. 34, no. 11, pp. 3720-3724, 2001.

[91] H. R. Brown *et al.*, *Molecular simulation fracture gel theory*. Springer Science & Business Media, 2001.

[92] K. Cho, H. Brown, and D. Miller, "Effect of a block copolymer on the adhesion between incompatible polymers. I. Symmetric tests," *Journal of Polymer Science Part B: Polymer Physics,* vol. 28, no. 10, pp. 1699-1718, 1990.

[93] B. Bernard, H. R. Brown, C. J. Hawker, A. J. Kellock, and T. P. Russell, "Adhesion of polymer interfaces reinforced with random and diblock copolymers as a function of geometry," *Macromolecules,* vol. 32, no. 19, pp. 6254-6260, 1999.

[94] J. Washiyama, C. Creton, E. J. Kramer, F. Xiao, and C. Y. Hui, "Optimum toughening of homopolymer interfaces with block copolymers," *Macromolecules,* vol. 26, no. 22, pp. 6011-6020, 1993.

[95] C.-A. Dai *et al.*, "Reinforcement of polymer interfaces with random copolymers," *Physical review letters,* vol. 73, no. 18, p. 2472, 1994.

[96] H. Brown, K. Char, V. Deline, and P. Green, "Effects of a diblock copolymer on adhesion between immiscible polymers. 1. Polystyrene (PS)-PMMA copolymer between PS and PMMA," *Macromolecules,* vol. 26, no. 16, pp. 4155-4163, 1993.

[97] M. Sikka, N. N. Pellegrini, E. A. Schmitt, and K. I. Winey, "Modifying a polystyrene/poly (methyl methacrylate) interface with poly (styrene-co-methyl methacrylate) random copolymers," *Macromolecules,* vol. 30, no. 3, pp. 445-455, 1997.

[98] E. Eastwood and M. Dadmun, "Multiblock copolymers in the compatibilization of polystyrene and poly (methyl methacrylate) blends: Role of polymer architecture," *Macromolecules,* vol. 35, no. 13, pp. 5069-5077, 2002.

[99] C. Creton, E. J. Kramer, C. Y. Hui, and H. R. Brown, "Failure mechanisms of polymer interfaces reinforced with block copolymers," *Macromolecules,* vol. 25, no. 12, pp. 3075-3088, 1992.

[100] M. Kanninen, "An augmented double cantilever beam model for studying crack propagation and arrest," *International Journal of fracture,* vol. 9, no. 1, pp. 83-92, 1973.

[101] H. R. Brown, "Effect of a diblock copolymer on the adhesion between incompatible polymers," *Macromolecules,* vol. 22, no. 6, pp. 2859-2860, 1989.

[102] M. Fernandez, J. Higgins, J. Penfold, R. Ward, C. Shackleton, and D. Walsh, "Neutron reflection investigation of the interface between an immiscible polymer pair," *Polymer,* vol. 29, no. 11, pp. 1923-1928, 1988.

[103] J. Guo *et al.*, "Aspect ratio effects of multi-walled carbon nanotubes on electrical, mechanical, and thermal properties of polycarbonate/MWCNT composites," *Journal of Polymer Science Part B: Polymer Physics,* vol. 52, no. 1, pp. 73-83, 2014.

[104] B. S. Yilbas, A. Al-Sharafi, and H. Ali, *Self-Cleaning of Surfaces and Water Droplet Mobility*. Elsevier, 2019.

[105] S. Kumar, T. Rath, B. B. Khatua, A. K. Dhibar, and C. K. Das, "Preparation and Characterization of Poly(methyl methacrylate)/Multi-Walled Carbon Nanotube Composites," *Journal of Nanoscience and Nanotechnology,* vol. 9, no. 8, pp. 4644-4655, 2009.

[106] Y. J. Choi *et al.*, "Preparation and characterization of PS/multi-walled carbon nanotube nanocomposites," *Polymer Bulletin,* vol. 53, no. 5-6, pp. 393-400, 2005.

[107] J. Washiyama, E. J. Kramer, and C. Y. Hui, "Fracture mechanisms of polymer interfaces reinforced with block copolymers: transition from chain pullout to crazing," *Macromolecules,* vol. 26, no. 11, pp. 2928-2934, 1993.

[108] J. Washiyama, E. J. Kramer, C. F. Creton, and C.-Y. Hui, "Chain pullout fracture of polymer interfaces," *Macromolecules,* vol. 27, no. 8, pp. 2019-2024, 1994.

Appendix A: Coalescence Suppression in PS/PMMA blends compatibilized with diblock CNTs

1. Background

The morphology of an immiscible polymer blend affects the properties of the blend. Immiscible blends have unstable morphologies and hence irreproducible mechanical properties. Blends where a phase is dispersed in another (i.e droplet/matrix morphology) can be regarded as emulsions; the high interfacial tension between the components in the blend results in flow-induced microstructure changes during processing due to a complex interplay between droplet deformation, break-up and coalescence. Copolymers that can adsorb at the interface between immiscible phases are added to stabilize the mean drop size. The reduction has been attributed to the ability of these compatibilizers to induce droplet breakup and prevent their coalescence during blending [1].

In droplet-matrix morphology, the deformation of droplets is an interplay between hydrodynamic forces and the interfacial tension. The latter tends to pull a drop back into a sphere while the viscosity of the surrounding fluid slows that motion down resulting in a form relaxation time, τ_s. Since direct measurements of interfacial viscoelasticity of polymer melts using an interfacial rheometer or a Langmuir trough are difficult, the form relaxation (i.e the frequency corresponding to a plateau in the storage modulus of the blend) derived from small angle oscillatory shear (SAOS) measurements is the only evidence of interfacial viscoelastic effects in immiscible polymer blends [2]. This form relaxation time, τ_s, depends on the size of the dispersed phase; a change in τ_s when a sample is sheared at different shear rates is indicative of droplet coalescence (i.e droplet size increases). The experiments consist of shearing the blend at a constant shear rate to produce an initial morphology. Flow is stopped and SAOS experiments are performed. The shear rate is then systematically decreased in each subsequent experiment. The storage modulus reflects the

structure generated during previous period of shearing [3]. A typical result for uncompatibilized blends is shown in Figure A.1. When the shear rate is reduced, droplets coalesce resulting in a new steady state morphology [4]. On the graph, this coalescence is reflected as a decrease in the plateau modulus which is indicative of droplet size increasing as shear rate is decreased.

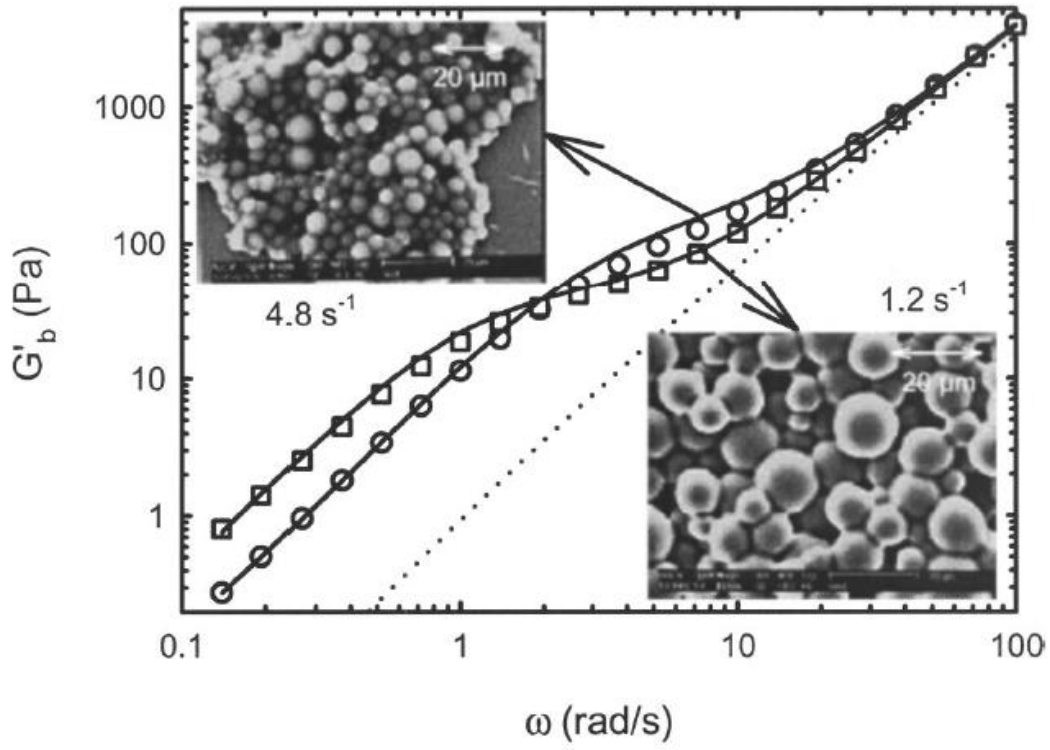

Figure A.1 G_b' of the uncompatibilized 10/90 PDMS/PI blend after a preshear of 4.8 s-1 for 3000 strain units (O) and after shearing at 1.2 s-1 until steady state (▭). The full lines are the fittings of G_b' using the model of Palierne. The dotted line is the component contribution to G_b', according to Dickie's model [5]. The SEM images of the blend after the same shear histories are added. Image taken from ref. [6]

Adding a compatibilizer to the blend results in an extra shoulder observed at lower frequencies. This extra shoulder, τ_β, is attributed to an additional interfacial stress that arises from the relaxation processes of the block copolymers at the interface during shearing [7]. As can be seen in Figure A.2, the shoulder gradually moves to higher frequencies as the amount of compatibilizer is

increased and eventually disappears at high concentrations[8] because as the concentration of compatibilizer increases at the interface, relaxation of the compatibilizer becomes faster. Eventually, the droplets and the compatibilizer relax on the same timescale and the two relaxation plateaus merge.

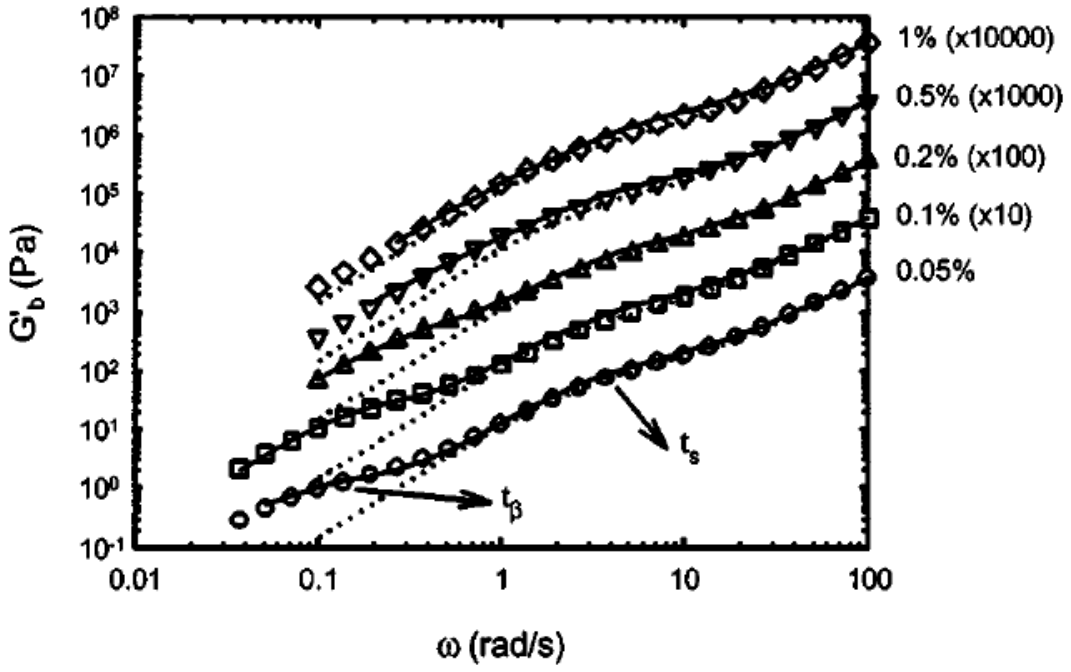

Figure A.2 G_b' for compatibilized blends with concentrations ranging from 0.05% to 1% after a preshear of 4.8 s-1 for 3000 strain units. The curves are shifted upwards with increasing block copolymer concentration. The full lines are the fittings of G_b' using the model of Palierne. G_b' for the uncompatibilized blend after the same shear history is added on the figure as a dotted line. Taken from ref. [6]

At high compatibilizer concentrations, the interface is saturated, coalescence is completely suppressed and the storage modulus of the blend will not evolve after step down in shear rate experiments (i.e a morphology will be achieved that is independent of the slower shear rate) as shown in Figure A.3.

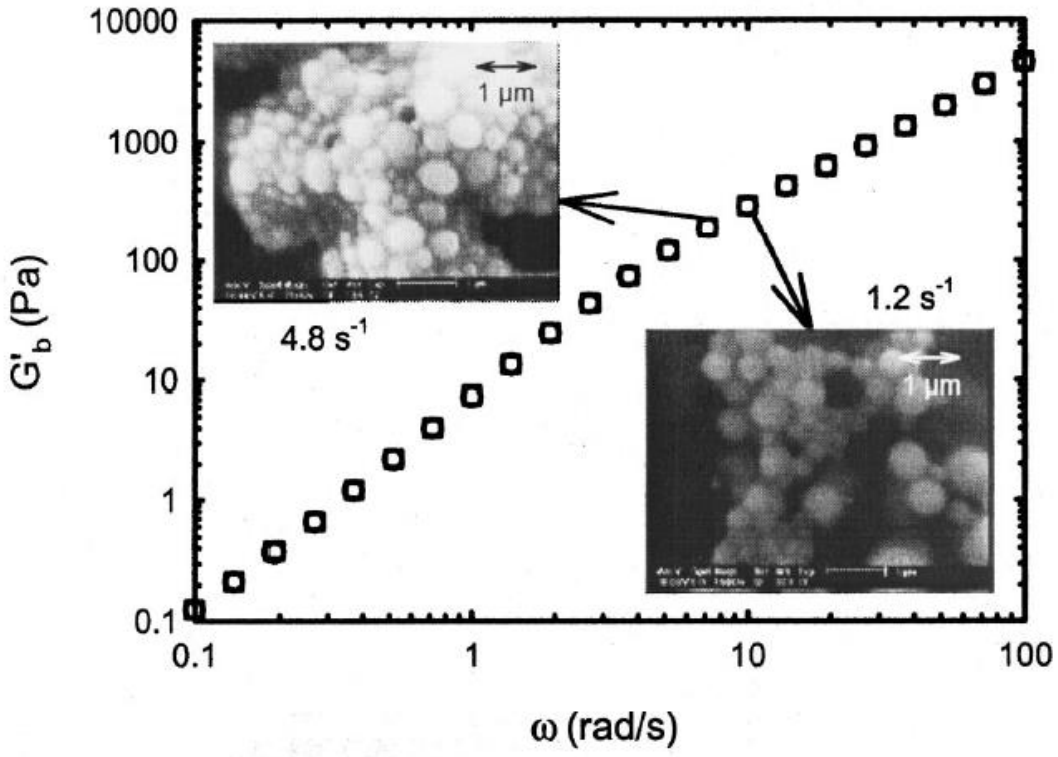

Figure A.3 G_b' of a 10% compatibilized blend after a preshear of 4.8 s^{-1} for 3000 strain units (○) and after shearing at 1.2 s^{-1} until steady state (□). The SEM images of the blend after the same shear histories are added. Taken from ref. *[6]*

Behavior represented by Figure A.2 and A.3 has been shown for a variety of blends and compatibilizers, including PDMS/PI [9, 10], PS/ PMMA [7, 11] and PS/PP [12].

Most of the work in the area has been done on low viscosity polydimethylsiloxane (PDMS)/polyisoprene (PI) polymers because experiments can be conducted at room temperature since the blends are liquid. Also, during SAOS experiments, changes can be seen at frequency ranges that are more easily probed. Relaxation of droplets in high molecular weight blends is about a factor of ten slower than in low molecular weight blends. However, a few have conducted experiments on high molecular polymers. Jacobs et al. [13] and Riemann et al. [7, 11] were the first to report the existence of a slow relaxation process in SAOS experiments using compatibilized

PS/PMMA blends. Figure A.4 show relaxation spectra for PS/PMMA blend obtained by Riemann and co-workers. Although the shapes of the graphs are different from those obtained for PDMS/PI blends, analogous behaviors are obtained. Two relaxation plateaus can be observed corresponding to droplet relaxation and interfacial viscoelasticity induced by the presence of copolymers. The other major difference is that relaxation occurs at much lower frequencies as molecular weight increases.

There are two procedures to find relaxation times from the storage modulus data. The first one is to fit the data to the Palierne equation; the second is to compute to plot the relaxation time spectra from the modulus data as shown in Figure A.4.b.

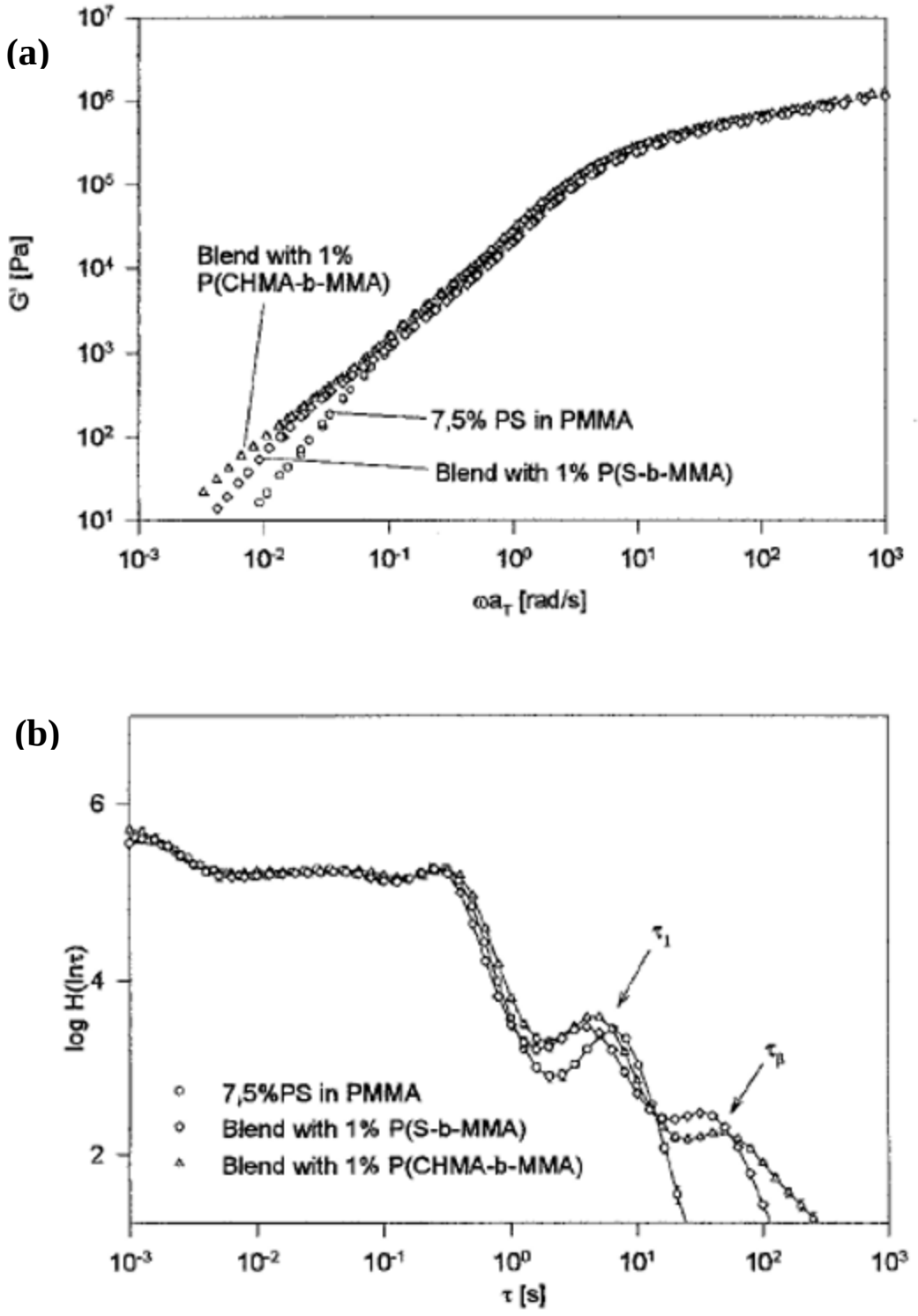

Figure A.4 (a) Storage modulus of the pure matrix material PMMA, the pure minor phase material PS and the blend with 7.5% PS in PMMA; (b) Relaxation time spectra of the blends in a. All data referenced at 190 °C.. Taken from ref. [11].

The effects of "particulate compatibilizers", particles that can adsorb at the interface of immiscible blends, on coalescence suppression has also been studied. Vermant et. al [14] used hydrophobic silica particles to compatibilize PIB/PDMS blends. The results from their SAOS measurements after a step down in shear rate are displayed in Figure A.5. A behavior analogous to that of copolymer compatibilized blends is obtained; there is a plateau that corresponds to the relaxation of the droplet phase. The plateau moves to lower frequencies until enough particles are added to effectively suppress coalescence. The main difference is that a second relaxation plateau is not observed when particles are added because particles in immiscible polymer blends do not act as classical compatibilizers, but as interfacial mobility modifiers [15]. Particles do not change IFT per se, they refine morphology by forming a dense layer of solid particles around the droplets that suppresses coalescence. Similar results were obtained for carbon black compatibilized PIB/PDMS [16], CNTs compatibilized PA12/EA [17], and silica compatibilized PP/PS blends [18].

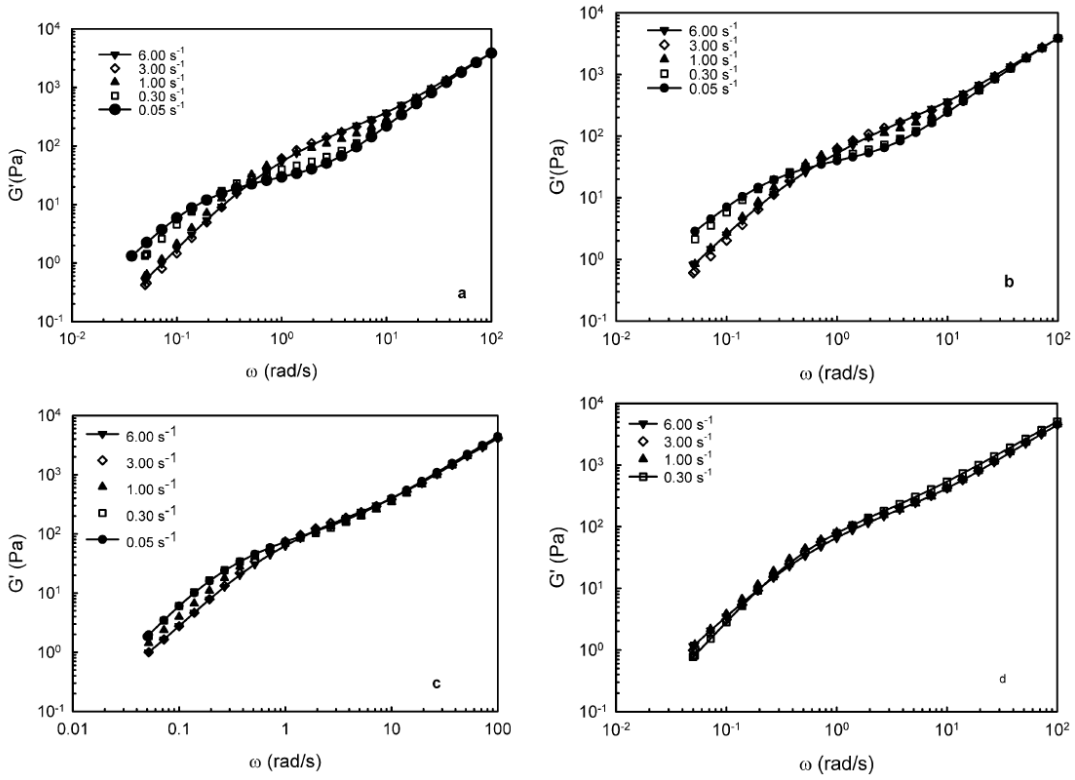

Figure A.5 Frequency dependence of the storage modulus after different pre-shear rates for 70/30 PDMS/PIB blends with varying amounts of silica particles: a) no filler added; b) 0.1 wt.% silica to the total blend; c) 0.5 wt.% silica to the total blend; d) 1 wt.% silica to the total blend (T = 25℃). Taken from ref. [14].

The emulsion model of Palierne has been used to analyze the storage moduli of immiscible polymer blends. The frequency, w, at which the relaxation shoulder in the moduli G' appears is inversely proportional to the form relaxation time, t_s , of the droplets. When either the average droplet radius, Rv , or the interfacial tension, α, is known; the other parameter can be calculated using Equation A.1.

$$t_s = \frac{\eta_m R_v}{4\alpha} \frac{(19p + 16)(2p + 3 - 2\Phi(p - 1))}{10(p + 1) - 2\Phi(5p + 2)} \qquad (A.1)$$

Where η_m is the viscosity of the matrix phase, p is the viscosity ratio and Φ is the volume fraction of the dispersed phase.

2. Objective of these studies

In the fracture toughness experiments, we have shown that diblock CNTs can improve the adhesion of immiscible polymer blends in the solid state. Rheological studies will demonstrate whether they can also stabilize the morphology during processing by effectively suppressing coalescence.

3. Experimental methods

PS/PMMA blends in 10/90 and 90/10 weight ratios were added to a glass vial and fed to a DSM Xplore^{TM} twin-screw extruder with corotating screws. The blends were mixed at a temperature of 190 °C at a speed of 150 rpm for 5 minutes under a nitrogen blanket. For the compatibilized blends, nanotubes were added to the dry blends and simultaneously fed into the extruder. Samples for rheological analysis were prepared by compression molding discs of 20 mm diameter and 1 mm thickness at 160 °C for blends without nanotubes and 180°C for composites for 10 minutes.

The rheological experiments are conducted on a Discovery Hybrid Rheometer-2 (DHR-2) from TA Instruments. A parallel plate configuration with a plate diameter of 20 mm and a 900 nm gap is used and SAOS experiments were conducted from 100 to 0.01 rad/s at 190 °C.

4. Preliminary results

Our hypothesis was that the modulus of PS/PMMA blends compatibilized with block CNTs will behave like particle compatibilized blends. Since nanotubes have been shown to not affect IFT [17], only the droplet relaxation plateau should be observed. Figure A.6 shows the modulus versus frequency before shearing the samples. Samples with 10% PMMA had modulus comparable to that of pure PS except at very low frequencies where a plateau corresponding to the relaxation of the droplet starts around 0.025 rad/s or 40 seconds relaxation time. For the samples with 10% PS, however, the modulus is lower than that of pure PMMA and the plateau is not clearly discernable; it seems to start around 1 rad/s and continues to the lowest frequency.

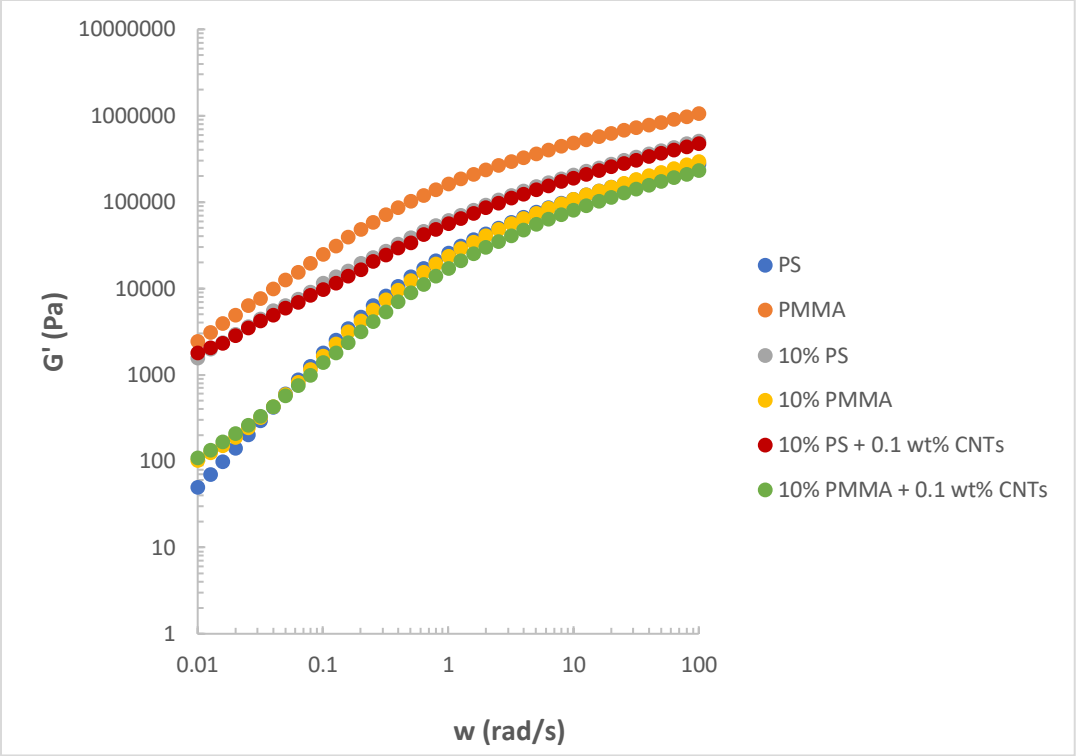

Figure A.6 Storage modulus of the neat polymers, uncompatibilized and compatibilized blends.

The behavior of the samples with PS as the dispersed phase is different from what is expected based on results from the literature. When polymers are blended, the interface between the polymers is elastic which should increase the storage modulus at lower frequencies (e.g when the relaxation of the droplets is probed). That behavior can be observed for the samples with dispersed PMMA. The plateau appears to be at the same frequency when 0.1 wt.% of CNTs are added which suggests that the nanotubes did not affect the sizes of the droplets in this case.

The discrepancy observed for the samples with dispersed PS is due to the fact that the samples degraded during the experiment; samples were visibly yellow at the end of the experiments which is an indication of thermo-oxidative degradation. The rheometer used in our studies is not equipped with a nitrogen supply and the SAOS experiments took about 2 hours to run with the frequency range used.

There were two main limitations to conducting further experiments. (1) The polymers degrading during the experiments kept us from completing the full experiment (i.e probing morphology after different pre-shear rates). Changing the current rheometer set up to add a nitrogen environment is necessary to be able to conduct experiments at such high temperatures. (2) No more block nanotubes were available.

Recommendations for future work

Sample preparation

The same procedure described above can be used but, it is recommended to try the following:

Different ratios of polymer blends (for example 92.5/7.5) because being able to use the Palierne model depends on the size of the dispersed phase; the volume average droplet radius divided by the number average droplet size (R_v/R_n) should be less than 2 [17]. The droplets sizes should be measured using TEM.

Different melt mixing conditions (mixing speed, time, temperature) should be tested to try and find optimum mixing conditions. Those conditions would yield the best possible dispersion at minimum nanotube breakage.

Rheological testing

The main reason experiments couldn't be continued was the degradation of the samples. It is not recommended to attempt these experiments until the experiment can be run in a nitrogen environment.

Only SAOS experiments were conducted because that step alone took over 2 hours and the samples degraded. However, since the objective of these experiments is to verify whether coalescence suppression is obtained, step-down in shear rate experiments should be conducted. The

experimental procedure is as follows: probe the initial morphology using SAOS experiments, shear the sample for a certain amount of time followed by another SAOS experiment; the second step is repeated decreasing the shear rate in each subsequent experiment.

The goal of the shearing experiments is to possibly generate a different morphology at each step and the SAOS data is used for the data analysis. There are three important parameters: $\tau_s, R_v, and\ \alpha$. The first parameter can be estimated by plotting the relaxation spectrum from the SAOS data using the NLREG program[11] to generate a plot similar to Figure A.4b. Different routes of analysis can be taken depending on the data. The assumption here is that the nanotubes won't change IFT, so the value can be assumed to be the same for compatibilized and uncompatibilized samples. However, a qualitative analysis of the modulus curves can easily verify whether that hypothesis is true. If the nanotubes are not affecting IFT, the second plateau that corresponds to their relaxation will not observed. Assuming that the nanotubes could affect IFT because half of their length has polymer attached, two scenarios can arise:

Scenario 1: No change in IFT

Here estimating R_v/α from Equation A.1 is enough to probe morphology. Any changes in the ratio can be attributed to changes in the droplet sizes. Since IFT doesn't change, it won't affect the results from one sample to the next. For a given sample, R_v/α is estimated before and after each shearing step using Equation A.1. When coalescence is suppressed, the value is no longer dependent on the shear rate applied.

Scenario 2: IFT changes

If IFT changes with nanotube additions, to be able to compare the morphologies between different samples (i.e no nanotubes vs. 0.1% nanotubes), then it would be better to estimate IFT for each

sample and calculate R_v. α can be calculated by using the data for the first SAOS experiments (i.e before any shearing occurs) and calculating α using R_v obtained from TEM experiments.

References

[1] U. Sundararaj, C. Macosko, R. Rolando, and H. Chan, "Morphology development in polymer blends," *Polymer Engineering & Science,* vol. 32, no. 24, pp. 1814-1823, 1992.

[2] P. Van Puyvelde, S. Velankar, and P. Moldenaers, "Rheology and morphology of compatibilized polymer blends," *Current opinion in colloid & interface science,* vol. 6, no. 5-6, pp. 457-463, 2001.

[3] I. Vinckier, P. Moldenaers, and J. Mewis, "Relationship between rheology and morphology of model blends in steady shear flow," *Journal of Rheology,* vol. 40, no. 4, pp. 613-631, 1996.

[4] I. Vinckier, P. Moldenaers, and J. Mewis, "Transient rheological response and morphology evolution of immiscible polymer blends," *Journal of rheology,* vol. 41, no. 3, pp. 705-718, 1997.

[5] R. Dickie, "Heterogeneous polymer–polymer composites. I. Theory of viscoelastic properties and equivalent mechanical models," *Journal of Applied Polymer Science,* vol. 17, no. 1, pp. 45-63, 1973.

[6] E. Van Hemelrijck, P. Van Puyvelde, S. Velankar, C. W. Macosko, and P. Moldenaers, "Interfacial elasticity and coalescence suppression in compatibilized polymer blends," *Journal of Rheology,* vol. 48, no. 1, pp. 143-158, 2004.

[7] R.-E. Riemann, H.-J. Cantow, and C. Friedrich, "Interpretation of a new interface-governed relaxation process in compatibilized polymer blends," *Macromolecules,* vol. 30, no. 18, pp. 5476-5484, 1997.

[8] Y. Huo, G. Groeninckx, and P. Moldenaers, "Rheology and morphology of polystyrene/polypropylene blends with in situ compatibilization," *Rheologica acta,* vol. 46, no. 4, pp. 507-520, 2007.

[9] E. Van Hemelrijck, P. Van Puyvelde, C. W. Macosko, and P. Moldenaers, "The effect of block copolymer architecture on the coalescence and interfacial elasticity in compatibilized polymer blends," *Journal of rheology,* vol. 49, no. 3, pp. 783-798, 2005.

[10] S. Velankar, P. Van Puyvelde, J. Mewis, and P. Moldenaers, "Steady-shear rheological properties of model compatibilized blends," *Journal of Rheology,* vol. 48, no. 4, pp. 725-744, 2004.

[11] R.-E. Riemann, H.-J. Cantow, and C. Friedrich, "Rheological investigation of form relaxation and interface relaxation processes in polymer blends," *Polymer Bulletin,* vol. 36, no. 5, pp. 637-643, 1996.

[12] A. M. C. d. Souza, P. S. Calvão, and N. R. Demarquette, "Linear viscoelastic behavior of compatibilized PMMA/PP blends," *Journal of applied polymer science,* vol. 129, no. 3, pp. 1280-1289, 2013.

[13] U. Jacobs, M. Fahrländer, J. Winterhalter, and C. Friedrich, "Analysis of Palierne's emulsion model in the case of viscoelastic interfacial properties," *Journal of Rheology,* vol. 43, no. 6, pp. 1495-1509, 1999.

[14] J. Vermant, G. Cioccolo, K. G. Nair, and P. Moldenaers, "Coalescence suppression in model immiscible polymer blends by nano-sized colloidal particles," *Rheologica acta,* vol. 43, no. 5, pp. 529-538, 2004.

[15] S. Vandebril, J. Vermant, and P. Moldenaers, "Efficiently suppressing coalescence in polymer blends using nanoparticles: role of interfacial rheology," *Soft Matter,* vol. 6, no. 14, pp. 3353-3362, 2010.

[16] J. Vermant, S. Vandebril, C. Dewitte, and P. Moldenaers, "Particle-stabilized polymer blends," *Rheologica acta,* vol. 47, no. 7, pp. 835-839, 2008.

[17] F. Tao, D. Auhl, A. C. Baudouin, F. J. Stadler, and C. Bailly, "Influence of multiwall carbon nanotubes trapped at the interface of an immiscible polymer blend on interfacial tension," *Macromolecular Chemistry and Physics,* vol. 214, no. 3, pp. 350-360, 2013.

[18] L. Elias, F. Fenouillot, J.-C. Majesté, and P. Cassagnau, "Morphology and rheology of immiscible polymer blends filled with silica nanoparticles," *Polymer,* vol. 48, no. 20, pp. 6029-6040, 2007.

Appendix B: Unique Plasticization of Ethylene-tetrafluoroethylene Copolymer reinforced with Fluorocopolymer-Coated Carbon Nanotubes

Fatoumata Ide Seyni[†], Jirayu Yuenyongsuwan[†,‡], Thirawudh Pongprayoon[‡], Brian P. Grady[†,*], and Edgar A. O'Rear[†]

[†]School of Chemical, Biological, and Materials Engineering, University of Oklahoma, Norman, Oklahoma

[‡]Department of Chemical Engineering, King Mongkut's University of Technology North Bangkok, Bangkok 10800, Thailand

*Corresponding author. E-mail: bpgrady@ou.edu

Abstract

Multiwall carbon nanotubes (MWCNTs) that were thought to be noncovalently functionalized with a fluorocopolymer were used to enhance performance of an ethylene- tetrafluoroethylene (ETFE). Initial FT-IR tests confirmed the presence of a functionalized material on the nanotubes but further SEM-EDS and TGA analyses showed otherwise. These CNTs slightly poorer tensile properties than as-received nanotubes. While the electrical percolation threshold was the same for both nanotube types, the rheological percolation threshold increased from 1-2 wt.% for as-received nanotubes to 3-4 wt.% for the functionalized nanotubes. The differences observed were attributed to trace elements of impurities in the CNTs after the functionalization attempt.

1. Introduction

Fluorinated polymers can be regarded as modified polyethylene (PE) where some or all of the hydrogen atoms are substituted with fluorine atoms.[1] These polymers possess several unique properties due to the unique features of the fluorine atom. Fluoropolymers have high thermal, chemical and corrosion resistance; low dielectric constant, surface energy and flammability; and possess excellent inertness to solvents, hydrocarbons and acids. Perhaps the most recognized fluoropolymer is poly(tetrafluoroethylene) (PTFE) commonly known as Teflon; a semicrystalline polymer used in everyday applications like coating for cooking pans because of its nonstick properties. Due to the difficulty of extrusion of PTFE, a well-known alternative is to copolymerize tetrafluoroethylene (TFE) with ethylene to yield ethylene-tetrafluoroethylene copolymer (ETFE). Aside from being melt processible, ETFE also is significantly more flexible than PTFE. ETFE is used in many applications including anticorrosion paintings, chemical resistant coatings, wires and cables insulation, and films for greenhouses.[2, 3] Despite the many excellent properties of ETFE, high rates of wear occur and cracks develop in moldings due to high temperature and stress.[4] One way to improve wear resistance, toughness and electrical conductivity of ETFE is to form composites with carbon nanotubes.[5]

Carbon nanotubes (CNTs) are often added to semicrystalline polymers to produce conductive composites at low filler loadings. CNTs have also been shown to increase stiffness and to nucleate crystallinity.[6, 7] While several studies have been conducted for composites of semicrystalline polymers like polyethylene (PE)[8, 9] and polypropylene (PP),[10, 11] to our knowledge, only one study, conducted by our group, examined ETFE/multi-wall carbon nanotubes (MWCNTs) composites .[12] The electrical percolation threshold was only 0.9 wt.% MWCNTs; a similar study conducted with polyamide 6,6 using the same nanotubes resulted in lower electrical conductivity

for the same filler concentration suggesting that the nanotubes dispersed better in ETFE.[13] However, no significant changes were observed for the crystallization and melting temperatures of the composites compared to that of pure ETFE up to filler loading of 5 wt.% and the tensile strength of the composites decreased compared to that of pure ETFE.

Although our group has been the only group to study ETFE, there are a significant number of papers involving nanotubes added to other fluoropolymers. For example, Solov'yanchik examined CNTs and CNTs functionalized with alkyl groups in a matrix of trifluorochloroethylene–vinylidene fluoride copolymer in a 10:1 ratio of ED-22 epoxy resin.[14] Surface resistance decreased with the amount of CNTs while higher resistance was observed with the functionalized CNTs which was attributed to worse contact between the carbon nanotubes. Further, addition of CNTs created greater roughness and an increase in contact angle. Wang et al. prepared superhydrophobic coatings by spraying a dispersion of CNTs with perfluoralkoxy resin (Teflon® PFA).[15] Nano-composites of Nafion® with MWCNTs have been studied for their potential to exhibit proton and electron conductivity.[16]

Extensive work has been conducted to prepare polymer nanocomposites because of the potential of CNTs in improving the mechanical, electrical and thermal properties of polymers.[17] However, taking full advantage of the properties of CNTs in polymeric matrices has been challenging because of their tendency to form aggregates and bundles. The poor dispersion in polymers is mainly due to the van der Waals forces between the tubes and the weak adhesion between CNTs and polymers.[18, 19] To obtain well dispersed CNTs in polymers, functionalization techniques that consist of covalently or non-covalently bonding polymers to the carbon nanotube surface has often been employed. [20-25] Covalent bonding can significantly improve the interfacial adhesion between CNTs and the polymer[26, 27], but most techniques involve strong acids which can

destroy the electronic structure of the nanotubes. Noncovalent techniques are more appealing because they preserve the integrity of the nanotubes. Such techniques consist of adhering the polymer around the nanotubes without breaking any bonds or introducing defects on the surface.[23]

Surfactant-assisted noncovalent polymerization techniques have gained interest because they can be used to form thin films of polymers on the surface of CNTs. Admicellar polymerization (AP) is one of those techniques and is known as the "surface analogue" to emulsion polymerization. AP has also been successfully used to form thin polymeric films on substrates like alumina, silica, cotton and recently on carbon nanotubes.[28-31] This technique consists of four steps: formation of an adsorbed surfactant layer on a surface, addition of monomers which are adsolubilized by the adsorbed surfactant, polymerization, and finally excess surfactant removal. This technique has been used for finishing textiles to achieve flame retardancy, UV protection and water repellency.[32] There has been considerable interest as well in using AP to modify the interphase of composites.[33] Poochai et al. [31] have successfully polymerized a thin film of polyacrylonitrile (PAN) on the surface of carbon nanotubes using admicellar polymerization to enhance their dispersion in a PAN matrix. They showed that the PAN/PAN-coated CNTs composites had higher tensile strength and were stiffer than the as-received CNTs/PAN composites. AP has also been used to form thin films of polymers on CNTs to enhance their dispersion in aqueous media. Monomers of sodium acrylate and methacrylate were used to form hydrophilic water-soluble segment for improving dispersion while also containing an insoluble polymeric segment to anchor the polymer to the nanotubes. These CNTs were shown to remain dispersed in water for up to 40 days.[30]

In this work, admicellar polymerization of 2,2,2 trifluoroethyl acrylate (TFEA) and 2,2,3,3,4,4,5,5 octafluoro pentyl methacrylate (OFPM) (see Structures in Figure 1) on a MWCNT surface was carried out using fluoroaliphatic amine oxide, a nonionic fluorosurfactant, for admicelle formation. The goal was to compare the performance of the functionalized carbon nanotubes in ETFE to those of unfunctionalized CNTs/ETFE composites by measuring the mechanical, electrical, and thermal properties of these composites with those of unfunctionalized CNTs/ETFE composites. Later TGA and SEM-EDS experiments revealed that the nanotubes were not functionalized, as initially thought. All the experiments were conducted before that finding was made.

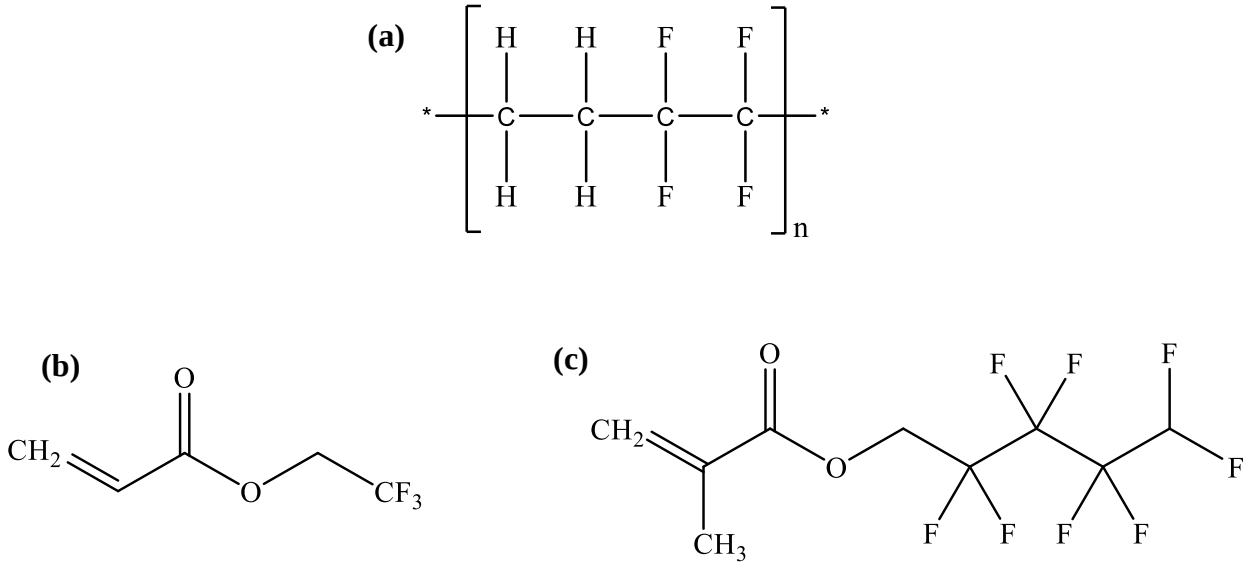

Figure B.1. Chemical Structures of (a) ETFE (b) TFEA (c) OFPM

1. Experimental

2.1 Materials

Ethylene tetrafluorethylene (ETFE) pellets were provided by Asahi Glass Company. This ETFE copolymer contains ~50% TFE comonomer. The melting temperature of 257°C measured indicated that it contains about 45 to 50% ethylene based on work by Arai and coworkers.[2] Nanocyl® 7000 MWCNTs with an average aspect ratio of 156 (length = 1.5 μm, diameter = 9.5 nm) were used and SMWTM-100 CNTs with an average aspect ratio of 94 (average length = 735 nm, average diameter = 7.8 nm) were provided by Southwest Nanotechnologies

2,2,2 trifluoroethyl acrylate (TFEA) and 2,2,3,3,4,4,5,5 octafluoro pentyl methacrylate (OFPM) were purchased from Sigma Aldrich. Isopropanol and the initiator ammonium persulfate were purchased from Fisher Scientific. Fluorourfactant nonionic FS230 (fluoroaliphatic amine oxide) was obtained from Masurf. All chemicals were used as received.

2.2 Functionalization of carbon nanotubes

An adsorption isotherm for this fluorosurfactant in 80:20 water/isopropanol has a CMC of ~300 ppm and 100 mg of surfactant adsorbed per gram of nanotube. This information was used to prepare a FS230 surfactant solution at 240 ppm assuming the same level of surfactant adsorption. The surfactant concentration in solution must be below the critical micelle concentration (CMC), to avoid emulsion polymerization.[34] The solution was then mixed with a 0.5:0.5 mmol solution of TFEA and OFPM. The vials were put in a shaker bath at room temperature for 1 hour at 60 rpm. 50 mg of carbon nanotubes was added to the solution and sonicated for 5 minutes with an ultrasonic probe. The initiator was then added in a 1:2 ratio with the monomer and vials were put in a shaker bath at 60°C and 120 rpm for 2 hours. Functionalized carbon nanotubes were removed from the

shaker bath, filtered with DI water until the filtrate did not foam (~1 hour) and then placed in an oven at 60°C until dry.

2.3 Carbon nanotube characterization

SEM images were collected with a JEOL JSM-880 scanning electron microscope (SEM) and a Nicolet IS10 Fourier-Transform Infrared Spectroscope (FT-IR) was used to collect infrared spectra.

2.4 Composite preparation

The desired amount of carbon nanotubes and ETFE pellets were mixed in a glass vial and fed to a DSM Xplore^{TM} twin-screw extruder with corotating screws. The composites were mixed at a rotation speed of 100 RPM at 270°C for 3 minutes under nitrogen gas. The extruded strands were compression molded using a Carver Laboratory Press at 280°C for 10 minutes.

2.5 Composite Characterization

2.5.1 Conductivity measurements

The electrical conductivity of high resistivity samples (> $1x10^7$ ohm-cm) were measured with an Agilent 4339B high resistance meter and 16008B resistivity cell. Composite films 8 cm in diameter and 0.5 mm thick were tested under 3 different voltages, on both sides, to obtain an average resistivity which was then converted to conductivity. For samples with moderate resistivity (< $1x10^7$ ohm-cm), a four-point probe geometry as outlined in the American Standard for Testing and Materials (ASTM) Standard D 4496 was used. Four copper electrodes were attached to rectangular pieces of composite films (30 mm x 10 mm) with a conductive silver epoxy (MG Chemicals 8331). A Keithley 2000 multimeter was used to measure resistance for each sample which was used to calculate the conductivity of the samples.

2.5.2 Dynamic Mechanical Analysis (DMA)

Storage and loss moduli were measured using a Rheometric Scientific RSA II. Film fixtures were used to take measurements on compression molded samples ~30 mm long and 5 mm wide at 1 Hz frequency and 0.05% strain. Glass transition temperatures were calculated by determining the temperature that corresponds to the maximum value in tan δ in the glass transition region.

2.5.3 Tensile tests

Tensile tests were performed using a United STM-2K tensile tester. Samples were cut using an ASTM D-1708 die from Dewes-Gumbs on a manual expulsion press. At least five replicates were used for samples at each nanotube content level.

2.5.4 Differential Scanning Calorimetry (DSC)

DSC measurements were performed using a TA instrument Q-1000 Calorimeter with 10-15 mg samples cut from compression molded films crimped in standard aluminum pans. Temperature calibration was performed during heating using indium, tin, and bisphenyl, and heat capacity calibration was performed with sapphire, Samples were heated to 320°C and held for 5 min, then cooled to -80°C at 10°C/min and held for 5 min (cooling run); the samples were reheated to 300°C at 10°C/min (heating run). The temperature corresponding to the maximum in heat evolution during the cooling run was recorded as the crystallization temperature. The melting temperature was assigned as the maximum heat influx upon heating, corresponding to the crystal-to-melt transition. No step change corresponding to the glass transition was visible.

2.5.5 Light Microscopy

Transmission light microscopy was performed using a Leica SP8 Confocal Laser Scanning Microscope to determine the area fraction of agglomerates. Thin sections from extruded samples

were cut using an ultramicrotome. The image analysis software ImageJ was used to determine the circle-equivalent diameter of the agglomerates, which in turn was used to calculate the carbon nanotubes agglomerate area. The area ratio was calculated by dividing the agglomerate area to the total area of the image. Only agglomerates with circle-equivalent diameters larger than 5 μm were used.

2. Results and Discussion

3.1 Carbon nanotube functionalization

As-received nanotubes and functionalized nanotubes were characterized by FT-IR as displayed in Figure B.2. No significant peaks can be seen on the spectrum of the as-received CNTs as expected. The strong peak observed in the spectra of the functionalized CNTs around 900-1000 cm^{-1} is a typical signal observed on spectra of functionalized CNTs [35] corresponding to C-H and C=C bonds in the copolymer. The double peak around 1300 cm^{-1} corresponds to both the stretching peak of the C-O present in the acrylate and methacrylate groups and to the C-F in the copolymer. The last strong peak observed around the 1800 cm^{-1} can be attributed to the C=O stretching peak from the ester linkages.

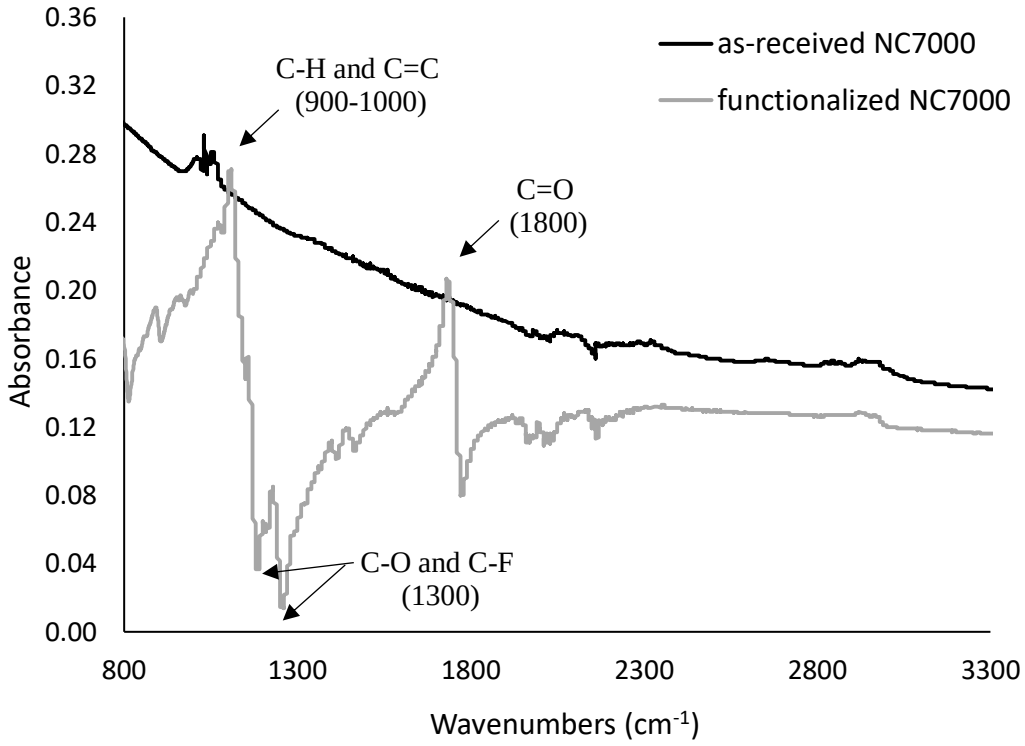

Figure B.2. FT-IR spectra of as-received and functionalized NC7000 CNTs

SEM micrographs were taken to visually characterize the structure of as-received and functionalized CNTs. As can be seen in Figure B.3, as-received CNTs have a smooth surface while the functionalized tubes appear a bit blurry due to the presence of the copolymer.

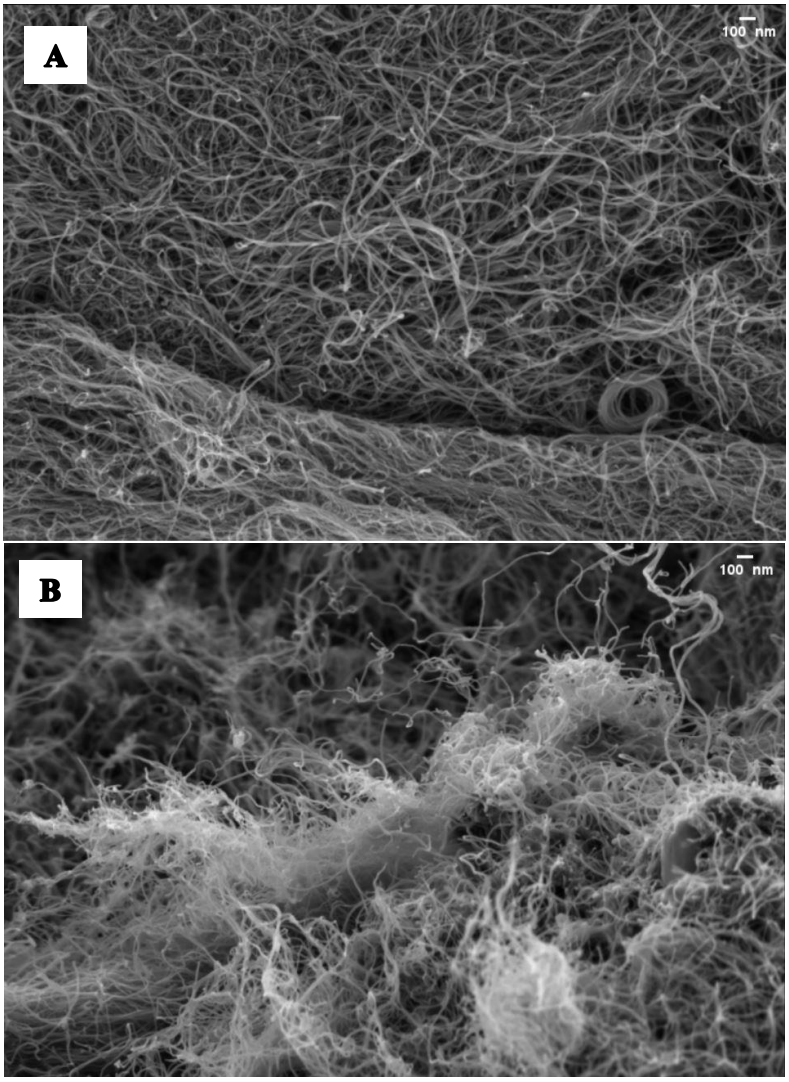

Figure B.3. SEM micrograph of (A) as-received NC7000 CNTs and (B) TFEA-OFPM functionalized NC7000 CNTs

Additional characterization experiments were requested after submission of the paper and the results of the TGA and SEM-EDS experiments are displayed in Figures B.4 and B.5. The TGA revealed that the two samples were the same in composition.

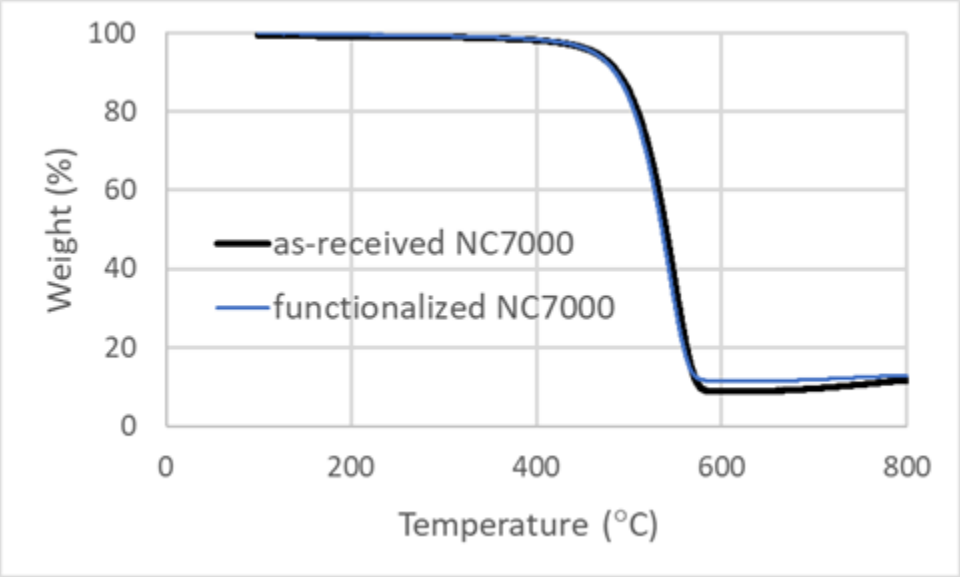

Figure B.4. Nanotubes weight % vs. temperature curves obtained after TGA experiments.

The EDS analysis shows that the only difference between the two samples is the presence of some trace elements. It is not clear why the initial FT-IR experiments showed pics that suggest that the functionalization was successful. Since trace elements can be seen in the sample that was supposed to be functionalized, the polymer may have been washed off during the rinsing. Because the functionalization was non-covalent, the affinity between the nanotubes and the TFEA-OFPM copolymer may have been too weak to keep the copolymer on the nanotubes.

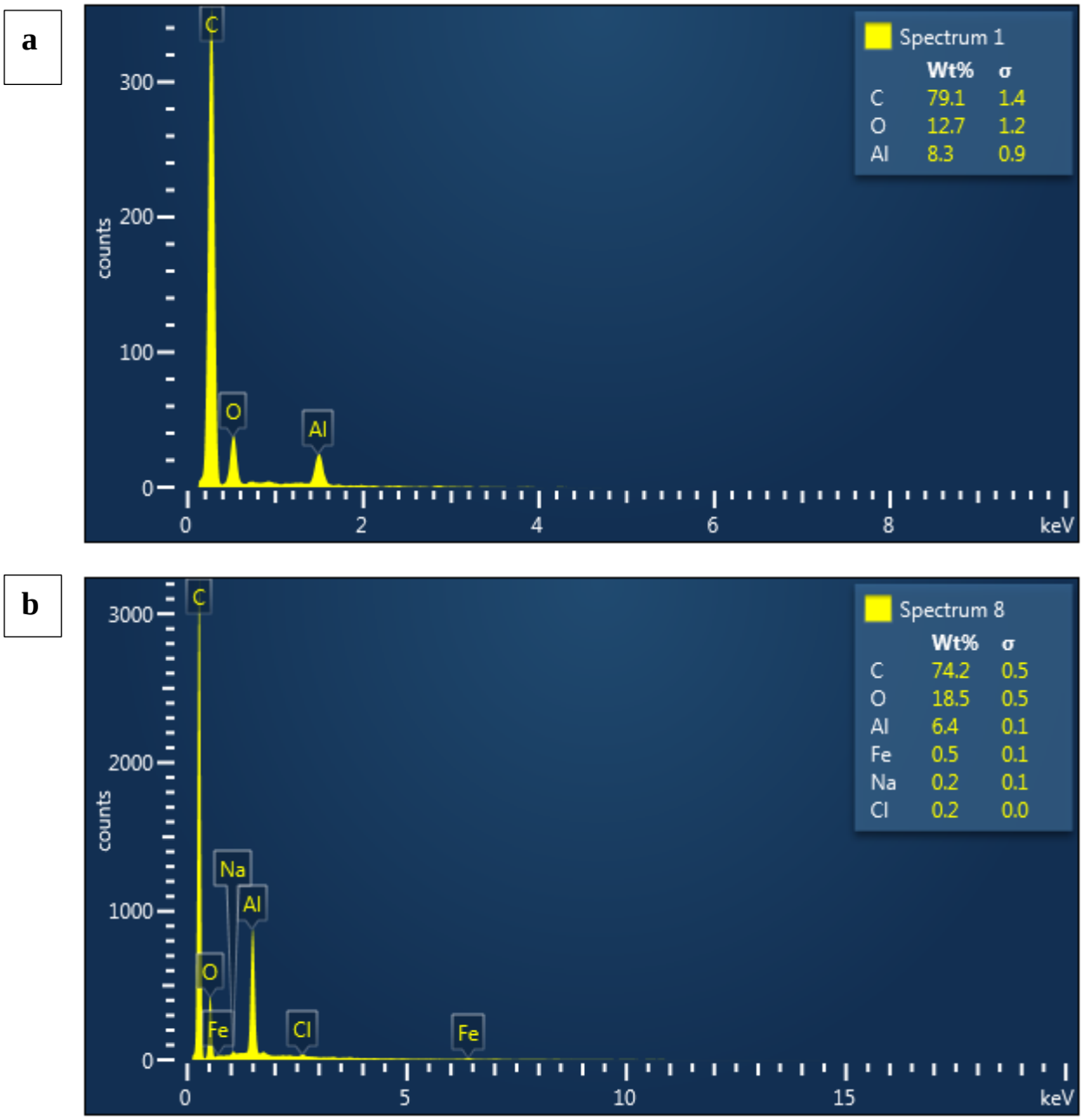

Figure B.5. Nanotubes chemical analysis obtained from SEM-EDS experiments. (a) as-received CNTs, (b) functionalized CNTs

All these subsequent experiments were conducted before the additional experiments revealed that the nanotubes were not functionalized. They will still be referred to as "functionalized" throughout to distinguish between the two types of nanotubes.

3.2 Electrical Conductivity

Polymer-carbon nanotube composites are often manufactured to produce conductive or electrically dissipative materials. Nanotubes increase conductivity because a continuous network will form at high enough concentrations and conductivity occurs both through nanotube-nanotube contacts as well as electron hopping or tunneling. Bulk conductivities of the ETFE/CNTs composites as a function of the type and weight fraction of CNTs are displayed in Figure B.6. The electrical percolation threshold using either functionalized or as-received CNTs was between 1-2 wt.% and the plateau conductivities were around 10^{-4} S/cm. This percolation threshold is on the lower end of typical values obtained for NC7000 CNTs in semicrystalline polymers as can be seen in Table A.1 implying good dispersion of these nanotubes in ETFE. However, the percolation threshold is slightly higher than the percolation threshold of 0.9 wt.% obtained with SMW-100 CNTs.[12]

Table B.1. Percolation threshold of various semicrystalline polymers filled with as-received NC7000 CNTs

Polymer	Electrical percolation threshold (wt.%)	Rheological percolation threshold (wt.%)	Reference
Polyamide 6	1%	-	Pötschke (2008)[36]
Poly (ether ether ketone)	1-1.5%	1 - 1.5%	Banganusampath (2009)[37]
Impact Modified Polypropylene	0.5 %	-	Müller (2011)[38]
Linear Low-Density Polyethylene	2.5 %	-	Müller (2012)[39]
Polyamide 6,6	3-4 %	-	Krause (2009)[40]
Polycaprolactone	0.50%	-	Pötschke (2013)[41]
Polyamide 12 with acid group excess	0.70%	-	Socher (2010)[42]
ETFE	1-2%	1-2%	This work

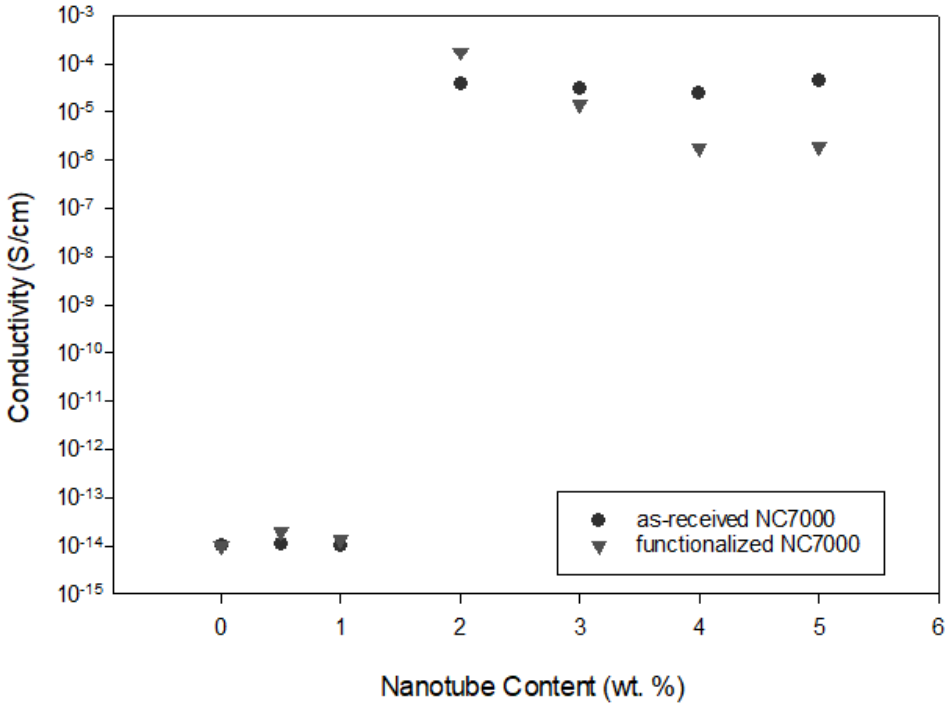

Figure B.6. Conductivity of MWCNT filled ETFE

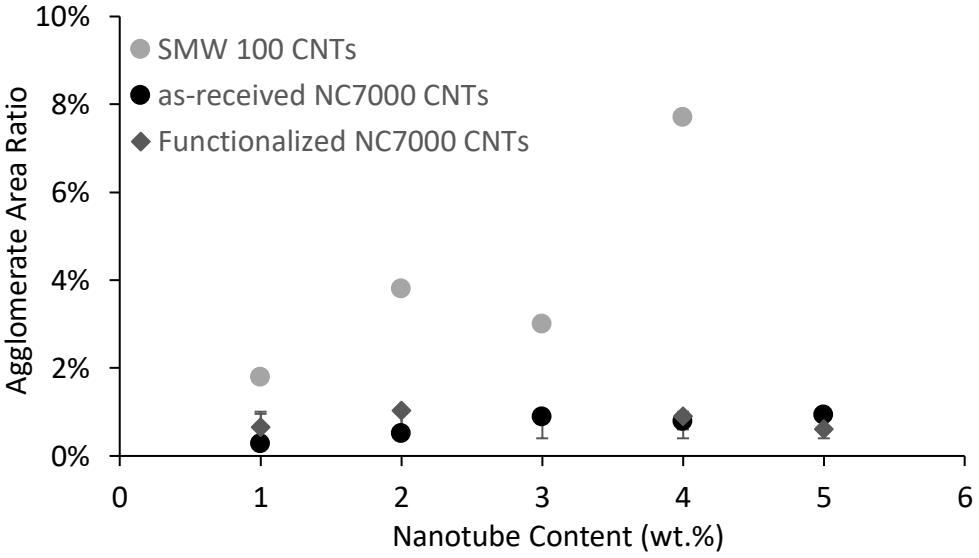

Figure B.7. Agglomerate area ratio of CNTs in ETFE as a function of nanotubes type and concentration. Error bars represent two standard deviations. SMW-100 data was taken from a previous publication and error bars are not available[12].

For carbon nanotubes to form a conductive network in polymers at low volume fractions, they must be well dispersed on a nanometer scale. As Figure B.7 shows, both NC7000 CNTs used in this work have lower agglomerate area ratios in this ETFE than SMW-100 CNTs which means the NC7000 CNTs are better dispersed, at least in a micron-level sense. However, composites made with NC7000 CNTs have higher percolation threshold and lower plateau conductivities. Better dispersion but higher percolation thresholds have been observed before with the same tubes in different polymers. Moud et al.[43] dispersed NC7000 nanotubes in polyamide 6 (PA6) and polypropylene (PP) and obtained higher percolation thresholds and lower conductivities in PA6 than in PP even though they saw better nanotubes dispersion in PA6. Their finding was attributed to better dispersion in PA6 leading to more isolated and broken tubes which decreases their physical contact and thus results in less conductive paths. They used the affinity of the nanotubes to PA6 as another causing factor because more affinity means the possibility that the polymer may be wrapped around the nanotubes which can also decrease the capacity of conducting electrons; the same conclusion was made elsewhere. [44]

Potschke's group has extensively studied the relationship between carbon nanotubes dispersion and electrical conductivity.[41, 45, 46] They concluded that maximum conductivity in polymer-carbon nanotube composites was related to an optimum mixing energy below which large carbon nanotubes agglomerates are present which prevent percolation and effective electron conduction and above which better nanotubes dispersion is achieved but because of significant tube breakage percolation is also inhibited.[45] In other words, a good balance between suitable dispersion and retaining the high aspect ratio of nanotubes is important for achieving low percolation thresholds [42]. This mixing energy depends on the mixing conditions (rotation speed of the motor, mixing

device characteristics, mixing time) but also on the properties of the polymer (i.e. viscosity) and the nanotubes (aspect ratio).

Another observation that can be made from Figure B.6 is that above the percolation threshold, functionalized CNTs composites have slightly lower conductivities than composites with as-received CNTs even though the percolation thresholds are close to identical. It was initially thought that the second issue raised by Moud et al.[43] could be used to explain this behavior. The presence of copolymer on the functionalized tubes would decrease the ability of the nanotube network to conduct electrons above the percolation threshold because of the nonconductive coating that would be forming. However, knowing that no copolymer is present on the nanotubes, the behavior can be explained the presence of the trace elements (Na, Fe…) decreasing the ability of the nanotube network to conduct electricity.

3.3 Dynamic mechanical analysis

Like electrical conductivity, adding CNTs to polymers affects rheological behavior. Above a certain concentration, CNTs can form a network capable of supporting significant stress. This rheological percolation threshold is achieved when a rubbery plateau forms in the storage modulus above the melting temperature of a semicrystalline polymer or the glass transition of an amorphous polymer.[47] It has been proposed that the rheological percolation threshold is reached when the distance between nanotubes is smaller than the radius of gyration of the polymer chains while for electrical percolation to occur, nanotubes must approach sufficiently to allow electron hopping or tunneling.[37] Stated more generally, the electrical percolation threshold is higher because the characteristic distance for the decay in resistance between two nanotubes is smaller than the characteristic distance for the decay in immobilized fraction. For this reason, in all amorphous materials to our knowledge and in some semicrystalline materials, the electrical percolation

threshold has been found to be higher than the rheological percolation threshold [48-56] while in a few other semicrystalline materials the opposite has been found [57, 58] . The latter arises because of the different states of the sample during measurement. Rheological measurements are made using the melt, and in a melt, nanotubes are distributed approximately uniformly. Electrical measurements are made using the solid and in a solid, nanotubes are preferentially located in the amorphous phase. Hence, the volume fraction in the amorphous phase is higher, and, if the amorphous phase is continuous, lower percolation thresholds will be measured.

As evidenced by the storage modulus curves in Figure 6, the rheological percolation threshold is in the same range as the electrical percolation threshold for as-received CNTs/ETFE composites but increases to 3-4 wt.% for functionalized CNTs/ETFE composites. This finding was surprising because functionalization typically has the opposite effect on the rheological percolation threshold.

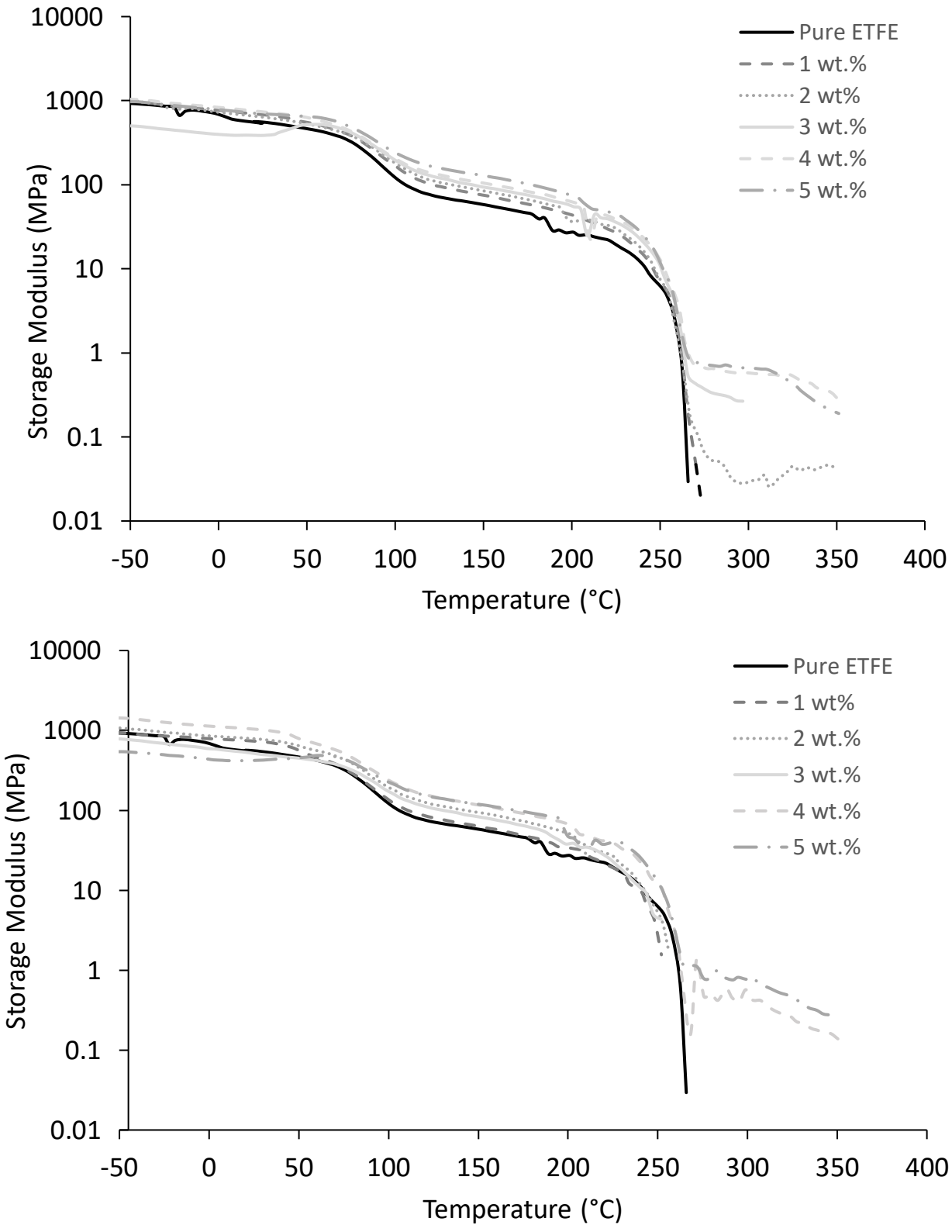

Figure B.8. Storage modulus of composites with as-received NC7000 CNTs (top) and functionalized NC7000 CNTs (bottom)

To explain this new finding, factors that affect percolation in polymer-CNT composites must be considered. The aspect ratio of the nanotubes and the quality of their dispersion in the polymer matrix affect both rheological and electrical percolation thresholds. Nanotubes alone determine the electrical percolation threshold; the rheological percolation threshold is due to both the nanotubes and the immobilized layer around the nanotubes. As stated previously, the electrical percolation threshold is almost always measured on a solid while the rheological percolation threshold is measured in a melt. However, to explain why the electrical percolation threshold was constant with functionalization while the rheological percolation threshold increased, the most important aspect to consider is polymer-CNT interactions.

With the nanotubes having a very weak nucleating ability for the ETFE copolymer, the electrical percolation threshold would be expected to be the same or lower than the rheological percolation threshold. However, the fact that changes only occurred in the melt indicates that differences in the solid material are likely not the cause of the qualitative differences in the behavior of the two percolation thresholds. An increase in rheological percolation threshold without any change in the electrical percolation threshold suggests that the impurities present in the functionalized nanotubes either reduces the thickness of the immobilized layer and/or plasticizes the immobilized layer. The elements present most likely changed the nature of the nanotube-filler interaction which resulted in a change in rheological percolation threshold without changing the electrical percolation threshold.

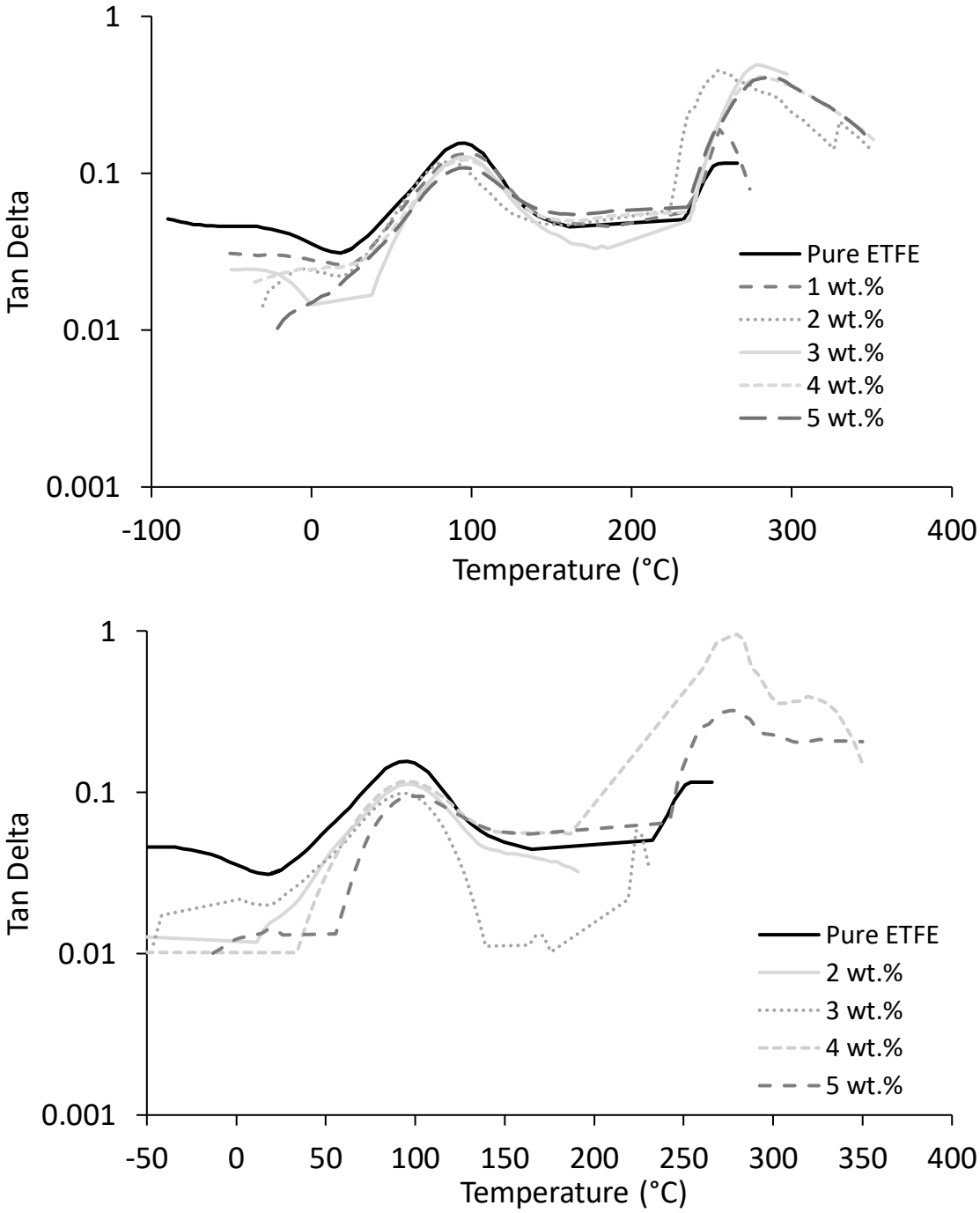

Figure B.9. tan δ for composites with as-received NC7000 CNTs (top) and functionalized NC7000 CNTs (bottom). Data was smoothed to improve presentation. Data for 1% MWCNTs was too noisy and was not included.

The peaks ~100°C on the tan δ curves, Figure B.8, can be attributed to the glass transition temperatures (T_g) of the pure ETFE and the composites which are displayed on Figure B.9. Two opposite trends can be observed for the composites with as-received and functionalized CNTs. For as-received tubes below percolation T_g increases while above percolation T_g decreases and eventually becomes constant. This behavior has been attributed to the immobilized amorphous polymer layer which is in a state of restricted mobility [59]. Below percolation this immobilized polymer decreases the amount of polymer chains that participate in the T_g, resulting in higher T_g. However, as the concentration of CNTs increases above the percolation threshold, the network of nanotubes formed also participates in the T_g which decreases its value. The value remains constant, somehow, because adding more nanotubes above percolation doesn't significantly affect the behavior of the network already formed. The behavior with functionalized tubes is due to an interplay between the plasticizing effect of the copolymer functionalized on the CNTs and the reinforcing effect of the nanotubes. Below 2 wt.%, a network of nanotubes is not formed so the plasticizing effect dominates and the T_g of the composite drops. Above 2 wt.%, when the network of polymer forms, an increase in T_g can be seen.

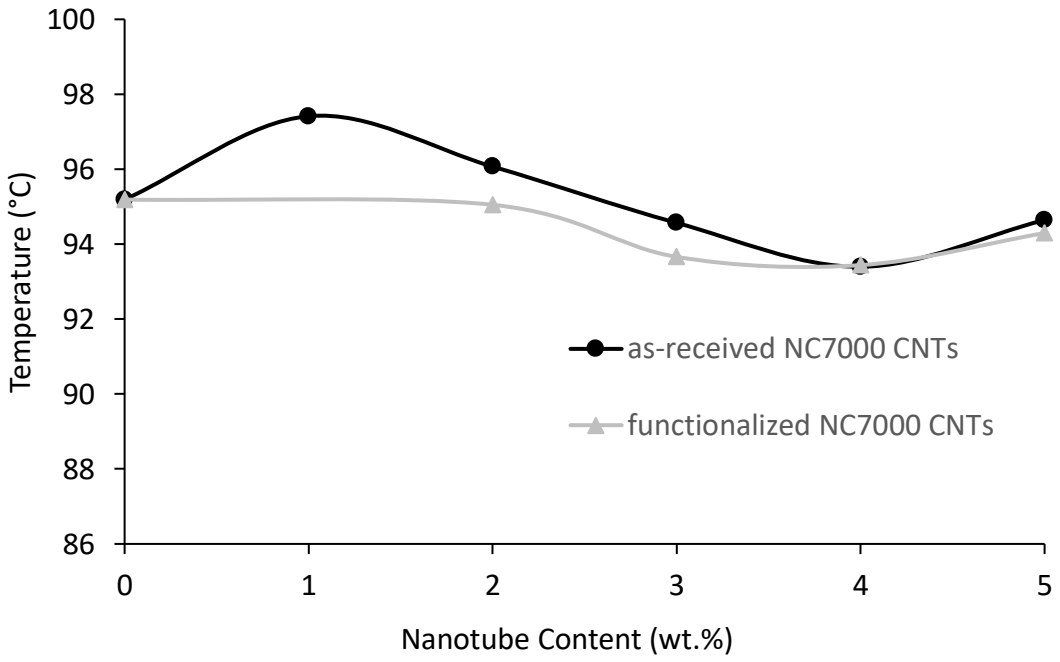

Figure B.10. T_g for MWCNT filled ETFE from peak in tan δ

3.4 Differential Scanning Calorimetry (DSC)

Crystallization and melting temperatures of ETFE as a function of CNT type are shown on Figure B.11; functionalization has no effect on either temperature. The crystallization temperature increases only slightly with nanotube addition which means that CNTs are not strong nucleating agents for ETFE, contrary to what was observed previously for other semicrystalline polymers like PE [60, 61] and PP.[62] The slight decrease in melting temperatures with CNT addition suggests that smaller crystals form in the presence of CNTs. The effect, as small as it is, seems to saturate at very low volume fractions, below 1 wt.% of added tubes.

The change in the enthalpy of fusion shows the same pattern regardless of the type of CNTs used as displayed in Figure B.12. When the nanotube content is below the percolation threshold, the enthalpy of fusion, i.e. fractional crystallinity, increases while decreasing above percolation. This behavior has been seen before and is attributed to the fact that crystal nucleation induced by CNTs

is more pronounced at low nanotube content; at high nanotube content, the formation of nanotube networks restricts the polymer chain motion which inhibits the proper growth of crystals.[7] So, even though the nucleating effect is small, this behavior will still be observed.

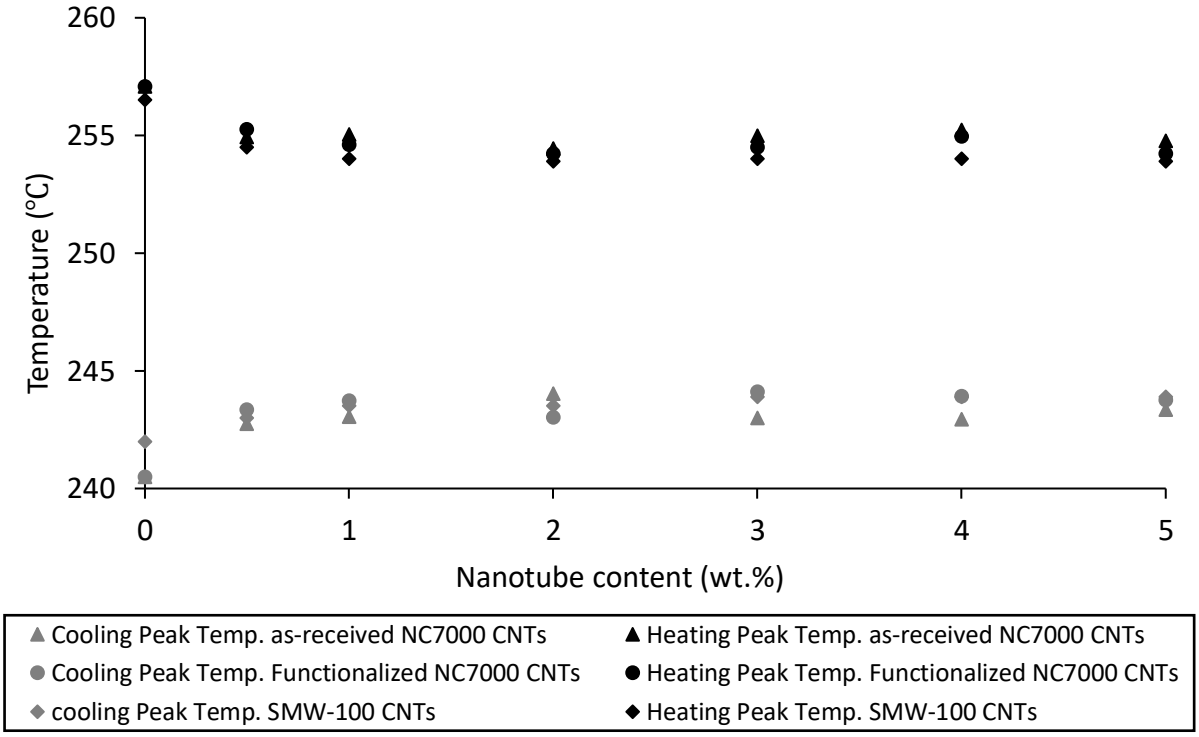

Figure B.11. Nonisothermal crystallization temperature and melting temperature of MWCNT filled ETFE

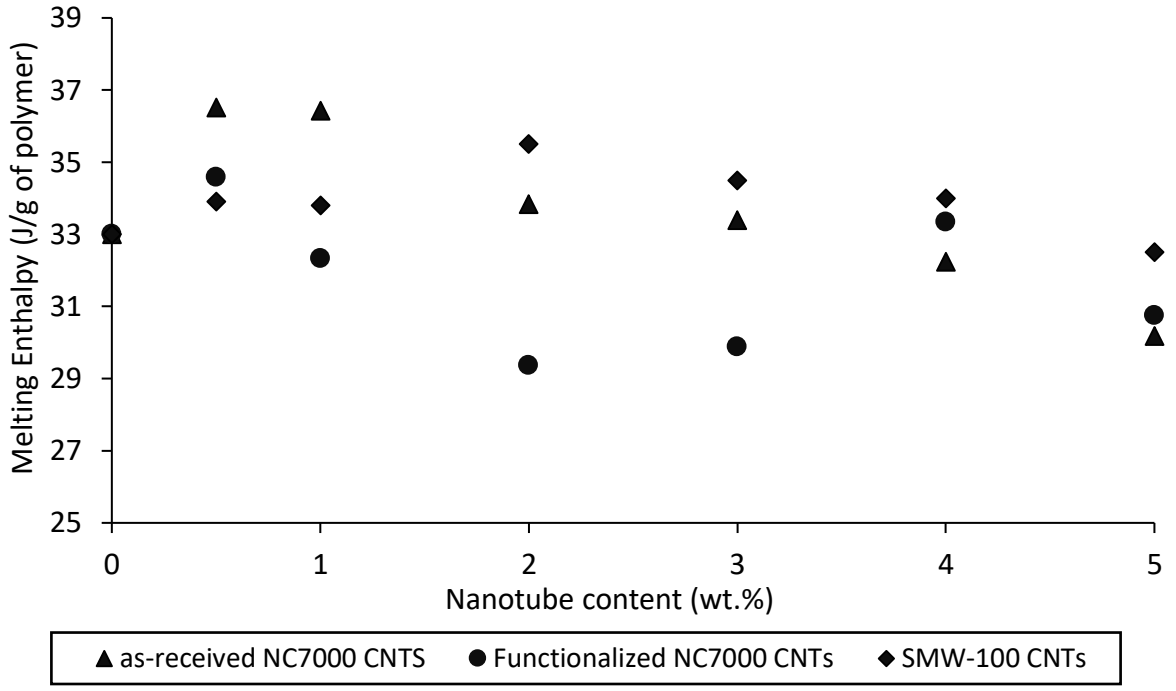

Figure B.12. Melting enthalpy of MWCNT filled ETFE

Nanotube type influences fractional crystallinity. From Figure 10, overall, ETFE/SMW-100 composites have the highest fractional crystallinity followed by ETFE/a-received NC7000 composites then ETFE/functionalized NC7000 composites. This variation can be attributed to the aspect ratio and surface chemistry difference of the CNTs. SMW-100 CNTs are shorter than NC7000 CNTs, which allows for more free volume in the copolymer matrix and thus more crystal formation while the functionalized tubes have additional trace elements which decrease the amount of crystals formed compared to the as-received NC7000 CNTs. An interesting observation here is that above 4 wt.%, the degree of crystallinity is the same for both NC7000 CNT types, as was observed for the T_g. It seems that at a certain concentration, the presence of impurities in the nanotubes no longer affect the behavior of the composites

3.5 Tensile tests

Results from tensile tests are shown in Figure B.13. The modulus increases as a function of as-received NC7000 CNTs addition, while tensile strength is only modestly improved and strain at break decreases significantly. In comparison, the functionalized NC7000 CNTs have much poorer performance; they only modestly improve the modulus and significantly decrease the tensile strength. The decrease in the strain at break is to a smaller extent than with the as-received CNTs. These results are almost certainly a manifestation of the differences in the nanotube-polymer interface, a more plasticized interface would be expected to yield a lower tensile strength and a higher strain to break.

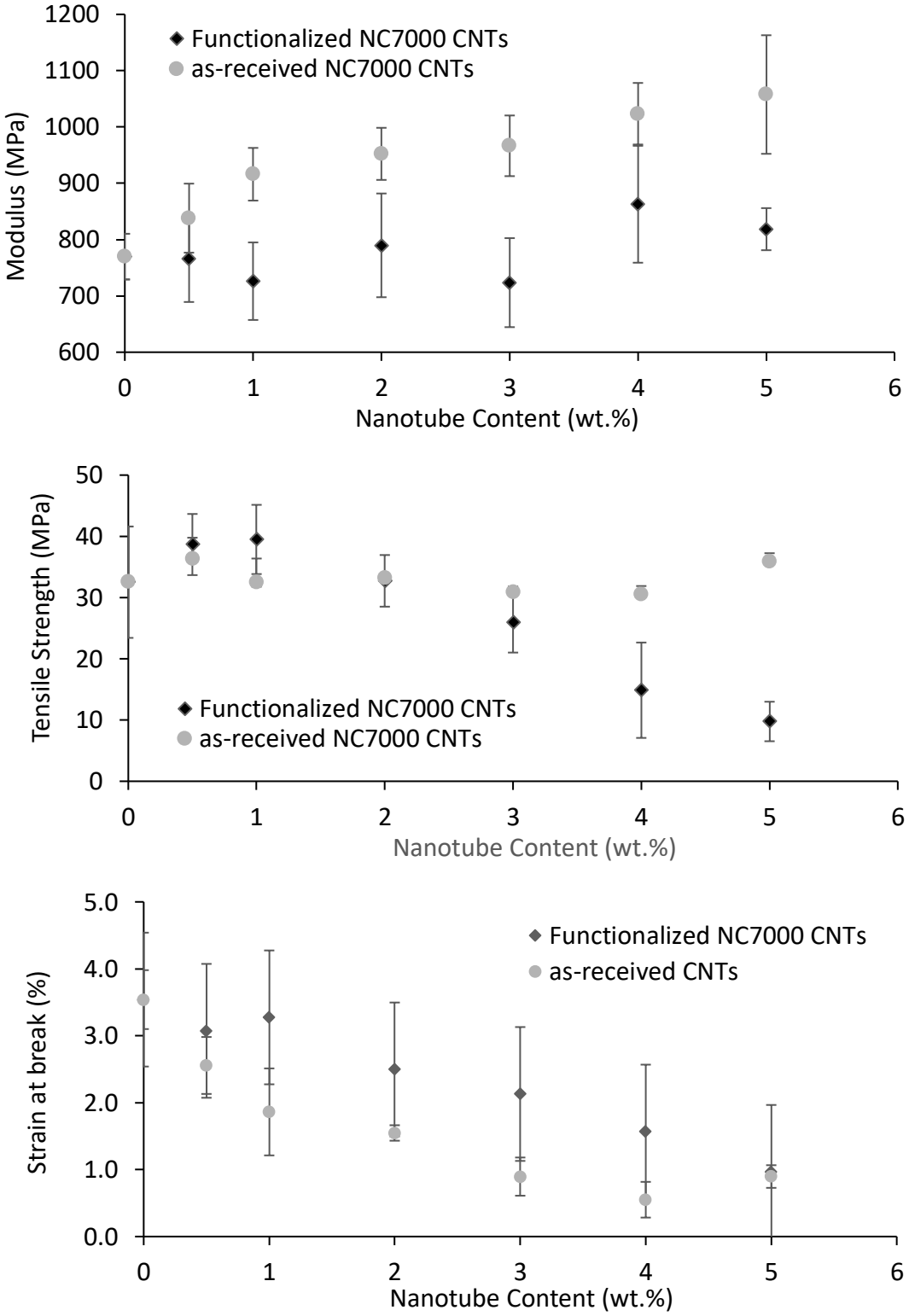

Figure B.13. Young's modulus, Tensile strength, Strain at break (top to bottom) for MWCNTs filled ETFE

3. Conclusions

This project shows the importance of using multiple characterization techniques for CNTs. FT-IR analysis suggested that the functionalization of the nanotubes was successful but subsequent SEM-EDS and TGA data showed otherwise. Only trace elements of Na, Fe, and other materials were present in the sample that was thought to be functionalized. We did notice certain differences in the electrical conductivity, rheological percolation threshold, and mechanical properties in the two composites which does show that the presence of impurities can affect the properties of CNT/polymer composites.

References

[1] T. Tanigami, K. Yamaura, S. Matsuzawa, M. Ishikawa, K. Mizoguchi, and K. Miyasaka, "Structural studies on ethylene-tetrafluoroethylene copolymer: 2. Transition from crystal phase to mesophase," *Polymer,* vol. 27, no. 10, pp. 1521-1528, 1986.

[2] K. Arai, A. Funaki, S. Aida, S. Phongtamrug, and K. Tashiro, "Influence of the monomer sequential distribution on the mechanical properties and temperature dependence of an ethylene–tetrafluoroethylene copolymer in association with the phase-transition behavior," *Journal of applied polymer science,* vol. 114, no. 3, pp. 1710-1716, 2009.

[3] K. Arai, A. Funaki, S. Phongtamrug, and K. Tashiro, "Influence of alternating sequential fraction on the melting and glass transition temperatures of ethylene–tetrafluoroethylene copolymer," *Polymer,* vol. 51, no. 21, pp. 4831-4835, 2010.

[4] A. Funaki, K. Arai, S. Aida, S. Phongtamrug, and K. Tashiro, "Influence of third monomer on the crystal phase transition behavior of ethylene–tetrafluoroethylene copolymer," *Polymer,* vol. 49, no. 25, pp. 5497-5503, 2008.

[5] J. Vail, D. Burris, and W. Sawyer, "Multifunctionality of single-walled carbon nanotube–polytetrafluoroethylene nanocomposites," *Wear,* vol. 267, no. 1-4, pp. 619-624, 2009.

[6] I. Alig, D. Lellinger, M. Engel, T. Skipa, and P. Pötschke, "Destruction and formation of a conductive carbon nanotube network in polymer melts: In-line experiments," *Polymer,* vol. 49, no. 7, pp. 1902-1909, 2008.

[7] S. Abbasi, A. Derdouri, and P. J. Carreau, "Properties of microinjection molding of polymer multiwalled carbon nanotube conducting composites," *Polymer Engineering & Science,* vol. 51, no. 5, pp. 992-1003, 2011.

[8] S. Sofie, D. Åkesson, and B. Martin, "Reprocessing of High-Density Polyethylene Reinforced with Carbon Nanotubes," *Journal of Polymers and the Environment,* vol. 28, no. 7, pp. 1967-1973, 2020.

[9] A. Li, Z. Wu, Z. Zhang, and K. Mai, "Preparation and characterization of ultrahigh molecular weight polyethylene composites with high content of multiwall carbon nanotubes," *Polymer Composites,* vol. 41, no. 5, pp. 1972-1978, 2020.

[10] H. Wang *et al.,* "Property improvement of multi-walled carbon nanotubes/polypropylene composites with high filler loading via interfacial modification," *RSC Advances,* vol. 9, no. 50, pp. 29087-29096, 2019.

[11] S. H. Yetgin, "Effect of multi walled carbon nanotube on mechanical, thermal and rheological properties of polypropylene," *Journal of Materials Research and Technology,* vol. 8, no. 5, pp. 4725-4735, 2019.

[12] Y. Rui, J. Guo, J. Harwell, T. Nakanishi, S. Kotera, and B. P. Grady, "Electrical, mechanical, and crystallization properties of ethylene-tetrafluoroethylene copolymer/multiwalled carbon nanotube composites," *Journal of Applied Polymer Science,* vol. 131, no. 22, 2014.

[13] C. Caamaño, B. Grady, and D. E. Resasco, "Influence of nanotube characteristics on electrical and thermal properties of MWCNT/polyamide 6, 6 composites prepared by melt mixing," *Carbon,* vol. 50, no. 10, pp. 3694-3707, 2012.

[14] L. V. Solov'yanchik, S. V. Kondrashov, V. S. Nagornaya, I. A. Volkov, T. P. D'Yachkova, and K. M. Borisov, "Highly Hydrophobic Conducting Nanocomposites Based on a Fluoropolymer with Carbon Nanotubes," *Russian Journal of Applied Chemistry,* vol. 91, no. 10, pp. 1654-1659, Oct 2018.

[15] K. W. Wang, N. X. Hu, G. Xu, and Y. Qi, "Stable superhydrophobic composite coatings made from an aqueous dispersion of carbon nanotubes and a fluoropolymer," *Carbon,* vol. 49, no. 5, pp. 1769-1774, Apr 2011.

[16] V. Ijeri, L. Cappelletto, S. Bianco, M. Tortello, P. Spinelli, and E. Tresso, "Nafion and carbon nanotube nanocomposites for mixed proton and electron conduction," *Journal of Membrane Science,* vol. 363, no. 1-2, pp. 265-270, Nov 2010.

[17] H. Zhang *et al.*, "Synergistic effect of carbon nanotube and graphene nanoplates on the mechanical, electrical and electromagnetic interference shielding properties of polymer composites and polymer composite foams," *Chemical Engineering Journal,* vol. 353, pp. 381-393, 2018.

[18] L. Vaisman, H. D. Wagner, and G. Marom, "The role of surfactants in dispersion of carbon nanotubes," *Advances in colloid and interface science,* vol. 128, pp. 37-46, 2006.

[19] B. P. Grady, *Carbon nanotube-polymer composites: manufacture, properties, and applications*. John Wiley & Sons, 2011.

[20] J. Rausch, R.-C. Zhuang, and E. Mäder, "Surfactant assisted dispersion of functionalized multi-walled carbon nanotubes in aqueous media," *Composites Part A: Applied Science and Manufacturing,* vol. 41, no. 9, pp. 1038-1046, 2010.

[21] H. Kuzmany, A. Kukovecz, F. Simon, M. Holzweber, C. Kramberger, and T. Pichler, "Functionalization of carbon nanotubes," *Synthetic Metals,* vol. 141, no. 1-2, pp. 113-122, 2004.

[22] J. Hilding, E. A. Grulke, Z. George Zhang, and F. Lockwood, "Dispersion of carbon nanotubes in liquids," *Journal of dispersion science and technology,* vol. 24, no. 1, pp. 1-41, 2003.

[23] P. Liu, "Modifications of carbon nanotubes with polymers," *European Polymer Journal,* vol. 41, no. 11, pp. 2693-2703, 2005.

[24] K. Shirvanimoghaddam, M. M. Abolhasani, Q. Li, H. Khayyam, and M. Naebe, "Cheetah skin structure: A new approach for carbon-nano-patterning of carbon nanotubes," *Composites Part A: Applied Science and Manufacturing,* vol. 95, pp. 304-314, 2017.

[25] K. Shirvanimoghaddam, M. M. Abolhasani, B. Polisetti, and M. Naebe, "Periodical patterning of a fully tailored nanocarbon on CNT for fabrication of thermoplastic composites," *Composites Part A: Applied Science and Manufacturing,* vol. 107, pp. 304-314, 2018.

[26] F. Avilés, J. V. Cauich-Rodríguez, P. Toro-Estay, M. Yazdani-Pedram, and H. Aguilar-Bolados, "Improving carbon nanotube/polymer interactions in nanocomposites," in *Carbon Nanotube-Reinforced Polymers*: Elsevier, 2018, pp. 83-115.

[27] D. G. Papageorgiou, I. A. Kinloch, and R. J. Young, "Mechanical properties of graphene and graphene-based nanocomposites," *Progress in Materials Science,* vol. 90, pp. 75-127, 2017.

[28] M. Seneewong-Na-Ayutthaya, T. Pongprayoon, and E. A. O'Rear, "Colloidal Stability in Water of Modified Carbon Nanotube: Comparison of Different Modification Techniques," *Macromolecular Chemistry and Physics,* vol. 217, no. 23, pp. 2635-2646, 2016.

[29] S. Hanumansetty and E. O'Rear, "Two-site adsolubilization model of incorporation of fluoromonomers into fluorosurfactants formed on cotton fabric," *Langmuir,* vol. 30, no. 13, pp. 3665-3672, 2014.

[30] S. Hanumansetty, E. O'Rear, and D. E. Resasco, "Encapsulation of multi-walled carbon nanotubes with copolymer to disperse in aqueous media," *Journal of Polymer Research,* vol. 24, no. 12, p. 228, 2017.

[31] C. Poochai and T. Pongprayoon, "Enhancing dispersion of carbon nanotube in polyacrylonitrile matrix using admicellar polymerization," *Colloids and Surfaces A: Physicochemical and Engineering Aspects,* vol. 456, pp. 67-74, 2014.

[32] K. N. Ulman and S. R. Shukla, "Admicellar polymerization and its application in textiles," *Advances in Polymer Technology,* vol. 35, no. 3, pp. 307-325, 2016.

[33] H. J. Barraza, Y. K. Hamidi, L. Aktas, E. A. O'Rear, and M. C. Altan, "Performance of glass woven fabric composites with admicellar-coated thin elastomeric interphase," *Composite Interfaces,* vol. 24, no. 2, pp. 125-148, 2016.

[34] P. Kothary, N. Yanumet, and A. Edgar, "Surfactant effects on application of a hydrophobic, fluoropolymer coating to cotton by admicellar polymerization," *Fibers and Polymers,* vol. 14, no. 5, pp. 710-717, 2013.

[35] B. Du, U. A. Handge, S. Majeed, and V. Abetz, "Localization of functionalized MWCNT in SAN/PPE blends and their influence on rheological properties," *Polymer,* vol. 53, no. 24, pp. 5491-5501, 2012.

[36] P. Pötschke, S. Pegel, M. Claes, and D. Bonduel, "A novel strategy to incorporate carbon nanotubes into thermoplastic matrices," *Macromolecular Rapid Communications,* vol. 29, no. 3, pp. 244-251, 2008.

[37] D. Bangarusampath, H. Ruckdäschel, V. Altstädt, J. K. Sandler, D. Garray, and M. S. Shaffer, "Rheology and properties of melt-processed poly (ether ether ketone)/multi-wall carbon nanotube composites," *Polymer,* vol. 50, no. 24, pp. 5803-5811, 2009.

[38] M. T. Müller, B. Krause, B. Kretzschmar, and P. Pötschke, "Influence of feeding conditions in twin-screw extrusion of PP/MWCNT composites on electrical and mechanical properties," *Composites Science and Technology,* vol. 71, no. 13, pp. 1535-1542, 2011.

[39] M. T. Müller, B. Krause, and P. Pötschke, "A successful approach to disperse MWCNTs in polyethylene by melt mixing using polyethylene glycol as additive," *Polymer,* vol. 53, no. 15, pp. 3079-3083, 2012.

[40] B. Krause, P. Pötschke, and L. Häußler, "Influence of small scale melt mixing conditions on electrical resistivity of carbon nanotube-polyamide composites," *Composites Science and Technology,* vol. 69, no. 10, pp. 1505-1515, 2009.

[41] P. Pötschke, T. Villmow, and B. Krause, "Melt mixed PCL/MWCNT composites prepared at different rotation speeds: Characterization of rheological, thermal, and electrical properties, molecular weight, MWCNT macrodispersion, and MWCNT length distribution," *Polymer,* vol. 54, no. 12, pp. 3071-3078, 2013.

[42] R. Socher, B. Krause, R. Boldt, S. Hermasch, R. Wursche, and P. Pötschke, "Melt mixed nano composites of PA12 with MWNTs: Influence of MWNT and matrix properties on macrodispersion and electrical properties," *Composites Science and Technology,* vol. 71, no. 3, pp. 306-314, 2011.

[43] A. Abbasi Moud, A. Javadi, H. Nazockdast, A. Fathi, and V. Altstaedt, "Effect of dispersion and selective localization of carbon nanotubes on rheology and electrical conductivity of polyamide 6 (PA 6), Polypropylene (PP), and PA 6/PP nanocomposites," *Journal of Polymer Science Part B: Polymer Physics,* vol. 53, no. 5, pp. 368-378, 2015.

[44] A. H. A. Hoseini, M. Arjmand, U. Sundararaj, and M. Trifkovic, "Significance of interfacial interaction and agglomerates on electrical properties of polymer-carbon nanotube nanocomposites," *Materials & Design,* vol. 125, pp. 126-134, 2017.

[45] G. R. Kasaliwal, S. Pegel, A. Göldel, P. Pötschke, and G. Heinrich, "Analysis of agglomerate dispersion mechanisms of multiwalled carbon nanotubes during melt mixing in polycarbonate," *Polymer,* vol. 51, no. 12, pp. 2708-2720, 2010.

[46] G. Kasaliwal, A. Göldel, and P. Pötschke, "Influence of processing conditions in small-scale melt mixing and compression molding on the resistivity and morphology of polycarbonate–MWNT composites," *Journal of Applied Polymer Science,* vol. 112, no. 6, pp. 3494-3509, 2009.

[47] M. L. Ha, B. P. Grady, G. Lolli, D. E. Resasco, and W. T. Ford, "Composites of Single-Walled Carbon Nanotubes and Styrene-Isoprene Copolymer Latices," *Macromolecular chemistry and physics,* vol. 208, no. 5, pp. 446-456, 2007.

[48] F. M. Du, R. C. Scogna, W. Zhou, S. Brand, J. E. Fischer, and K. I. Winey, "Nanotube networks in polymer nanocomposites: Rheology and electrical conductivity," (in English), *Macromolecules,* vol. 37, no. 24, pp. 9048-9055, 2004.

[49] M. L. P. Ha, B. P. Grady, G. Lolli, D. E. Resasco, and W. T. Ford, "Composites of single-walled carbon nanotubes and styrene-isoprene copolymer latices," (in English), *Macromolecular Chemistry and Physics,* vol. 208, no. 5, pp. 446-456, Mar 5 2007.

[50] G. J. Hu, C. G. Zhao, S. M. Zhang, M. S. Yang, and Z. G. Wang, "Low percolation thresholds of electrical conductivity and rheology in poly(ethylene terephthalate) through

the networks of multi-walled carbon nanotubes," *Polymer,* vol. 47, no. 1, pp. 480-488, 2006.

[51] J. I. Lee, S. B. Yang, and H. T. Jung, "Carbon Nanotubes-Polypropylene Nanocomposites for Electrostatic Discharge Applications," *Macromolecules,* vol. 42, no. 21, pp. 8328-8334, 2009.

[52] D. S. Bangarusampath, H. Ruckdaschel, V. Altstadt, J. K. W. Sandler, D. Garray, and M. S. P. Shaffer, "Rheology and properties of melt-processed poly(ether ether ketone)/multi-wall carbon nanotube composites," *Polymer,* vol. 50, no. 24, pp. 5803-5811, 2009.

[53] S. Z. Yu, W. M. Wong, X. Hu, and Y. K. Juay, "The Characteristics of Carbon Nanotube-Reinforced Poly(phenylene sulfide) Nanocomposites," *Journal of Applied Polymer Science,* vol. 113, no. 6, pp. 3477-3483, 2009.

[54] R. A. Kalgaonkar and J. P. Jog, "Copolyester nanocomposites based on carbon nanotubes: reinforcement effect of carbon nanotubes on viscoelastic and dielectric properties of nanocomposites," (in English), *Polymer International,* vol. 57, no. 1, pp. 114-123, Jan 2008.

[55] Y. Kazemi, A. R. Kakroodi, L. H. Mark, T. Filleter, and C. B. Park, "Effects of polymer-filler interactions on controlling the conductive network formation in polyamide 6/multi-Walled carbon nanotube composites," *Polymer,* vol. 178, Sep 2019, Art. no. Unsp 121684.

[56] F. Faridirad, S. Ahmadi, and M. Barmar, "Rheological and electrical percolation thresholds of multi-walled carbon nanotube/in-situ polymerised Nylon12 nanocomposites," *Micro & Nano Letters,* vol. 13, no. 11, pp. 1594-1599, Nov 2018.

[57] J. Kim, S. M. Hong, S. Kwak, and Y. Seo, "Physical properties of nanocomposites prepared by in situ polymerization of high-density polyethylene on multiwalled carbon nanotubes," *Physical Chemistry Chemical Physics,* vol. 11, no. 46, pp. 10851-10859, 2009.

[58] T. Chatterjee, K. Yurekli, V. G. Hadjiev, and R. Krishnamoorti, "Single-walled carbon nanotube dispersions in poly(ethylene oxide)," (in English), *Advanced Functional Materials,* vol. 15, no. 11, pp. 1832-1838, Nov 2005.

[59] E. Logakis *et al.*, "Structure–property relationships in polyamide 6/multi-walled carbon nanotubes nanocomposites," *Journal of Polymer Science Part B: Polymer Physics,* vol. 47, no. 8, pp. 764-774, 2009.

[60] J. Vega *et al.*, "Rheology, processing, tensile properties, and crystallization of polyethylene/carbon nanotube nanocomposites," *Macromolecules,* vol. 42, no. 13, pp. 4719-4727, 2009.

[61] M. Trujillo *et al.*, "Thermal fractionation and isothermal crystallization of polyethylene nanocomposites prepared by in situ polymerization," *Macromolecules,* vol. 41, no. 6, pp. 2087-2095, 2008.

[62] K. Wiemann, W. Kaminsky, F. H. Gojny, and K. Schulte, "Synthesis and properties of syndiotactic poly (propylene)/carbon nanofiber and nanotube composites prepared by in situ polymerization with metallocene/MAO catalysts," *Macromolecular Chemistry and Physics,* vol. 206, no. 15, pp. 1472-1478, 2005.